FOSSIL

DOE/PC/90301-T6
(DE94014367)
Distribution Category UC-113

Comparative Study of the Reactions of Metal Oxides and Carbonates with H_2S and SO_2

Final Technical Report

September 1990 - February 1994

Prepared by:

Prof. Stratis V. Sotirchos

March 1994

Work Performed under Grant No.: DE-FG22-90PC90301

Performed for:

U.S. Dept. of Energy
University Coal Research Program
Pittsburgh Energy Technology Center
Pittsburgh, Pennsylvania

Performed at:

University of Rochester
Dept. of Chemical Engineering
Rochester, NY 14627

EXECUTIVE SUMMARY

The primary objective of this project had been the investigation of the effects of pore structure on the capacity of porous metal oxides for removal of gaseous pollutants from flue gases of power plants (SO_2) and hot coal gas (primarily H_2S). Porous calcines obtained from natural precursors (limestones and dolomites) and sorbents based on zinc oxide were used as model systems in our experimental studies, which included reactivity evolution experiments and pore structure characterization using a variety of methods. The key idea behind this project was to appropriately exploit the differences of the sulfidation and sulfation reactions (for instance, different molar volumes of solid products) to elucidate the dependence of the sorptive capacity of a porous sorbent on its physical microstructure.

In order to be able to proceed faster and more productively on the analysis of the above defined problem, it was decided to employ in our studies solids whose reaction with SO_2 (limestone calcines) or H_2S (sorbents based on zinc oxide) had been investigated in detail in past studies by our research group. Calcines derived from limestones of high (> 95%) calcium carbonate content and commercially available desulfurization sorbents (e.g., zinc oxide) of qualitatively (or quantitatively) different pore size distributions were used in our experiments. Reactivity vs. time or conversion vs. time studies were conducted using thermogravimetry and fixed-bed and fluidized-bed reactors. The pore structure of partially reacted samples collected at selected time instants or conversion levels was analyzed by gas adsorption and mercury porosimetry. For better characterization of the pore structure of the solid samples, we also carried out intraparticle diffusivity measurements by the peak-broadening (chromatographic) method, using a system developed for this purpose in our laboratory. In the context of this part of the project, we also conducted a detailed theoretical investigation of the measurement of effective diffusivities in porous solids using the diffusion-cell method.

Our experiments on the reaction of ZnO-based sorbents with SO_2 showed that it proceeded with extremely low rate. As a result, conclusions on the effects of pore struc-

ture on the sulfidation and sulfation reactions were mainly reached from the comparative analysis of the CaO-SO_2 and CaO-H_2S reactions. The comparison of model predictions and experimental data showed that the key factor influencing the behavior of a sorbent during sulfidation and sulfation was the connectivity of its pore space. In both cases, the reactivity of the sorbent and the connectivity of its pore structure were found to, in general, increase with increasing average grain in the precursor stone, and the same behavior was also exhibited by the calcination rates of the precursors. Detailed models for transport, reaction, and structure evolution in porous media undergoing gas-solid reactions were used to analyze the experimental data. Among these mathematical models was a novel structural model developed under this project, which uses an assemblage of partially overlapping grains to represent the solid phase of the porous medium. Very good agreement between model and experiment was obtained using in almost all cases the same pore connectivity parameter for sulfidation as for sulfation. The particle models were used as basis to develop a predictive design model for desulfurization in beds, and experimental data obtained for the ZnO-H_2S reaction in a fixed-bed reactor were used for its testing and validation.

Results and conclusions on the reaction of CaO with H_2S and SO_2 at atmospheric pressure cannot be applied to flue gas and coal gas desulfurization by limestone addition in units (combustors and gasifiers) operating at high pressures since calcination is, in general, not favored in such units. For this reason, we decided to comparatively investigate the direct reaction with H_2S and SO_2 of the limestones we used as CaO precursors. Reactivity evolution experiments were thus carried out in a thermogravimetric analysis system under simulated high pressure conditions, that is, in the presence of enough CO_2 to prevent decomposition of $CaCO_3$. The direct sulfidation reaction of limestones was found to be much faster than their direct sulfation, but both direct reactions were much slower than the corresponding reactions of the calcined solids. In agreement with the behavior seen in the study of the indirect reactions, the direct reactivity of limestone with H_2S and SO_2

was found to increase with decreasing grain size.

The preliminary analysis of the experimental data using a shrinking core model suggested that the effective diffusivity in the product layer depended on the distance from the external surface of the reacting particles. A variable diffusivity, shrinking core model was thus developed and then employed to extract from the experimental conversion vs. time profiles the effective diffusivity in the product layer as a function of distance from the external surface. Several interesting conclusions about the resistance for diffusion in the product during the direct and indirect reactions were reached from the estimated values of effective diffusivities. For instance, it was concluded that the product layer formed during direct sulfation presented much less resistance to diffusion than that formed during the indirect process. On the other hand, the diffusional resistance of the product formed during direct sulfidation was found to be much larger than what should be expected for a 30% porous solid – as it should be the case if the particle did not change size during reaction. In agreement with this result, pore structure characterization of fully sulfided particles revealed that the product layer formed during sulfidation underwent extensive sintering.

TABLE OF CONTENTS

1. BACKGROUND STATEMENT

The reactions of metal oxides with sulfur-containing compounds, such as SO_2 and H_2S, find extensive use in controlling emissions of gaseous pollutants from coal utilization systems. Limestone and dolomite, for instance, are used in the control of emissions of sulfur dioxide from coal-fired power plants. In the high temperature environment of a combustor, the limestone or dolomite particles undergo calcination, and the calcined product (CaO or MgO) reacts with the sulfur dioxide produced during coal combustion forming, mainly, calcium or magnesium sulfate. Calcium oxide and other metal oxide sorbents (iron oxide, zinc oxide, zinc ferrite, zinc titanate, etc.), on the other hand, are used to remove sulfur-containing compounds (predominantly H_2S) from hot coal gas.

The reaction of metal oxides with SO_2 and H_2S are typical examples of noncatalytic gas solid reactions with solid product formation and pore closure behavior. Such gas-solid reactions with solid product are encountered in a number of chemical process industries with applications ranging from ceramic material manufacture to gas scrubbing for pollution control. The calcination and sulfation reactions of limestone and dolomite have been the subject of extensive experimental investigation, but unambiguous experimental evidence that leads to a clear understanding of the effects of pore size distribution of calcined stones on their capacity for SO_2 removal is still lacking. Most investigators tend to focus on the global kinetics of the sulfation or sulfidation reactions while paying little attention to the pore structure of the calcined solid. A review of the experimental evidence of the literature reveals an anomalous dependence of the reactivity and SO_2 uptake of calcined limestones on the initial values of average properties of their pore structure, such as porosity and surface area, indicating strong effects of the pore size distribution on the overall reactivity of the calcined solids (Borgwardt and Harvey, 1972; Wen and Ishida, 1973; Hartman and Coughlin, 1974, 1976; Simons and Garman, 1986; Yu, 1987; Gullett and Bruce, 1987).

Analogous observations apply to the reaction of metal oxides (calcium oxide, zinc oxide, zinc ferrite, zinc titanate, etc.) with H_2S. A good deal of experimental effort has been put in the area of hot gas desulfurization into the investigation the reactivity and capacity of various metal/metal oxide sorbents for sulfur compound removal from coal

gas (e.g., see studies by Gibson and Harrison (1980), Tamhankar et al., (1981 and 1985), Ranade and Harrison (1981), Jalan (1983), Sick and Schwerdtfeger (1987), and Sa et al. (1989)). However, limited work has been done on the characterization of these sorbents in terms of their pore size distribution and resistance for intraparticle diffusion. Simplistic models of structure evolution are usually employed for data treatment and interpretation, while few studies have looked into the variation of the properties of the pore structure, such as the internal surface area (Caillet and Harrison, 1982; Sa et al., 1989), with the progress of the reaction.

A systematic investigation of the dependence of the transient behavior of large limestone particles reacting with SO_2 in the presence of oxygen on pore structure and particle size related factors has been carried out by my research group (Zarkanitis and Sotirchos, 1989; Yu, 1987). Our results have shown strong dependence of the transient behavior of reacting particles of calcined limestone and, consequently, of their sorptive capacity for SO_2 removal on their initial pore size distribution, but this dependence seems to follow an anomalous pattern when the sulfation capacities of calcines obtained from different precursors (stones) are compared. Specifically, calcines of similar composition and pore structure properties have been found to exhibit considerably different capacities for removal of SO_2 from flue gases. Comparison of the experimental data with the predictions of a generalized pore model for gas-solid reactions with solid product (Yu and Sotirchos, 1987) showed that these differences could be due to the formation of inaccessible pore space in the course of the reaction, which takes place when the small feeder pores of finite clusters of large pores or large cavities, in aperture-cavity pore structures, are filled with solid product.

Similar conclusions have been reached by analyzing reactivity data for zinc oxide sulfidation obtained in our laboratory (Efthimiadis and Sotirchos, 1989). However, an important difference exists between the reaction of metal oxides with H_2S and their reaction with SO_2. The sulfide produced during reaction with H_2S occupies less space than the solid product produced during sulfation (sulfate (mainly) or sulfite), and as a result, complete pore closure in the case of sulfidation can happen only for low initial porosities. This difference suggests that a comparative study of the reactions of porous metal oxides with SO_2 and H_2S can lead to a better assessment of the effects of pore structure on sorptive

capacity than studies of the effects of the parameters of a single reaction only.

On the basis of the above observations, a research program has been formulated for the comparative investigation of the reactions of metal oxides with SO_2 and H_2S. Initially, it was planned to work with CaO, limestone-derived, and ZnO solids and specifically with solids whose reactions with SO_2 (limestone calcines) and H_2S (zinc oxide sorbents) had been studied in detail in the past with our research group. However, in order to make our results and conclusions useful to those interested in SO_2 or H_2S removal from high pressure units (combustors or gasifiers), it was decided to extend our work to the case in which sulfidation or sulfation occurs under noncalcining conditions. Reactivity evolution experiments for limestone sulfation and sulfidation were thus carried out in a thermogravimetric analysis system under simulated high pressure conditions, that is, in the presence of enough CO_2 to prevent decomposition of $CaCO_3$ to CaO.

In this technical report, we present some of the most important results that we obtained on the study of the above problems using various experimental and theoretical methods. Each section of the report is developed in a self-contained manner, and as a result, it can be read and followed independently of the others. Section 2 presents experimental and theoretical results on the reaction of calcined limestones with H_2S and compares them with those obtained for the sulfation of the same solids in our past studies. Section 3 deals with the investigation of the direct (i.e., under noncalcining conditions) sulfation of limestones, while Section 4 discusses the development of a variable diffusivity shrinking core model and its application to the analysis of the direct limestone sulfation data. Section 5 examines the effective diffusivity changes that occur during calcination, carbonation, recalcination, and sulfation of limestones – studied using pulse chromatographic experiments on reacted samples – and discusses these changes in conjunction with the behavior seen in sulfation and sulfidation experiments. The study of the direct sulfidation of limestones and the comparison of the obtained results with those for direct sulfation and indirect sulfidation is the subject of Section 6. The subject of Section 7 is the validation of a predictive model for desulfurization in fixed beds using thermogravimetric single particle reactivity data and breakthrough curves from fixed-bed experiments for zinc oxide particles. Section 8 presents a new grain model for gas-solid reactions, which allows for

partial overlapping of the constituent grains and, as a result, can cover the whole range between the nonoverlapping and randomly overlapping models. Finally, in Section 9, we present a detailed theoretical analysis of the problem of effective diffusivity measurement in porous solids using the diffusion-cell method. The motivation behind this study was to elucidate the effects of the connectivity of the pore structure on the interpretation of mass transport data and the estimation of effective diffusion coefficients.

Literature References

Borgwardt, R.H.; Harvey, R.D., Environ. Sci. Technol., **6**, 350 (1972).

Caillet, D.A.; Harrison, D.P, Chem. Eng. Sci., **37**, 625 (1982).

Efthimiadis, E.A.; Sotirchos, S.V., "Reactivity Evolution during Sulfidation of Porous Zinc Oxide," AIChE Annual Meeting, San Francisco (1989).

Gibson, J.B.; Harrison, D.P., Ind. Eng. Chem. Process Des. Dev., **19**, 231 (1980). Gullett, B.K.; Bruce, K.R., AIChE J., **33**, 1719 (1987).

Hartman, M.; Coughlin, R.W., Ind. Eng. Chem., Process Dec. Dev., **13**, 248 (1974). Hartman, M.; Coughlin, R.W., AIChE J., **22**, 490 (1976).

Jalan, V., Studies Involving High Temperature Desulfurization/Regeneration Reactions of Metal Oxides for Fuel Cell Development, Final Report, DOE/MC/16021-1486 (1983).

Ranade, P.V.; Harrison, D.P., Chem. Eng. Sci., **36**, 1079 (1981).

Sa, L.N.; Focht, G.D.; Ranade, P.V.; Harrison, D.P., Chem. Eng. Sci., **44**, 215 (1989).

Sick, G.; Schwerdtfeger, K., Met. Transactions B, 18, 603 (1987).

Simons; G.A.; Garman, A.R., AIChE J., **32**, 1491 (1986).

Tamhankar, S.S.; Garimella, S.; Wen, C.Y., Chem. Eng. Sci., **40**, 1019 (1985).

Tamhankar, S.S., Hasatani, M., Wen, C.Y., Chem. Eng. Sci., **36**, 1181 (1981).

Wen, C.Y.; Ishida, M., Environ. Sci. Technol.,**7**, 703(1973).

Yu, H.C.; Ph.D. Thesis, University of Rochester (1987).

Yu, H.C.; Sotirchos, S.V., AIChE J., **33**, 382 (1987).

Zarkanitis, S.; Sotirchos, S.V., AIChE J., **35**, 821 (1989).

2. SULFIDATION OF LIMESTONE-DERIVED CALCINES

2.1. Introduction

The sulfidation of CaO particles is of importance in the control of toxic emissions from Limestone Injection Multistage Burners (LIMB) (Borgwardt et al., 1984). The same reaction is also encountered in the desulfurization unit of an Integrated Gasification Combined Cycle (IGCC) (Jalan (1983)). Limestones and dolomites are the most common sources of calcium oxide used in these applications. The thermal decomposition of the calcium carbonate and the sulfidation of the produced calcium oxide can be described by the overall reactions:

$$CaCO_3 \rightarrow CaO + CO_2 \tag{2.1}$$

$$CaO + H_2S \rightarrow CaS + H_2O \tag{2.2}$$

The kinetics of reaction (2.2) were investigated in a number of past studies in thermogravimetric analysis systems (TGA) and other types of reactors, using fully calcined limestones or reagent grade CaO as the solid reactant. In most studies, the carbonates were calcined under an inert atmosphere (usually nitrogen) at temperatures in the range 700-900 $^{\circ}C$, and they were subsequently sulfided at the calcination or at a lower temperature. Mixtures of H_2S, a reducing gas (H_2 or CO), and nitrogen were used as the reactive gas in most cases. Experiments performed in TGA reactors showed in most cases a weak influence of the reaction temperature on the initial sulfidation rates and, as a result, gave low activation energies for Arrhenius-type dependence of the sulfidation rate on temperature (e.g., 5.16 $kcal/mol$ (Westmoreland et al., 1977) and 3.6 $kcal/mol$ (Kamath and Petrie, 1981). Low activation energies were also determined for the reaction of COS with CaO, which is similar to reaction (2.2), in the same temperature range as that of the previous studies (e.g., 3.9 $kcal/mol$ (Kamath and Petrie, 1981) and 4.3 $kcal/mol$ (Yang and Chen, 1979)). The reactivity experiments in these studies were carried out isothermally in the temperature range of 300-900$^{\circ}C$ using solid material in particle form from 1 to about 400 μm in size. Much larger in size dolomite-derived pellets (spheres of about 7 mm in diameter) were sulfided by Squires et al. (1971) in a thermogravimetric analysis system. Reaction rates were measured at different temperatures and gave an activation energy of 30 $kcal/mol$ for

sulfidation in the temperature range 475-700°C. However, the reaction rate measured at 800°C was found to deviate significantly from the value estimated from the Arrhenius plot for reaction at temperatures between 475 and 700°C. Control of the overall reaction by pore diffusion at high temperatures was postulated by Squires et al. (1971) to explain this behavior. The sulfidation experiments of Westmoreland et al. (1977) gave a linear relation between the initial reaction rate of reagent grade CaO and the H_2S concentration in the reactive mixture at temperatures in the range of 300-800°C, and this led these investigators to conclude that reaction (2.2) is of first order with respect to H_2S.

The reaction of calcined limestones in a differential fixed-bed reactor was studied by Borgwardt et al. (1984). Small amounts of solid sorbent (particles of 1-9.4 μm size) and large reactive gas flow rate were used to ensure differential operation of the reactor. Preparation of calcines under different conditions gave solid reactants covering a broad range of initial internal surface areas. The sulfur uptake was determined by chemical analysis of the solid product at different sulfidation times, and an activation energy of 31 $kcal/mol$ was computed from the reaction rates at 50% conversion. Experiments in a fixed-bed reactor were carried out by Freund (1984) who impregnated amorphous carbon particles with CaO and sulfided them at high temperatures (1120-1425 °C), where significant H_2S dissociation takes place. The rate of CaO consumption was determined from the analysis of the outlet stream of the reactor after correction for the loss of H_2S by dissociation. By assuming intraparticle mass transport control – the effectiveness factor of 115 μm particles was estimated to be about 0.002 – and first-order reaction, an estimate of 45.5 $kcal/mol$ was obtained for the activation energy. Attar and Dupuis (1979) reacted minerals found in coal (calcite, dolomite, and siderite) with H_2S in a pulsed differential reactor. The reaction rate was determined from the analysis of the outlet gaseous stream, and an activation energy of 37 $kcal/mol$ was estimated in the temperature range 560-670 °C for the calcite-H_2S reaction. A much lower activation energy (4 $kcal/mol$) was observed at higher temperatures, and this was attributed to mass transfer limitations in their apparatus.

In most of the above experimental studies, the experimental data were interpreted by considering that the rate of reaction was controlled by intrinsic kinetics or one of the transport mechanisms of the gaseous reactant and by assuming that negligible structural

changes occurred in the solid during the reaction. Variants of the shrinking-core and grain models (Szekely et al., 1976) were used in most cases to analyze the experimental data (e.g., Yang and Chen (1979), Borgwardt et al. (1984), and Squires et al. (1971)) for the extreme cases of local reactivity (intrinsic kinetics and (or) product layer diffusion) and intraparticle mass transport control, respectively. However, highly porous sorbent particles result from limestone or dolomite calcination, and as a result, the overall rate of sulfidation reaction is in general influenced by both the transport and reaction details in the intraparticle space. Moreover, since the solid product (CaS) in reaction (2.2) has larger molar volume than the solid reactant (CaO), various phenomena associated with pore structure evolution (such as pore plugging and formation of inaccessible pore space) may play an important role in determining the evolution of the reactivity of the solid with the progress of its sulfidation.

Gas-solid reactions with solid product were modelled by Yu and Sotirchos (1987) in the so-called generalized random pore model. This model represents the void volume in the solid using pore segments randomly distributed in space around the bonds of a three-dimensional lattice and predicts the evolution of the reactivity of the solid as well as of its pore structure with the progress of the reaction. The generalized random pore model was applied by Zarkanitis et al. (1990) and Sotirchos and Zarkanitis (1992) to the sulfation of calcined limestones, where it was found to provide satisfactory approximations to the experimentally determined conversion vs. time curves over a rather broad range of operating conditions. It was also used successfully for the interpretation of reactivity evolution data for the reaction of porous zinc oxide sorbents with H_2S (Efthimiadis and Sotirchos, 1993). In both cases, it was found that depending on particle size, reaction temperature, and extent of the reaction (average solid conversion), the overall reaction rate could be controlled by intraparticle diffusion, reaction at the unreacted-reacted solid interface, diffusion in the product layer, or by a combination of these three processes.

The reaction of limestone-derived calcines with H_2S-N_2 mixtures was investigated experimentally in this study. Reactivity evolution experiments were carried out in a thermogravimetric analysis system, and the structure of the unreacted solid was characterized using gas adsorption and mercury porosimetry. Calcines prepared from the calcination of precursors of high (>95%) calcium carbonate content were used in our experiments.

Calcination was carried out at 750 or 850°C, while the produced material was sulfided at 650 or 750°C. We chose to work with these precursors and the above calcination temperatures because the behavior of these calcines during sulfation was investigated in detail by Zarkanitis and Sotirchos (1989), Zarkanitis (1991), and Sotirchos and Zarkanitis (1992). The sulfidation and sulfation of CaO solids are gas-solid reactions with solid product formation involving the same solid reactant but different solid products. Their most important difference is that the solid formed during sulfation ($CaSO_4$) occupies considerably more volume than that formed during sulfidation (CaS). The solid product to solid reactant volume ratio is the parameter that has the strongest effect on the predictions of the mathematical models for gas-solid reactions with solid product. Therefore, comparison of the reactivity evolution results of the same sorbents during sulfation and sulfidation can provide information on the effects of pore structure than cannot be obtained by changing any of the other parameters of the process.

2.2. Materials and Procedures

The solid sorbents used for sulfidation were obtained through the decomposition of two high purity calcitic limestones, a limestone supplied by Greer Limestone Co. and a marble supplied by Georgia Marble Co., and calcitic single crystals (Iceland spar) supplied by Wards Inc. The Greer limestone (GL) and the Georgia marble (GM) samples were provided in the form of about 5 mm fragments, while the Iceland spar (IS) came in the form of large crystals of a few cm in size. The precursors were crushed into particles and sieved to isolate the following ranges of particle sizes: 53-62, 88-105, 210-250, and 297-350 μm. The carbonate content of the stones (magnesium and calcium) is summarized in Table 2.1, while a detailed compositional analysis of the three samples is given elsewhere (Zarkanitis, 1991). It is seen from Table 2.1 that all samples contain more than 95% $CaCO_3$, with the Iceland spar consisting almost entirely of $CaCO_3$ and the Georgia marble exhibiting the highest $MgCO_3$ content. Mineralogical analysis of the solids showed that Greer limestone consisted mainly of fine calcitic grains, while the structure of Georgia marble was spanned by much larger calcitic grains (Zarkanitis, 1991).

Precursor	GL	GM	IS
% $CaCO_3$	97.84	95.19	99.14
% $MgCO_3$	0.95	3.04	0.35

Table 2.1: Carbonate content of the precursors. GL=Greer limestone, GM=Georgia marble, and IS=Iceland spar.

The pore structure of the solids was characterized by mercury porosimetry using a Micromeritcs porosimeter and gas adsorption (N_2 in 77 K) using a flow-type apparatus. The mercury porosimetry results for the precursors showed little mercury penetration, and this only at very high pressures. Since mercury penetration is plagued by several uncertainties at high pressures, mainly because of mercury and sample compressibility, we did not think that it was possible to reach reliable quantitative conclusions about the porosity of the precursors from the mercury intrusion data. The BET analysis of the nitrogen adsorption data showed that all samples had significantly larger surface area than that corresponding to nonporous spheres of diameter equal to the arithmetic mean of the two limits of the particle size range. Moreover, application of the capillary condensation theory to the isotherm data revealed that the precursors possessed some natural porosity, which increased in the direction Greer limestone → Georgia marble → Iceland spar, that is, in the direction of increasing grain size. Almost the same average pore radius was computed from the surface area and the pore volume data of the three precursor solids. More results on the characterization of the precursor are given by Efthimiadis (1991).

Mercury porosimetry and gas adsorption measurements were also carried out for the calcined samples. The relatively large samples needed for the structural analysis were prepared in a fluidized-bed reactor under reaction conditions identical to those employed to study reactivity evolution. About 4 g of each sample (710-850 μm particles) was placed in a 1.5 cm I.D. quartz reactor. The reactor was brought to the calcination temperature under CO_2 to prevent decomposition of the solid. Decomposition was started by replacing the CO_2 with N_2 flowing at 2 l/min (at standard conditions). The BET surface area of the calcined sorbents ranged from 30 to 80 m^2/g and increased in the direction

Greer limestone → Georgia marble → Iceland spar, with the calcines produced at $850°C$ exhibiting lower surface areas. In general, the results obtained from our pore structure characterization experiments were similar, both qualitatively and quantitatively, to those obtained by Zarkanitis (1991) even though he used samples prepared in small batches in a fixed-bed reactor and smaller particles (88-105 μm in size). Nevertheless, in order to make our sulfidation results directly comparable with those of Zarkanitis (1991) for the sulfation of the same sorbents, it was decided to use the pore size distributions reported in his study for the analysis of our sulfidation data using the mathematical model of Yu and Sotirchos (1987).

The porosity distribution curves that were determined for the six samples (three precursors at two calcination temperatures) from the mercury porosimetry results, by assuming a perfectly interconnected network of cylindrical pores, are shown in Fig. 2.1 ($750°C$) and Fig. 2.2 ($850°C$). If no change in the particle dimensions takes place during calcination, the porosity of the resulting calcines should be about 54%, without accounting for the natural porosity of the precursors. As the curves of Figs. 2.1 and 2.2 show, the measured total porosities were indeed around this value. For both calcination temperatures, the most probable pore radius of the Greer limestone calcine – the point where there is a sharp rise in the intrusion volume – is larger than those of the other two samples. The porosity distribution curves of Figs. 2.1 and 2.2 were estimated from the mercury porosimetry data using the skeletal density based on the chemical analysis of the oxides. This value was found to agree with that measured experimentally by N_2 pycnometry.

Particles of 53-62, 88-105, 210-250, and 297-350 μm were calcined, and subsequently sulfided in a thermogravimetric analysis system. The samples (3-5 mg) of the precursor solids were placed on a circular quartz pan, hang from the sample arm of the microbalance, and were outgassed under CO_2 during the heating period to prevent thermal dissociation of the carbonates. Calcination was carried out isothermally at 750 or $850°C$ by sending N_2 through the system. The reactor was then brought to the sulfidation temperature (same as the calcination or lower) and the calcined samples were sulfided using a mixture of H_2S and N_2 flowing at 200 ml/min (standard conditions). The percentage of H_2S consumed during the initial stages of the reaction was estimated by performing a mass balance on the

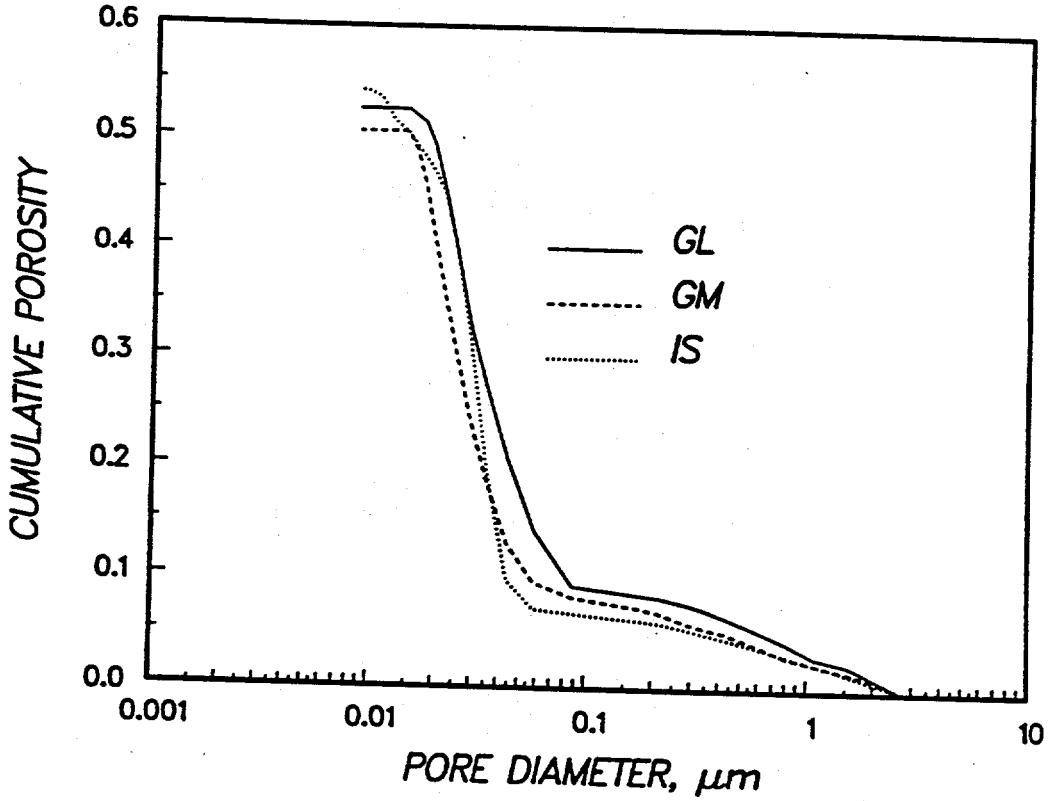

Figure 2.1: Pore size distributions of calcines produced at $750^{o}C$.

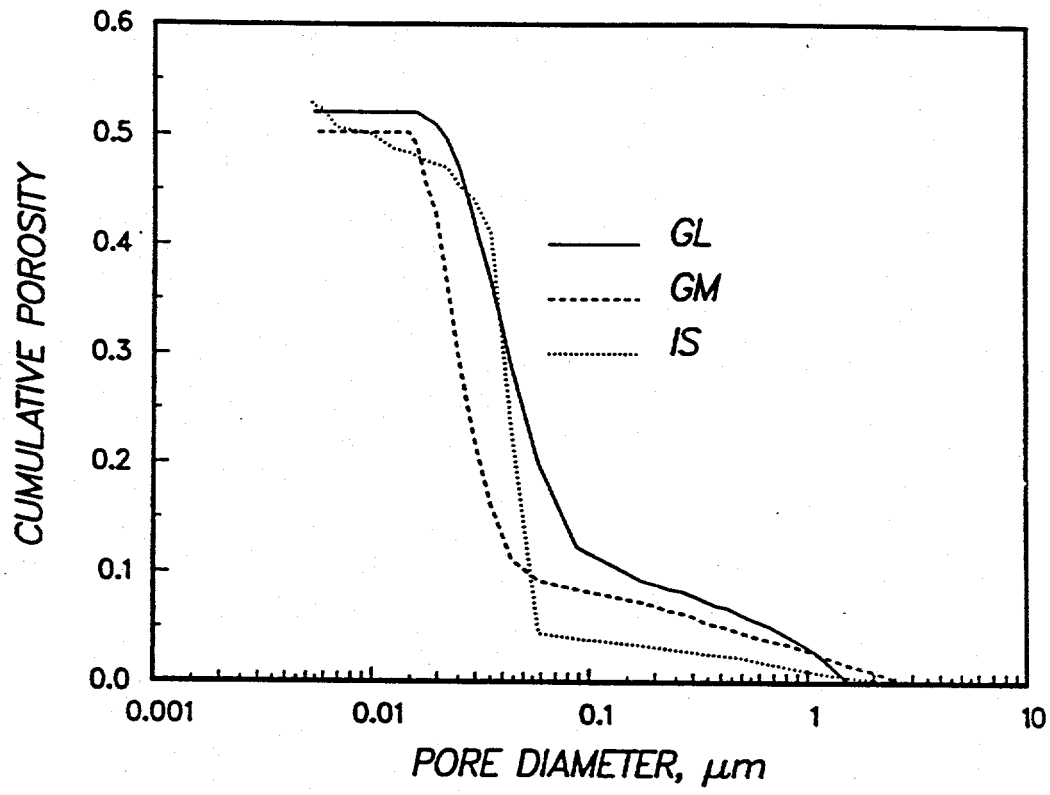

Figure 2.2: Pore size distributions of calcines produced at $850°C$.

H_2S entering and leaving the reactor, and it was found to be less than 10% for all cases studied. In view of this result, the operation of the reactor was assumed to be differential, and the measured weight gain vs. time data were converted to conversion vs. time curves by attributing the observed weight change to transformation of CaO to CaS.

2.3. Calcination Experiments

The decomposition of calcium carbonate produces a porous oxide whose physical properties depend on the calcination conditions and the morphology of the precursor stone. Experimental studies have shown that parameters influencing the final product of the calcination reaction are the sample size, the calcination temperature, the heating rate (for nonisothermal calcination), and the sweep gas flow rate and composition. For instance, experiments in TGA reactors showed that the decomposition rate of particles of 20-44 μm depended on the sample size (Gallagher and Johnson, 1973) and the composition of the reactive mixture (Caldwell et al., 1977). Caldwell et al. (1977) calcined 4 mg of 20-44 μm particles under flow of gases of different thermal conductivity. Higher reaction rates were measured when the thermal conductivity of the reactive gas increased, implying effects of heat transfer limitations. No effects of sample size and of the thermal conductivity of the sweep gas were observed by Borgwardt (1985), who had samples of 7-50 mg dispersed in a differential packed-bed reactor and calcined under flow of inert gases with velocities of the order of 9 m/s (24-44 l/min). Calcination conditions like the above cannot be applied in TGA systems, and thus it is possible that mass and heat transfer limitations may compete with the intrinsic kinetics of the $CaCO_3$ decomposition in such reactors.

The calcination conditions of this study were similar to those used in the preparation of the solids for the sulfation experiments of Zarkanitis and Sotirchos (1989) and Sotirchos and Zarkanitis (1992). The particle size effect on the experimental results is shown in Fig. 2.3 for the Iceland spar sample calcined at $750°C$. Qualitatively similar results were obtained for the other two solids. The calcination rates of the three solids are compared in Fig. 2.4 for calcination of three particle sizes at $750°C$ and Fig. 2.5 for calcination of two particles sizes at $850°C$. The calcination data are presented in Figs. 2.3-2.5 as the evolution with time of the ratio of the weight of the calcined material to the initial sample weight.

The horizontal line in Figs. 2.3-2.5 corresponds to the ratio of the molecular weight of CaO to that of $CaCO_3$. At the completion of calcination, the weight ratio vs. time curves should coincide with this line if the precursor rocks consisted of 100% $CaCO_3$. It can be easily verified that the final weight ratios reached by the various samples of Figs. 2.3-2.5 are in good agreement with the values expected on the basis of the carbonate content of the precursor stones (see Table 2.1).

The results of Figs. 2.3-2.5, and especially those shown in Fig. 2.3, clearly show that there is strong particle size effect on the calcination rate in all cases, implying strong mass, and possibly heat, transfer limitations in the interior of the calcining particles. Significant differences exist among the calcination rates of same size particles of different sorbents. The calcination rate of Iceland spar is influenced more strongly by the particle size than the rates of the other two samples. As a result, even though there are not very large differences in the calcination rates of small (53-62 μm) particles, much larger reaction times are required for complete calcination of Iceland spar samples of large particle size (Figs. 2.4 and 2.5). The Greer limestone sample was found to exhibit higher calcination rate for all particle sizes but the largest one, while exactly the opposite behavior was demonstrated by the Georgia marble sample. If we assume that the calcination rates of the three sorbents are mostly controlled by intraparticle mass transport, the obtained results for the 53-62, 210-250, and 297-350 μm particles (see Fig. 2.4) point to the conclusion that the intraparticle mass transport resistance increases in the direction of increasing grain size in the precursors, that is, in the order Greer limestone $\rightarrow$ Georgia marble $\rightarrow$ Iceland spar. Zarkanitis (1991) explained this phenomenon by arguing that pores formed during calcination at the periphery of the grains are larger and better interconnected than those formed in the interior of the crystallites. This, however, does not offer an explanation as to why the large (297-350 μm) Georgia marble particles present higher calcination rates than the other samples.

Georgia marble samples of large particle size (larger than 200 μm) behaved differently during heating under 1 atm of CO_2 to the reaction temperature. Unless very low rates of heating (temperature rise) were employed, the large Georgia marble particles tended to explode, thus leading to loss of solid material from the pan and, as a result, abortion

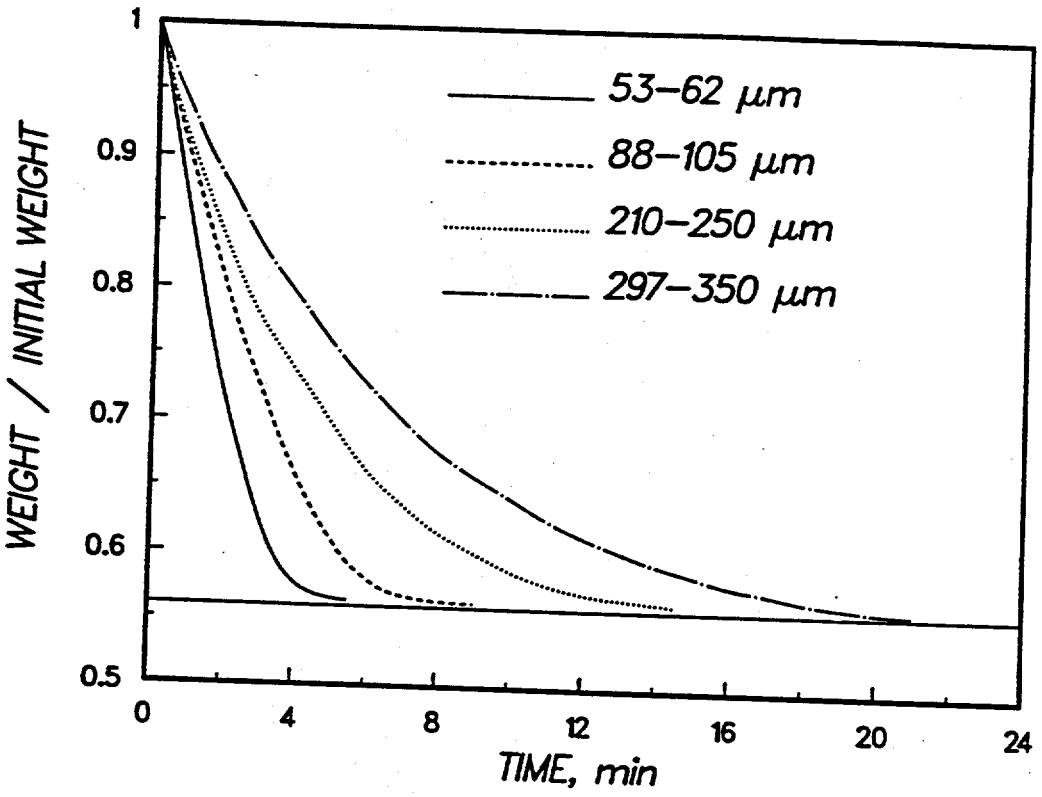

Figure 2.3: Particle size effect on rate of calcination of Iceland spar at $750°C$.

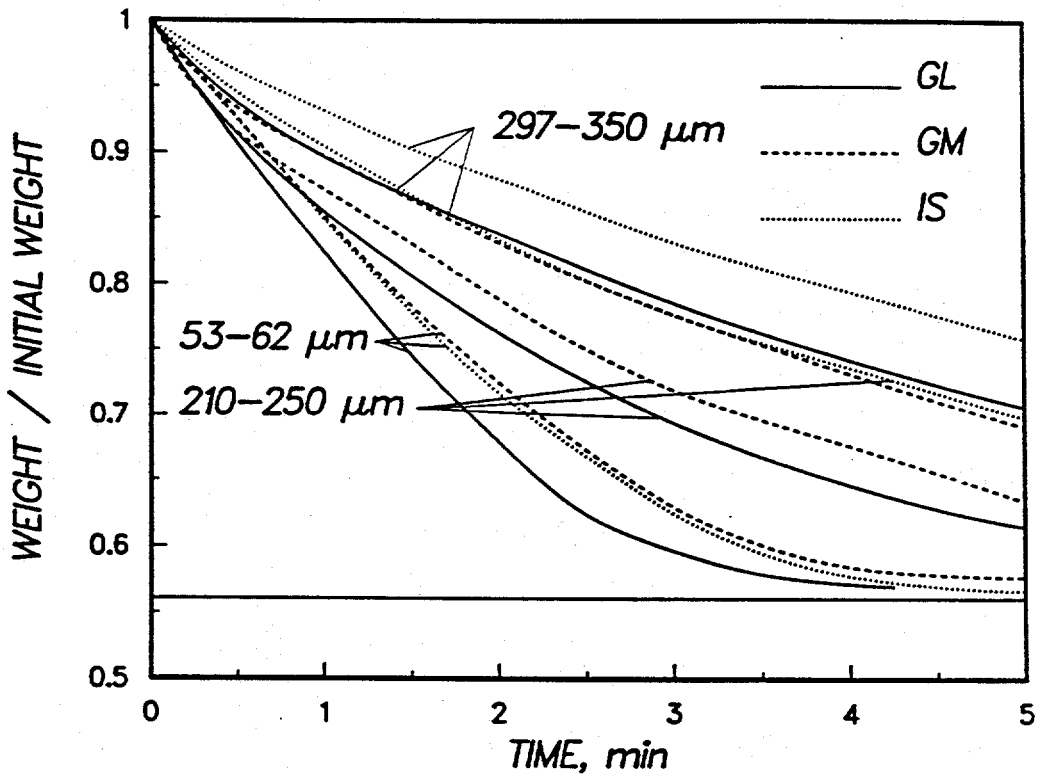

Figure 2.4: Comparison of the calcination rates of the three solids at $750°C$.

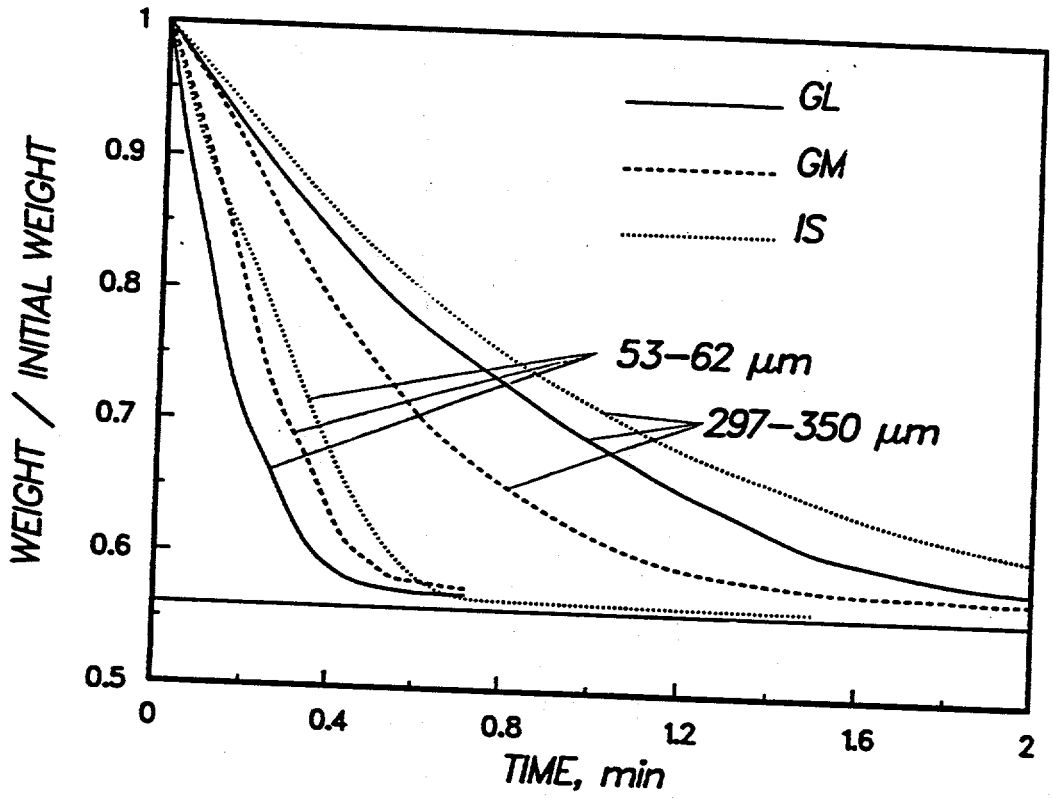

Figure 2.5: Comparison of the calcination rates of the three solids at $850°C$.

of the experiment. This phenomenon occurs at temperatures above 500-600°C and is most probably caused by the decomposition of the magnesium carbonate contained in the Georgia marble sample and the resulting pressure build-up in the interior of the particles as the released CO_2 is trying to escape through the low porosity matrix. Such behavior was also observed by Hasler et al. (1984) for some of the samples they studied, and the term 'popcorn' effect was used to describe it. We thus believe that the apparently weak effect of particle size on the calcination of Georgia marble samples is caused by the existence of cracks in the interior of the larger particles, formed during heating of the precursor particles under CO_2. It should be pointed out even when explosion of the heated particles is avoided by using low heating rates – as it was done in our experiments – it is still possible the pressure build-up in the interior of the particles to lead to formation of cracks in uncalcined particles. We will discuss the behavior of the large Georgia marble particles in more detail in the next two sections.

2.4. Sulfidation Experiments

It is usually assumed in sulfidation studies that reaction (2.2) is irreversible. We examined the validity of this assumption by estimating the equilibrium constant of reaction (2.2) at the sulfidation temperatures employed in our study (650 and 750°C) using thermodynamic data from Barin and Knacke (1973). The equilibrium H_2S concentrations at the reaction conditions of this study (10,500 *ppm* H_2S in nitrogen) was found to be 2.5 and 5.6 *ppm* at 650 and 750°C, respectively, thus indicating that the above assumption can be considered valid for all practical purposes. Comparative thermodynamic calculations for the sulfidation of twelve metal oxides were performed by Furimsky and Yumura (1986), who found that CaO had the second largest equilibrium constant (after ZnO) in a wide temperature range. Moreover, they concluded that in a reducing atmosphere CaO is the most resistant to reduction among the twelve metal oxides examined. It can thus be argued that efficient and satisfactory removal of hydrogen sulfide from a hot coal gas stream can be achieved using CaO-based sorbents.

All results presented and discussed in this study were obtained using a reaction mixture of 1.05% H_2S in nitrogen. We examined the concentration dependence of the

sulfidation rates of the solids used in our study by carrying out experiments with lower concentrations of H_2S. A linear relationship was fo· :d to exist between the initial rate of sulfidation and the concentration of H_2S. Moreover, the reactivity evolution curves for different concentrations but with all the other conditions being the same were found to practically coincide with each other when plotted as conversion vs. normalized time, with the latter defined as (real time) $\times$ (H_2S percentage in the reactive mixture). On the basis of these two findings it was concluded that the reaction of CaO with H_2S is of first order with respect to the concentration of H_2S. A similar conclusion was reached from our reactivity evolution studies during sulfidation of ZnO-based sorbents (Efthimiadis and Sotirchos, 1993).

Figs. 2.6, 2.7, and 2.8 present reactivity evolution data, in the form of conversion vs. time curves, for the sulfidation at $750°C$ of calcines produced at the same temperature for Greer limestone, Georgia marble, and Iceland spar, respectively, for four particle sizes. Shown in the figures are also the conversion vs. time curves measured for the sulfation of the same sorbents at $750°C$ by Sotirchos and Zarkanitis (1992) using a mixture of 3,000 ppm SO_2 and 12% O_2 in N_2. A general observation from the experimental sulfidation data of Figs. 2.6-2.8 is that there is a strong influence of particle size on the overall rate of the CaO-H_2S reaction, indicating that the process occurs under strong intraparticle diffusional limitations. Consequently, it is necessary to use a model for mass transport and reaction in the interior of the porous particles to analyze the obtained conversion vs. time data.

Comparison of the sulfidation data of Figs. 2.6-2.8 with the corresponding sulfation results shows that while the sulfidation reaction always reaches complete conversion, the sulfation reaction stops before complete conversion is reached. Moreover, the maximum conversion reached during sulfation decreases drastically with increasing particle size. This difference in the behavior of the two reactions is caused by the fact that the molar volume of the solid product formed during sulfidation (CaS) is smaller (by a factor of two) than that of $CaSO_4$ produced during sulfation of CaO. Assuming that the physical dimensions of a particle do not change during reaction, a mass balance on the volume of the solid phase gives the following relation between the maximum conversion that can be attained

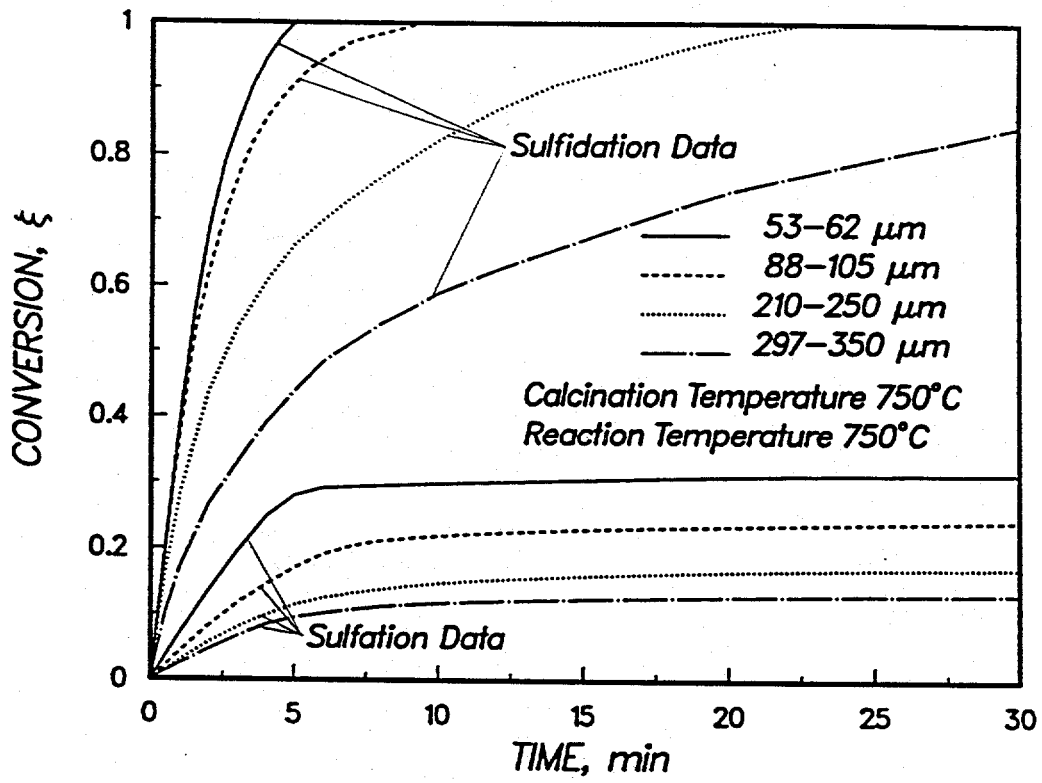

Figure 2.6: Effect of particle size on the conversion vs. time results during sulfidation at $750°C$ of Greer limestone calcines produced at the same temperature. The sulfation data shown were obtained by Zarkanitis (1990) at the same temperature with 0.3% SO_2 and 12% O_2 in N_2.

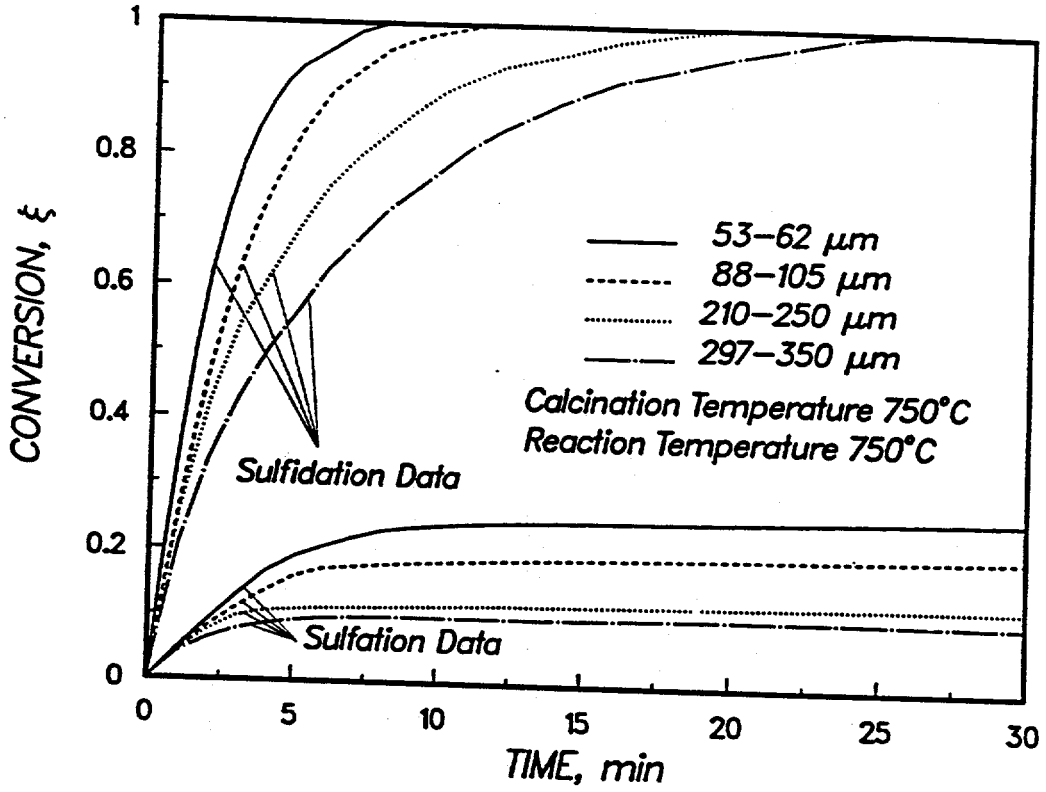

Figure 2.7: Effect of particle size on the conversion vs. time results during sulfidation at $750°C$ of Georgia marble calcines produced at the same temperature. The sulfation data shown were obtained by Zarkanitis (1990) at the same temperature with 0.3% SO_2 and 12% O_2 in N_2.

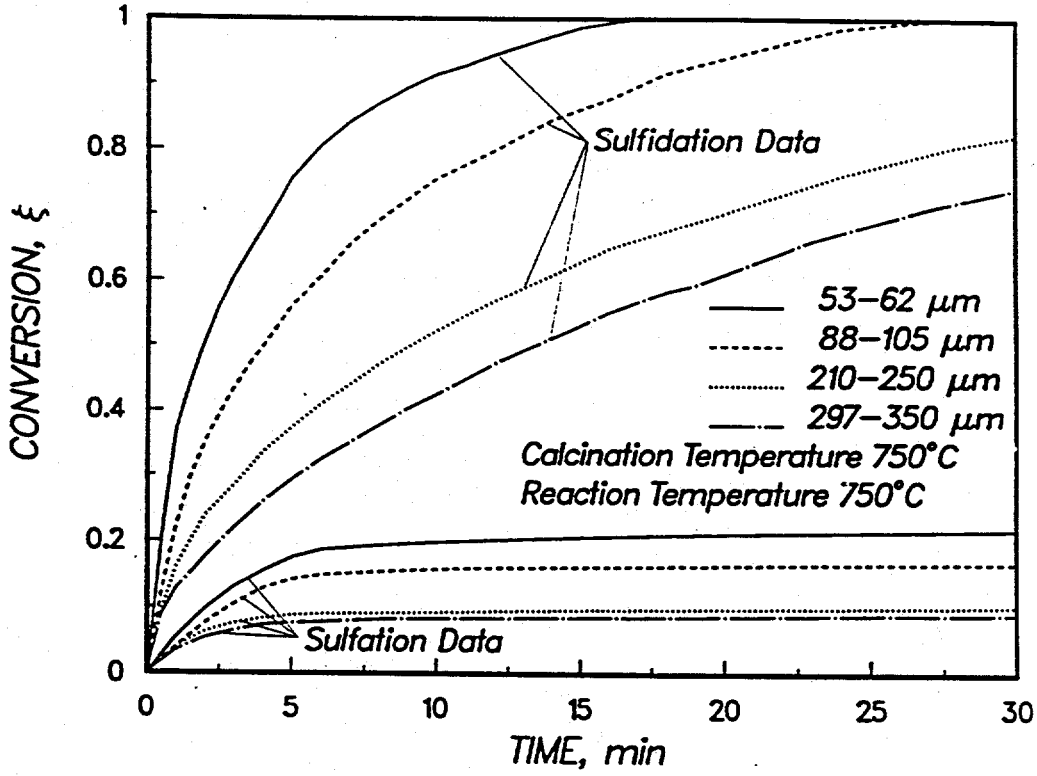

Figure 2.8: Effect of particle size on the conversion vs. time results during sulfidation at $750°C$ of Iceland spar calcines produced at the same temperature. The sulfation data shown were obtained by Zarkanitis (1990) at the same temperature with 0.3% SO_2 and 12% O_2 in N_2.

before the interior of the porous sorbent is completely filled with the solid product, ξ_{max}, and the initial porosity of the solid, ε_0:

$$\xi_{max} = \frac{\varepsilon_0}{(1-\varepsilon_0)(Z-1)} \tag{2.3}$$

Z is the stoichiometric volume ratio of the gas-solid reaction, defined as volume of reacted solid phase per unit volume of a stoichiometrically equivalent amount of unreacted solid phase. For a pure sorbent (100% CaO), Z is equal to the ratio of the molar volume of CaS or $CaSO_4$ to that of CaO. In the presence of impurities, Z may be estimated using the equation:

$$Z = \psi \frac{v_{CaSorCaSO_4}}{v_{CaO}} + (1-\psi) \tag{2.4}$$

ψ is the volume fraction of CaO in the unreacted calcine, and v_i is the molar volume of solid i. The stoichiometric volume ratios for the calcines used in our experiments are shown in Table 2.2 which also lists the volume of the solid phase of the unreacted calcines per mole of CaO ('molar' volume, $v_s = v_{CaO}/\psi$). Introducing the Z values of Table 2.2 in eq. (2.3), we find that porosities lower than about 0.67 lead to incomplete conversion during sulfation, while the corresponding porosity limit for sulfidation is about 0.33. On the other hand, for an initial porosity of 0.5, as it is approximately the case with all the solids used in this study (see Figs. 2.1 and 2.2), eq. (2.3) predicts complete conversion for sulfidation with 0.25 final porosity ($\xi = (\varepsilon_0 - \varepsilon)/[(1-\varepsilon_0)(Z-1)]$) but about 50% maximum conversion for sulfation. The sulfation conversions reached in Figs. 2.6-2.8 are much lower than 50% since the presence of in aparticle mass transport limitations causes the pore openings at the external surface of the particles to be plugged first. The maximum conversion may also be limited by inaccessible pore volume formation, a situation occurring when small feeder pores of a cluster of large pores are filled with solid product.

The conversion vs. time results of Figs. 2.6-2.8 reveal that the sulfation reactivity of the CaO sorbents and the maximum conversion they reach decrease significantly in the order Greer limestone → Georgia marble → Iceland spar, that is, with increasing grain size in the precursors. Since there are no significant qualitative differences in the pore size distributions of the calcines (see Fig. 2.1) to justify the differences seen in the sulfation reactivities, Sotirchos and Zarkanitis (1992) concluded that decreasing grain size in the

precursor leads to a better interconnected pore structure in the calcine and, hence, lower intraparticle diffusion resistance and smaller inaccessible pore space. This explanation is in agreement with the observed sulfidation behavior of the Greer limestone and Iceland spar samples, as it can be seen from the results of Figs. 2.9-2.11 which compare the sulfidation results of the three sorbents at the various combinations of calcination and sulfidation temperature employed in our experiments. It also applies to the small particles of the Georgia marble calcines (53-62 and 88-105 μm), which in general exhibited reactivity intermediate to that of the other two sorbents, but it is in obvious contradiction with the behavior of the large particles (210-250 and 297-350 μm), which showed much larger reactivities than same particle sizes of the other sorbents.

Precursor	GL	GM	IS
Z for sulfidation	1.508	1.492	1.522
Z for sulfation (MgO treated as inert)	3.015	2.952	3.070
v_s of the unreacted solid phase, $cm^3/gmol$	18.1	17.5	17.1

Table 2.2: Stoichiometric volume ratio (Z) and 'molar' volume (v_s) of the unreacted solids used in the application of the generalized random pore model. GL=Greer limestone, GM=Georgia marble, and IS=Iceland spar.

The behavior of the Georgia marble samples during sulfidation in relation to the behavior of the other sorbents, is strikingly similar to their behavior during calcination (Fig. 2.4 and 2.5), where it was seen that the Georgia marble sample exhibited higher overall reactivity for the large particle size (297-350 μm) even though its reactivity for smaller particles was lower than or between those of the other solids. This observation points out to the conclusion that the apparently weak effect of particle size on the sulfidation of Georgia marble samples is caused by the existence of large pores in the interior of the larger particles, formed from the cracks in the heat-treated precursors. These pores facilitate transport of the reactive gas (H_2S) in the interior of the calcine, thus reducing the effective size of the particle. The presence of cracks (large pores) in the interior of the Georgia marble calcines does not have an effect of the same magnitude on their sulfation

behavior since sulfation leads to complete pore plugging, and as a result, even these large pores are eventually filled with solid product. The peculiar behavior of the Georgia marble calcines will be discussed in some more detail in the next section of our paper.

Comparison of the conversion vs. time curves of Fig. 2.9 with the respective results shown in Fig. 2.11 suggests that calcination at higher temperatures yields sorbents of higher overall reactivity. Similar conclusions were reached by Zarkanitis and Sotirchos (1989) and Sotirchos and Zarkanitis (1992) from the study of the sulfation of the same sorbents. The theoretical analysis of the sulfation data of Zarkanitis and Sotirchos (1989) using the generalized random pore model of Yu and Sotirchos (1987) showed that the sulfation reactivity of the calcines improves with increasing calcination temperature because the connectivity (degree of interaction) of their pores increases as the calcination temperature is raised. We will reach a similar conclusion in this study from the analysis of the sulfidation data that we will carry out in the next section.

The effects of sulfidation temperature on the sulfidation reactivity of the CaO sorbent can be determined by comparing the conversion vs. time results of Fig. 2.9 with those of Fig. 2.10. It is seen that sulfidation at a lower temperature slows down the overall reaction rate, but not significantly. The initial slopes of the conversion vs. time curves in Fig. 2.10 are slightly smaller than the slopes of the corresponding curves of Fig. 2.9, indicating weak dependence of the reaction rate constants on temperature and, hence, small activation energies. The temperature effect is in general stronger for the small particles, and only the behavior of the large particles of the Iceland spar calcines is significantly influenced by the temperature. This is not unexpected since the overall reaction rate of the small particles is usually controlled by intrinsic reaction (low conversions) and diffusion in the product layer (high conversions), whose rates increase exponentially with the temperature. On the other hand, the reaction of large particles is more influenced by the rate for intraparticle diffusion, which for Knudsen diffusion – as it is most probably the case in this study – varies proportionally to the square root of the temperature. In order to be able to derive any quantitative conclusions on the effects of the above processes on the sulfidation of the sorbents, it is necessary that a mathematical model be used to analyze the experimental data. This is done in the following section.

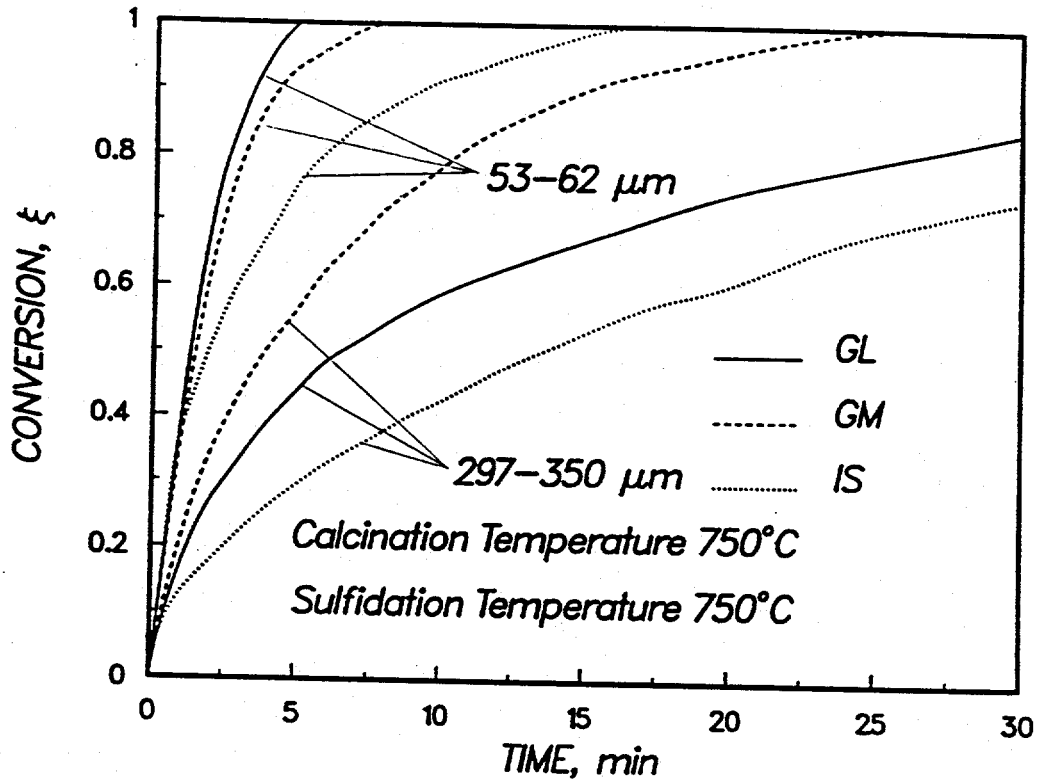

Figure 2.9: Comparison of the sulfidation rates at $750°C$ of calcines produced at the same temperature for two particle sizes.

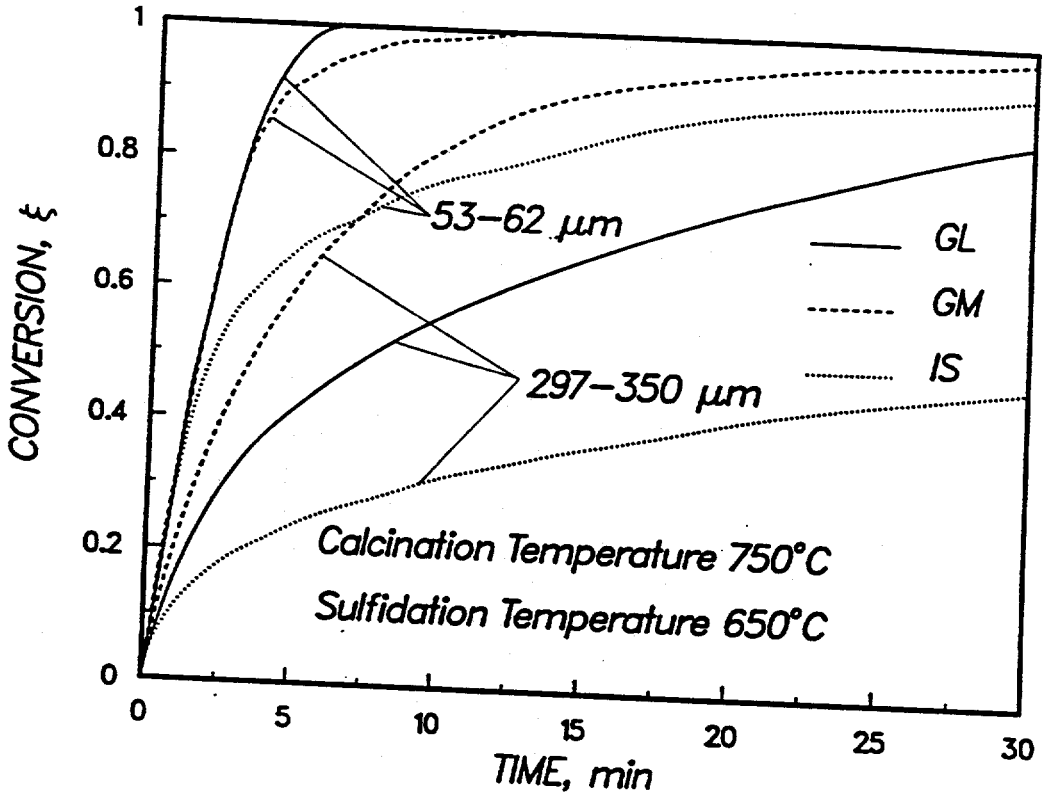

Figure 2.10: Comparison of the sulfidation rates at $650°C$ of calcines produced at $750°C$ for two particle sizes.

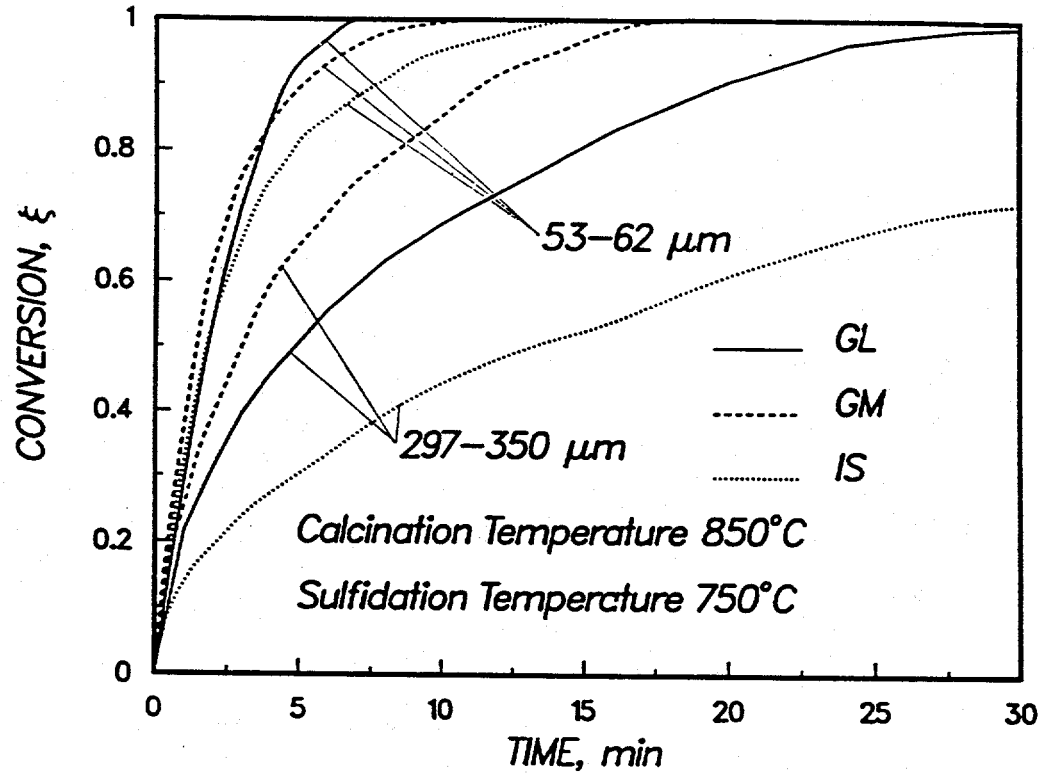

Figure 2.11: Comparison of the sulfidation rates at $750°C$ of calcines produced at $850°C$ for two particle sizes.

2.5. Experimental Results and Model Predictions

Past studies on CaO sulfidation, employed particles of a few μm in size (Yang and Chen, 1979; Borgwardt et al., 1984) or large pellets (Squires et al., 1971) in order to eliminate the effects of intraparticle diffusional limitations or make the diffusion the controlling step of the process. However, the need for a controlling step in the interpretation of the experimental data can be avoided by analyzing the experimental data using a mathematical model developed by Yu and Sotirchos (1987), which accounts not only for reaction and diffusion of the reactive gaseous species but also for the evolution of the internal pore structure of the solid with the progress of the reaction. The model represents the void space using a network of cylindrical capillaries arranged around the bonds (with the bonds serving as axes) of a three-dimensional lattice. The reactive gas diffuses through the product layer and reacts with the solid at a sharp interface between reacted and unreacted solid. The effective diffusivity in the porous medium is computed using the effective medium theory-smooth field approximation approach developed by Burganos and Sotirchos (1987), which is consistent with the network structure assumed in the structural model. Readers interested in the equations and the details of the model are advised to consult the papers of Yu and Sotirchos (1987) and Zarkanitis et al. (1990).

For the application of the generalized random pore model to our sulfidation data, the only parameters are the diffusion coefficient in the product layer, D_P, and the topology of the network. The topology of the network is determined by a three-dimensional lattice formed by the axes of the pore segments. Like in past applications of the generalized random pore model, the topology of the lattice will be assumed to be that of a Bethe lattice (Fisher and Essam, 1961). Bethe lattices are tree-like structures, whose characteristics are completely defined by their coordination number, z, that is, the number of bonds (pore segments) per node. D_P and z are determined by fitting the experimental data to the model predictions under the conditions that D_P depend only on sorbent and sulfidation temperature and z depend only on sorbent. Obviously, since the topology of the initial structure of the solid is independent of the reaction that the solid undergoes, z should, in principle, be the same both for sulfidation and sulfation reactions. All other parameters are estimated using the experimental data.

The mass transfer coefficient was estimated from correlations for mass transfer during flow past spherical objects (Bird et al., 1960). Using these correlations, it was found that the Sherwood number was equal to 2 (based on diameter) and practically independent of particle size. The reaction rate constant was estimated from the initial reaction rates of 53-62 μm particles after correcting them for the effects of intraparticle diffusion using the expression for the effectiveness factor of a first-order reaction (Smith, 1981). Negligible H_2S dissociation was assumed to occur at the temperatures used for sulfidation. Thermodynamic calculations showed that even if the reaction reached equilibrium in the reactor, less than 5.2% of H_2S would dissociate at 750^oC.

The coordination numbers, product layer diffusivities, and reaction rate constants that had to be used in the mathematical model to reproduce the reactivity evolution data are shown in Table 2.3. The reaction rate constants of Table 2.3 were obtained using the initial reaction rates of 53-62 μm particles. At least four independent measurements of the initial reaction rate were used to arrive at an average value for the initial reaction rate for each set of operating conditions. Since the calcination temperature affects only the physical structure of the resulting product, calcines produced from the same sorbent at different temperatures were assumed to have the same reaction rate constant. Notice that for the Georgia marble sample, parameter values are shown for two coordination numbers at each temperature. We will explain the use of two coordination numbers later during the discussion of the model predictions for sulfidation of this solid.

It is seen from the results of Table 2.3 that the differences among the intrinsic reaction rate constants of the three sorbents are very small. This is not an unexpected result since the initial reaction rates of the three sorbents are comparable (see Figs. 2.9-2.11) and their pore size distributions are not much different from each other (see Figs. 2.1 and 2.2). Relatively small differences were also found to exist between the diffusivities in the product layer. The largest product layer diffusivities was estimated for the Greer limestone calcines and the smallest for the Iceland spar samples. The activation energies that are determined from the results of Table 2.3 if k_s and D_P are assumed to obey an Arrhenius-type equation are given in Table 2.4. The activation energies of Table 2.4 should be used with some caution since only two temperatures were used for their estimation. Similar

values of reaction rate constant, solid product layer diffusivity, and activation energy were determined by Sotirchos and Zarkanitis (1992) for sulfation of these sorbents. For example, the intrinsic reaction rate constant for sulfidation at $750°C$ was found to have an average value of 1.5×10^{-3} cm/s, which is about 2 times smaller than the value estimated here for sulfidation.

Precursor	GL	GM	GM	IS
Coordination number, z for calcination at $750°C$	6	3	1000	3
k_s at $750°C$, cm/s	3.6×10^{-3}	3.7×10^{-3}	3.3×10^{-3}	3.8×10^{-3}
D_P at $750°C$, cm^2/s	7×10^{-8}	1×10^{-8}	1×10^{-8}	2×10^{-9}
k_s at $650°C$, cm/s	2.5×10^{-3}	2.6×10^{-3}	2.3×10^{-3}	2.7×10^{-3}
D_P at $650°C$, cm^2/s	3×10^{-8}	5×10^{-9}	5×10^{-9}	1×10^{-9}
Coordination number, z for calcination at $850°C$	12	4	4000	6.5
k_s at $750°C$, cm/s	3.6×10^{-3}	3.8×10^{-3}	3.4×10^{-3}	3.7×10^{-3}

Table 2.3: Reaction rate constants (k_s) estimated from the initial sulfidation rates of particles of 53-62 μm and diffusion coefficients in the product layer (D_P) used in the application of the generalized random pore model. GL=Greer limestone, GM=Georgia marble, and IS=Iceland spar.

Figs. 2.12 and 2.13 compare the predictions of the generalized random pore model with the experimental data for sulfidation at $750°C$ of Greer limestone calcines produced at 750 and $850°C$, respectively. Very good agreement is seen to exist between model and experiment in both figures and for all particle sizes. The model was also successful in reproducing the experimental data at $650°C$. Only the product layer diffusivity was used as free parameter to fit the model predictions to the experimental data since the coordination number was set equal to the value estimated for each calcination temperature by Sotirchos and Zarkanitis (1992) in their sulfation study. The successful use of the generalized random pore model to describe the behavior of the sulfidation reaction of the

Greer limestone calcines using parameters determined independently from the study of their sulfation behavior underscores its capacity to function as a predictive model for gas-solid reactions with solid product. The comparison of the predictions of the mathematical model with the experimental data for the Georgia marble calcines led to the conclusion that a particle size dependent coordination number had to be used to successfully reproduce the experimental data. Fig. 2.14 compares the experimental data for sulfidation at $750°C$ of Georgia marble calcines produced at the same temperature with the model predictions for two values of coordination number. A coordination number equal to 3, the value used by Sotirchos and Zarkanitis (1992) for the sulfation of the same calcines, was found to provide very good approximation to the conversion vs. time results of the 53-62 and 88-105 μm particles, but a much larger coordination number ($z = 1,000$) had to be used to reproduce the behavior displayed by the largest (297-350 μm) particles. For the calcines prepared at $850°C$, the corresponding values of coordination number were 4 and 4,000 (see Table 2.3). This result indicates that there is much smaller resistance for mass transport in the interior of the large particles since larger coordination numbers imply increased interaction of pores of different size. Indeed, as it can be seen in Table 2.5 which lists initial and final effective diffusivities predicted by the model for the Georgia marble sample, the initial effective diffusivity for $z = 1,000$ is about two times larger than the diffusivity for $z = 3$, but smaller by about the same factor than that for perfectly interconnected pores ($z = \infty$). This rather peculiar dependence of the effective diffusivity on the coordination number will be discussed in detail later.

Precursor	GL	GM	IS
Activation energy for k_s, $kcal/gmol$	6.8	6.9	6.2
Activation energy for D_P, $kcal/gmol$	16	13	13

Table 2.4: Activation energies estimated from the reaction rate constants and the diffusion coefficients of Table 2.3. GL=Greer limestone, GM=Georgia marble, and IS=Iceland spar.

Coordination number, z	3	1,000	∞
Initial diffusivity, cm^2/s	6.14×10^{-3}	13.5×10^{-3}	28.32×10^{-3}
Diffusivity ratio at $\xi = 0$, $D_e^z/D_e^{z=\infty}$	0.217	0.477	1
Final diffusivity, cm^2/s	0.57×10^{-3}	6.19×10^{-3}	21.87×10^{-3}
Diffusivity ratio at $\xi = 1$, $D_e^z/D_e^{z=\infty}$	0.026	0.283	1

Table 2.5: Initial effective diffusivities computed from the generalized random pore model for the Georgia marble for different coordination numbers. Calcination temperature=$750°C$; Sulfidation temperature=$750°C$.

The need to use very large coordination numbers to reproduce the results for Georgia marble sulfidation suggests that a pore network model, with all pores participating in the network in the same way, is not appropriate for describing the pore structure of this solid. It was argued during the presentation of the calcination and sulfidation results that the apparently lower resistance of the large Georgia marble particles for mass transport in their interior is caused by formation of cracks and possibly fragmentation into smaller pieces during heating under CO_2. We tested this explanation by carrying out the following experiment: A sample of 297-350 μm Georgia marble particles was treated under CO_2 for about 30 min. It was then cooled down to room temperature, resieved to remove the fragmented material, and used for calcination and sulfidation experiments in exactly the same manner as the fresh samples. Since decomposition of $MgCO_3$ had already taken place, no explosions were observed during heating of the treated material under CO_2. Typical results of those test experiments are shown in Fig. 2.15. The overall reactivities of calcines obtained from the treated samples were found to be systematically lower than those of calcines prepared from fresh material, indicating that particle disintegration indeed took place during treatment of the Georgia marble under CO_2. Comparison of the results of Figs. 2.14 and 2.15 reveals that the reactivity of the treated samples is still higher than that predicted by the mathematical model using the coordination number of the sulfation study (e.g., $z = 3$ for calcination at $750°C$). This is not unexpected since sieving removes the fragments but does not have any effect on cracks formed in the interior of the heated particles.

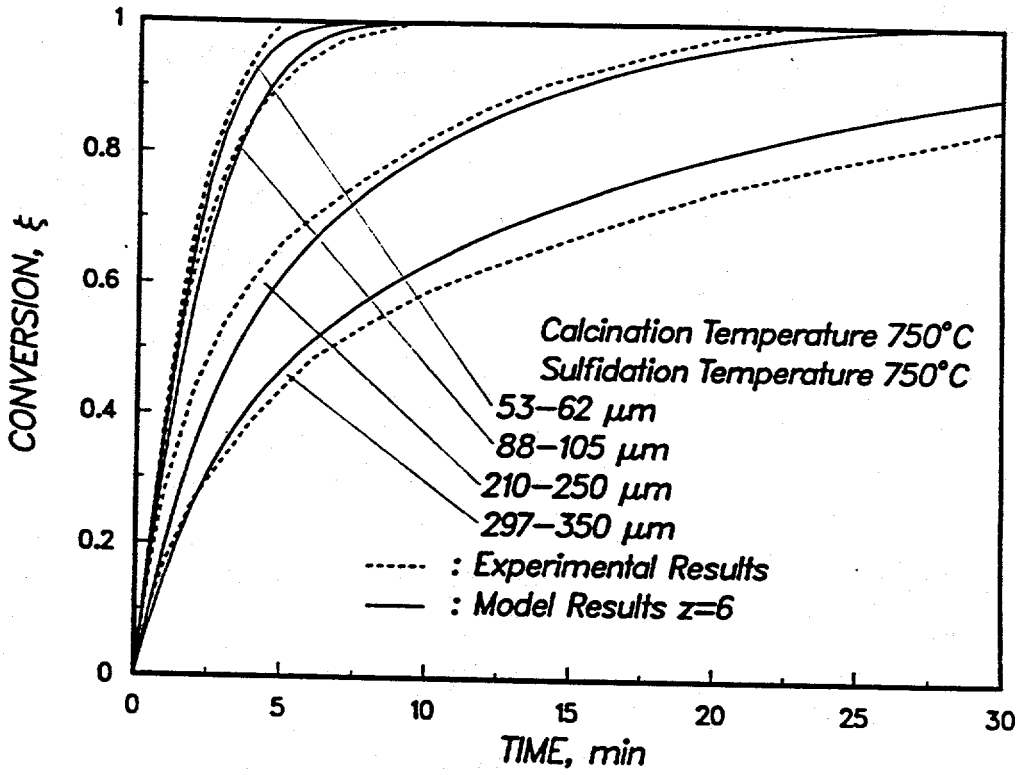

Figure 2.12: Comparison of experimental data and model predictions for sulfidation at $750°C$ of Greer limestone calcines produced at $750°C$.

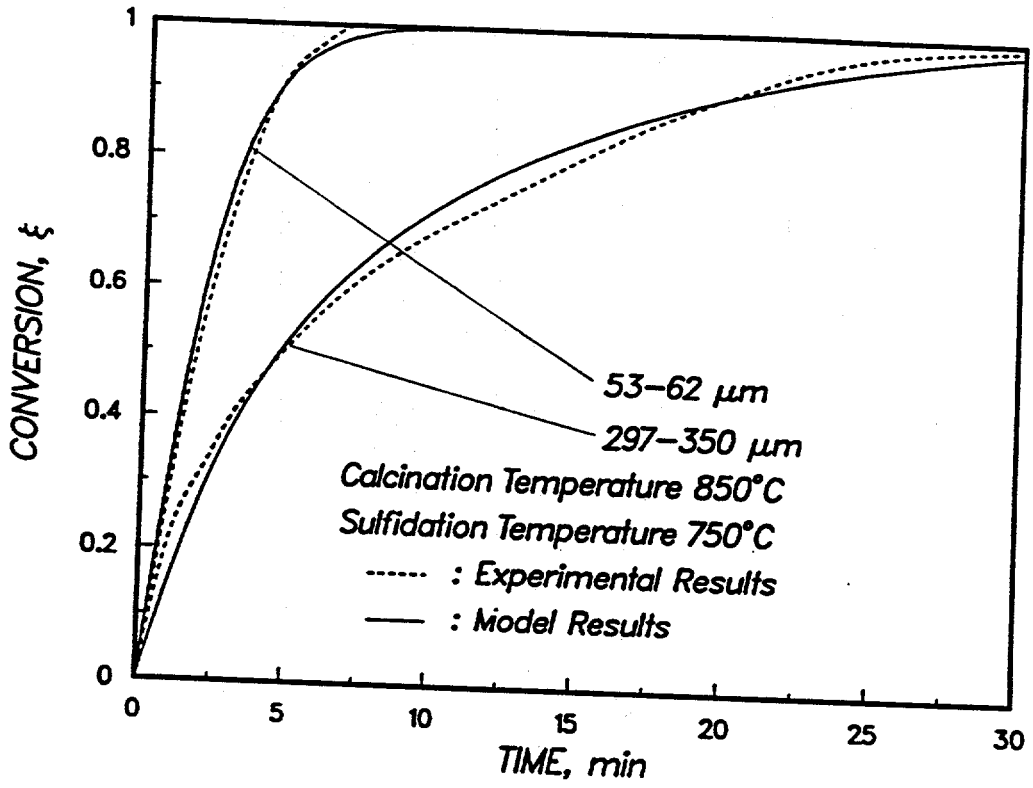

Figure 2.13: Comparison of experimental data and model predictions for sulfidation at $750°C$ of Greer limestone calcines produced at $850°C$.

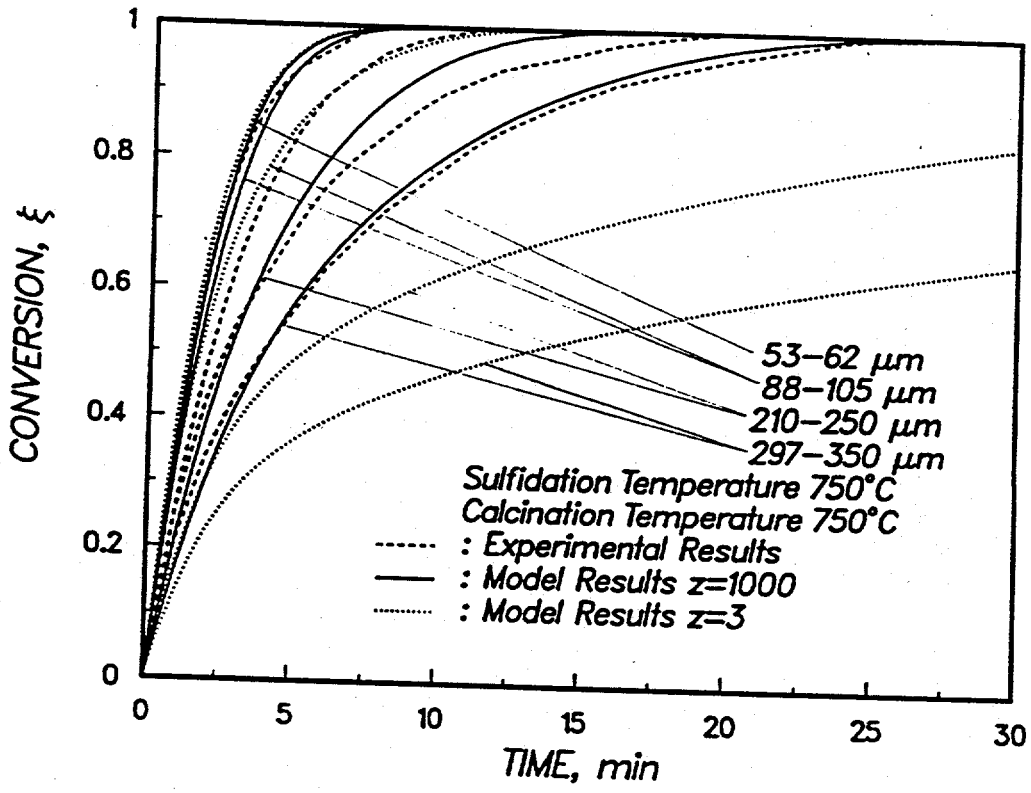

Figure 2.14: Comparison of experimental data and model predictions for sulfidation at $750°C$ of Georgia marble calcines produced at $750°C$.

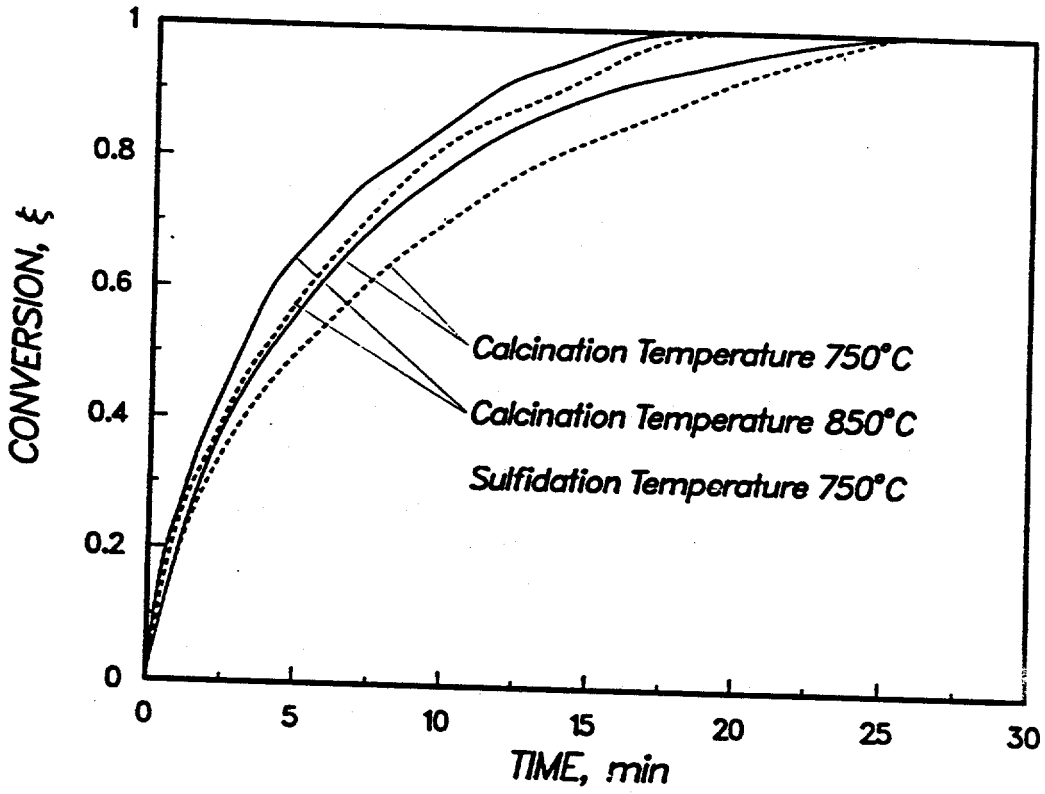

Figure 2.15: Dependence of the sulfidation rate of Georgia marble calcines produced at $750°C$ on the pretreatment of the precursor (———: fresh sorbent particles; – – –: particles heat-treated under 1 *atm* of CO_2 at the calcination temperature and resieved).

Good agreement between model and experiment was also observed for the Iceland spar experimental data when the coordination numbers estimated by Sotirchos and Zarkanitis (1992) for sulfation were used in the mathematical model. The experimental and theoretical results for sulfidation at $750°C$ of sorbents calcined at the same temperature are shown in Fig. 2.16. The mathematical model successfully reproduced the effect of particle size on the evolution of the reactivity of the Iceland spar, but it tended – as it can be seen in Fig. 2.16 – to overestimate the reaction rate at the initial stages of the reaction and underestimate it at high conversions. The pore structure of the calcined Iceland spar sample was examined by Michail et al. (1980). Crystals of 1-2 mm in thickness and 1 cm in length were calcined under vacuum in the temperature range of 580-$750°C$. The physical structure of fresh and calcined samples was analyzed using nitrogen adsorption and scanning electron microscopy. The obtained results showed that the pore structure of the calcined materials consisted primarily of slit-shaped (parallel plate) mesopores. The development of this pore structure was attributed to the decomposition of initial plate-like carbonate layers. The slow variation of the reaction rate of Iceland spar calcines with time after the initial stages of the reaction is in qualitative agreement with the findings of Michail et al. (1980) since such behavior is typical – as those with some experience in the analysis of gas-solid reaction data using pore or grain-based model know – of plate-like pores or grains.

As the results of Table 2.3 show, higher coordination numbers had to be used to reproduce the experimental data for calcines produced at $850°C$. Since the pore size distributions are shifted toward larger pores with increasing calcination temperature (compare Figs. 2.1 and 2.2), this indicates that calcination at higher temperatures leads to better interconnected pore structures. For the same calcination temperature, higher coordination numbers had to be used for the Greer limestone calcines than for the Iceland spar samples, and therefore, it can be argued that the higher reactivities of the former sample are primarily due to the higher connectivity of their pore structure. For the coordination numbers needed to reproduce the sulfidation results for the small particles and the sulfation results for all particle sizes (Sotirchos and Zarkanitis, 1992), the Georgia marble calcines exhibit pore space connectivity intermediate to that of the other two solids. This is not obvious

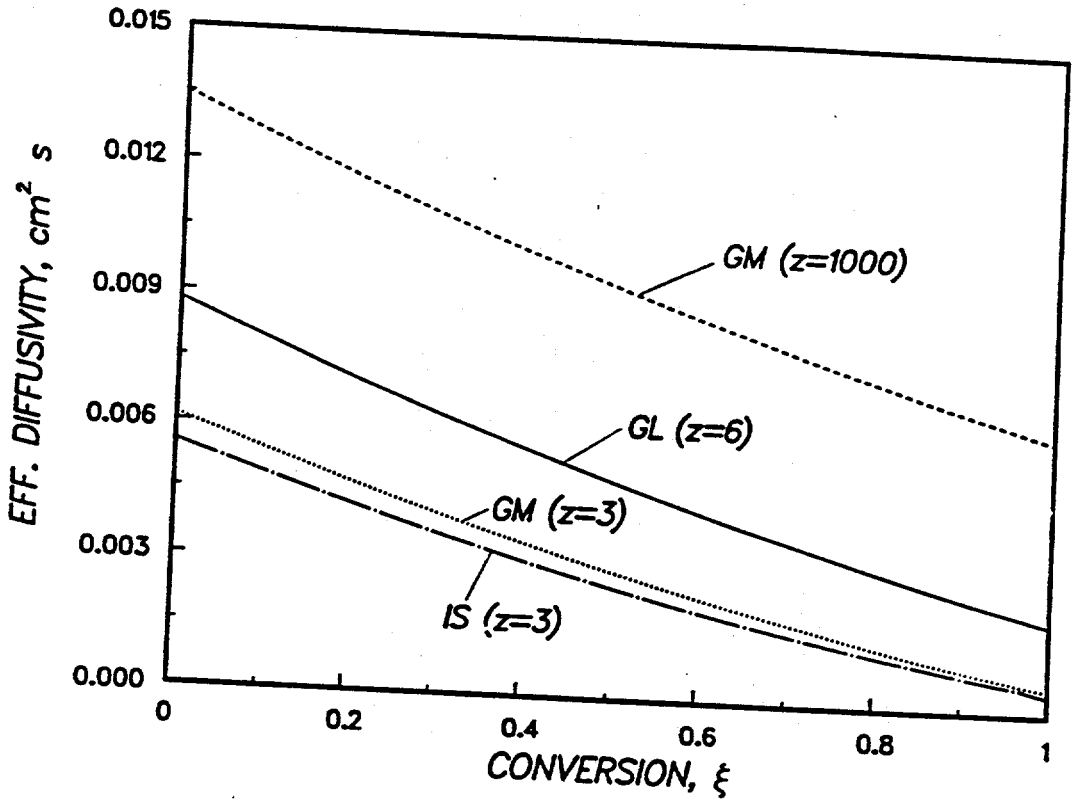

Figure 2.16: Comparison of experimental data and model predictions for sulfidation at $750°C$ of Iceland spar calcines produced at $750°C$.

from the coordination numbers of Table 2.3, since the coordination number of Iceland spar and Georgia marble are the same at $750°C$, while the latter is larger at $850°C$. However, the coordination number gives only the number-based percolation threshold ($= 1/(z-1)$), that is, the number fraction of pores that must be eliminated (blocked) in order to get an inaccessible pore structure. Thus, a better measure of the accessibility and connectivity characteristics of the pore space of a porous medium is offered by its porosity-based percolation threshold, namely the porosity of small pores that must be removed to obtain an inaccessible pore structure. The porosity threshold depends on the coordination number and the pore size distribution of the solid. A rough estimate for the number distribution density can be obtained by dividing the porosity distribution density by the volume of a pore segment $\pi R^2 \bar{l}$, with R being the pore radius and $\bar{l}$ the pore length. Therefore, shifting a small fraction of porosity toward the small pores can make a big difference in the location of the coordination number for a given coordination number. Using the pore size distributions of Fig. 2.1 for calcination at $750°C$, we find that the internal pore structure of Greer limestone ($z = 6$) becomes inaccessible when pores accounting for 0.23 initial porosity are plugged (<140 Å in radius), that of Georgia marble ($z = 3$) when pores accounting for 0.12 initial porosity (<94 Å in radius) are plugged, and that of Iceland spar when pores accounting for 0.085 initial porosity (<94 Å in radius) are plugged. Clearly, the initial porosity that must be removed to obtain an inaccessible pore structure (starting from the lower limit of the pore size range) increases from Greer limestone, to Georgia marble, to Iceland spar, that is, in the order decreasing overall reactivity during sulfidation (for the small particles of Georgia marble) and sulfation.

In the case of sulfation, the location of the percolation threshold affects both the amount of inaccessible pore volume and the effective diffusion coefficient. In the case of sulfidation, it only affects the intraparticle diffusion coefficient variation since the final porosity is far from being zero (about 0.25). The conversion dependence of the effective diffusion coefficients that are predicted by the mathematical model for the calcines produced at $750°C$ for sulfidation at the same temperature is shown in Fig. 2.17. We see that the effective diffusivity coefficient varies among the samples in the same order as the accessibility (or pore connectivity) of the pore structure, as it is quantified by the porosity-based

percolation threshold. Fig. 2.17 also gives the variation of the effective diffusivity that is predicted by the model for the larger coordination number that is needed to reproduce the sulfidation results for large Georgia marble particles. As it can also be seen from Table 2.5 which gives the initial and final diffusivities predicted by the mathematical model for the Georgia marble calcines at $750°C$, much larger diffusivities are needed for these particles. It is interesting to point out that despite having very large coordination numbers ($z = 1,000$ for calcination at $750°C$), the predicted diffusivity for the large Georgia marble particles is still two times lower than that predicted for a thoroughly interconnected structure of pores ($z = \infty$) or equivalently for a structure of parallel, infinitely long pores. This is a direct consequence of the broad form of the pore size distribution of the Georgia marble samples. The number-based percolation threshold ($1/(z\text{-}1)$) is equal to 0.9989, that is almost unity, but the corresponding initial pore radius is 385 Å and the corresponding porosity-based percolation threshold is 0.42. As a result, the large pores that are mainly responsible for the large diffusion coefficient for $z = \infty$ are still governed by transport in smaller size pores.

2.6. Summary and Conclusions

A detailed investigation of the sulfidation of calcines prepared from three limestones of high (>95%) calcium carbonate content was carried out in this study. Reactivity experiments were carried out in a thermogravimetric analysis system, the solids were characterized by mercury porosimetry ad gas adsorption, and the obtained sulfidation data were analyzed using the generalized random pore model of Yu and Sotirchos (1987), a model describing reaction, transport, and structure evolution in gas-solid reactions with solid product.

Our results showed very strong dependence of the overall reaction rate of each sorbent and of its evolution with the progress of the reaction on particle size. The overall reactivity of the solids increased with the calcination temperature, but the sulfidation temperature was found to influence weakly the conversion vs. time behavior of all sorbents, with its effect diminishing with increasing particle size. The results and conclusions of our sulfidation study were in relative agreement with those reached by Sotirchos and Zarkanitis (1992)

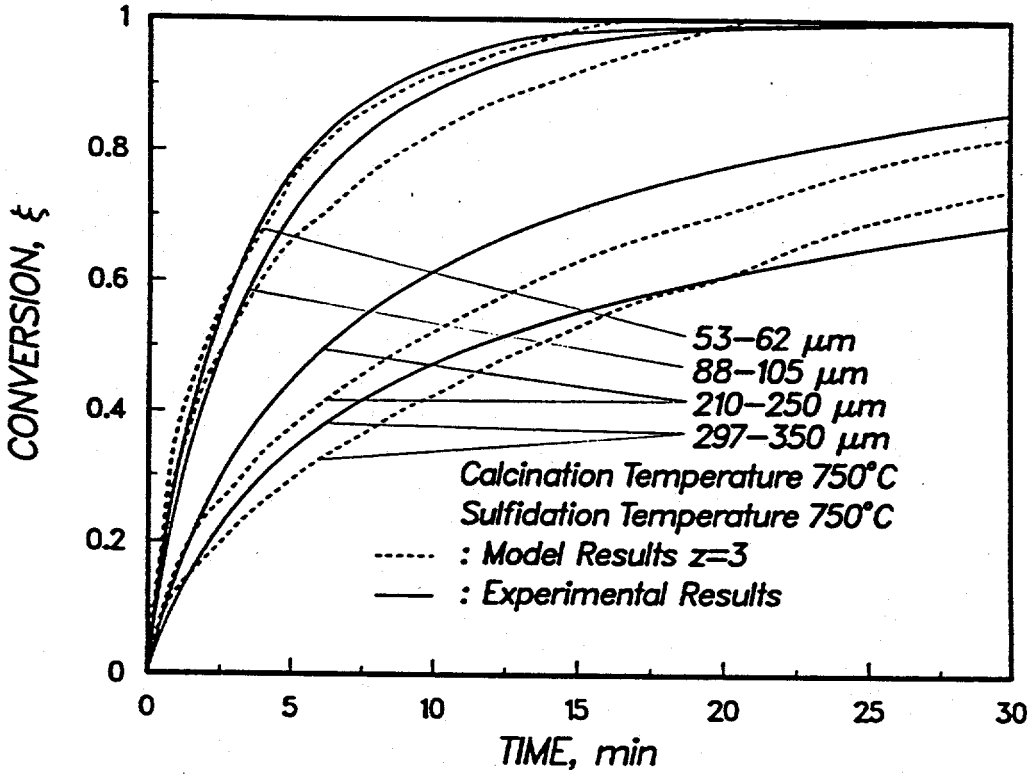

Figure 2.17: Variation of the effective diffusivities with the conversion for calcines produced and sulfided at $750°C$.

from the study of the sulfation of the same solids. In both cases, the reactivity of the sorbent was found to increase with increasing average grain in the precursor stone, and the same behavior was also exhibited by the calcination rates of the precursors. The only exception was observed for large ($> 200\ \mu m$) particles of one of the sorbents, a calcitic marble (Georgia marble), which had larger calcination and sulfidation rates than same size particles of the other sorbents even though smaller size particles exhibited intermediate reactivity. Since large particles of Georgia marble tended to explode during heating under CO_2 at high heating rates, it is believed that the apparently aberrant behavior of these particles during calcination and sulfidation is due to development of cracks in their interior, which lower the resistance for mass transport in their pore space.

With the exception of the data for large Georgia marble particles, very good agreement was obtained between model and experiment using parameter values consistent with those needed to describe the sulfation of the same solids (Sotirchos and Zarkanitis, 1992). In general, the comparison of model predictions and experimental data showed that the key factor influencing the behavior of a sorbent during sulfidation and sulfation is the connectivity of its pore space.

2.7 Notation

D_e	effective diffusivity, cm^2/s
D_P	diffusivity in the product layer, cm^2/s
R	pore radius, cm
v_s	volume of unreacted solid phase per mole of CaO, $cm^3/gmol$
v_i	molar volume of unreacted solid i, $cm^3/gmol$
z	coordination number
Z	volume of reacted solid phase per unit volume of unreacted phase (see Eq. (2.4))

Other Symbols

GR	Greer limestone
GM	Georgia marble

IS Iceland spar

Greek

ε porosity

ε_0 initial porosity

ξ conversion

ξ_{max} maximum conversion for complete pore plugging

ψ volume fraction of CaO in the sorbent

2.8. Literature References

Attar, A.; Dupuis, F., "The Rate and the Fundamental Mechanisms of the Reaction of Hydrogen Sulfide with Basic Minerals in Coal," Ind. Eng. Chem. Process Des. Dev., **18**, 607-618 (1979).

Barin, I.; Knacke, O., *Thermochemical Properties of Inorganic Substances*, Springer-Verlag, Berlin (1973).

Bird, R.B.; Stewart, W.E.; Lightfoot. E.N., *Transport Phenomena*, John Wiley, New York (1960).

Borgwardt, R.H., "Calcination Kinetics and Surface Area of Dispersed Limestone Particles," AIChE J., **31**, 103-111 (1985).

Borgwardt, R.H.; Roache, N.F.; Bruce, K.R., "Surface Area of Calcium Oxide and Kinetics of Calcium Sulfide Formation," Environ. Prog., **3**, 129-135 (1984).

Burganos, V.N.; Sotirchos, S.V., "Diffusion in Pore Networks: Effective Medium Theory and Smooth Field Approximation," AIChE J., **33**, 1678-1689 (1987).

Caldwell, K.M.; Gallagher, P.K.; D.W. Johnson, J., "Effect of Thermal Transport Mechanisms on the Thermal Decomposition of $CaCO_3$," Thermochim. Acta, **18**, 15-19 (1977).

Efthimiadis, E.A., "Reactivity and Pore Structure Changes in Hot Coal Gas Desulfurization Sorbents," Ph.D. Thesis, University of Rochester (1991).

Efthimiadis, E.A.; Sotirchos, S.V., "Reactivity Evolution during Sulfidation of Porous Zinc Oxide," Chem. Eng. Sci., **48**, 829-843 (1993).

Fisher, M.E.; Essam, J.W., "Some Cluster Size and Percolation Problems," J. Math. Phys., **2**, 609-619 (1961).

Freund, H., "Intrinsic Global Rate Constant for the High-Temperature Reaction of CaO with H_2S," Ind. Eng. Chem. Fundam., **23**, 338-341 (1984).

Furimsky, E.; Yumura, M., "Solids Adsorbents for Removal of Hydrogen Sulphide from

Hot Gas," Sci. and Technol., **39**, 163-172 (1986).

Gallagher, P.K.; Johnson, D.W., Jr., "The Effects of Sample Size and Heating Rate on the Kinetics of the Thermal Decomposition of $CaCO_3$," Thermochim. Acta, **6**, 67-83 (1973).

Hasler, J.R., Jr.; Robl, T.L.; Adibhatla, S.; Cunningham, R.D.; Withers, H.W., "Testing of Limestone Samples from the TVA Region as Sulfur Dioxide Sorbents in Atmospheric Fluidized-Bed Combustors," Technical Report, Institute for Mining and Mineral Research, University of Kentucky (1984).

Jalan, V., "Studies Involving High Temperature Desulfurization/Regeneration Reactions of Metal Oxides for Fuel Cell Development," Final Report, DOE/MC/16021-1486 (1983).

Kamath, V.S.; Petrie, T.W., "Rate of Reaction of Hydrogen Sulfide-Carbonyl Sulfide Mixtures with Fully Calcined Dolomite," Environ. Sci. Technol., **15**, 966-968 (1981).

Mikhail, R.S.; Hanafi, S.; Abo-el-Enein, S.A.; Good, R.J.; Irani, J., "Morphology and Surface Area Changes in the Thermal Dissociation of Iceland Spar," J. Colloid Interface Sci, **75**, 74-84 (1980).

Smith, J.M., *Chemical Engineering Kinetics*, McGraw-Hill, New-York (1981).

Squires, A.M.; Graff, R.A.; Pell, M., "Desulfurization of Fuels with Calcined Dolomite. I. Introduction and First Kinetic Results," Chem. Eng. Chem. Prog. Symp. Ser., **67**, 23-34 (1971).

Sotirchos, S.V.; Zarkanitis, S., "Inaccessible Pore Volume Formation during Sulfation of Calcined Limestones," AIChE J., **38**, 1536-1550 (1992).

Szekely, J.; Evans, J.W.; Sohn, H.Y., *Gas-Solid Reactions*, Academic Press, London (1976).

Westmoreland, P.R.; Gibson, J.B.; Harrison, D.P., "Comparative Kinetics of High-Temperature Reaction between H_2S and Selected Metal Oxides ," Environ. Sci. Technol., **11**, 488-491 (1977).

Yang, R.T.; Chen, J.M., "Kinetics of Desulfurization of Hot Fuel Gas with Calcium Oxide. Reaction between Carbonyl Sulfide and Calcium Oxide," Environ. Sci. Technol., **13**, 549-553 (1979).

Yu, H.C.; Sotirchos, S.V., "A Generalized Pore Model for Gas-Solid Reactions Exhibiting Pore Closure," AIChE J., **33**, 382-393 (1987).

Zarkanitis, S., "Pore Structure and Reactivity Evolution during Limestone Sulfation," Ph.D. Thesis, University of Rochester (1991).

Zarkanitis, S.; Efthimiadis, E.A.; Sotirchos, S.V., "Experimental Evaluation of a Class of Distributed Pore Size Models for Gas-Solid Reactions with Solid Product," Chem. Eng. Sci., **45**, 2761-2768 (1990).

Zarkanitis, S.; Sotirchos, S.V., "Pore structure and Particle Size Effects on Limestone Capacity for SO_2 Removal," AIChE J., **35**, 821-830 (1989).

3. SULFATION OF HIGH PURITY LIMESTONES UNDER SIMULATED PFBC CONDITIONS

3.1. Introduction

Fluidized-bed combustion (FBC) possesses a number of environmental and operational advantages over conventional combustion systems, with the former becoming increasingly attractive as stricter limits are imposed on the concentration of gaseous pollutants (primarily, NO_x and SO_2) in the flue gases of coal combustion facilities. Fluidized-bed combustion exhibits high flexibility with respect to the sulfur and ash content of the coal feed and does not require a separate flue gas desulfurization unit. Moreover, because of lower combustion temperatures, it presents smaller concentrations of NO_x in the flue gases than combustion in other units (METC, 1984). When combustion of the coal matter in the fluidized bed is carried out under pressure, several additional advantages are encountered in comparison to having the process occurring under atmospheric pressure. These include smaller fluidized beds and smaller equipment size for comparable power - which make possible modular fabrication of the units - larger volumetric rates of heat release, lower combustion temperatures and, hence, smaller NO_x concentrations in the flue gas, and increased thermal efficiencies for combined cycle systems (METC, 1984). All these interesting features make pressurized fluidized-bed combustion (PFBC) very attractive as a high-efficiency alternative to the better developed atmospheric fluidized-bed combustion (AFBC), although the latter is still favored in the industry, especially by boiler manufacturers (Fox et al., 1986).

In a fluidized-bed combustor, a bed of combustible (coal) and noncombustible material is fluidized using air blown upward. Using dolomite or limestone as the noncombustible material, it is possible to have fuel combustion and flue gas desulfurization taking place simultaneously in the combustion vessel. If operation occurs under atmospheric pressure, the average partial pressure of carbon dioxide in the combustor (typically, 10-15% of the total pressure) is considerably lower than the equilibrium CO_2 pressure for decomposition of limestone ($CaCO_3$) or dolomite ($CaCO_3 \cdot MgCO_3$) at the temperatures usually encountered in FBC units (800- 950^oC). In the high temperature environment of the AFBC unit,

the limestone or dolomite particles undergo calcination, yielding a highly porous product (CaO or MgO), which reacts with the sulfur dioxide produced during coal combustion forming, mainly, calcium or magnesium sulfate. The sulfates occupy more space than the oxides they replace, and as a result, the pores of the calcine are completely plugged with solid product before complete conversion takes place. (The conversion for complete pore plugging is about 50% for the calcine of a stone consisting of $CaCO_3$ only.) Pores of different size are plugged at different conversion levels, and it is thus possible to have formation of inaccessible pore space in the interior of the particles when the small feeder pores of clusters of large pore are filled with solid product (Zarkanitis and Sotirchos, 1989). Moreover, under conditions of strong internal diffusional limitations, complete pore closure may first take place at the external surface of the particles while there is still open pore space left in the interior. In reactors operating at higher temperatures, porosity loss may also occur through CO_2-activated sintering (Newton et al., 1989). For these reasons, ultimate conversions much lower than those predicted by the stoichiometry of the reaction for complete plugging of the internal pore space (less than 30-40%) are seen in AFBC units.

The reaction of calcined limestones (primarily) and dolomites with SO_2 has been the subject of extensive investigation. The experimental evidence gathered in most of the past studies indicates strong effects of the pore size distribution on the overall reactivity of the calcined solids (Borgwardt and Harvey, 1972; Wen and Ishida, 1973; Hartman and Coughlin, 1974, 1976; Ulerich et al., 1977; Simons and Garman, 1986; Yu, 1987; Gullett and Bruce, 1987; Zarkanitis and Sotirchos, 1989; Sotirchos and Zarkanitis, 1992). Unfortunately, the immense volume of information that has accumulated over the years on the reaction of calcined limestones and dolomites with SO_2 is not applicable to SO_2 emissions control by limestones and dolomites under PFBC conditions. PFBC units normally operate under a pressure of 1600 kPa, which for an average CO_2 content of 15% gives a partial pressure of CO_2 in the reactor of about 240 kPa. Thermodynamic calculations show that the temperature for $CaCO_3$ calcination in the presence of 240 kPa of CO_2 must be larger than 980^oC, that is, well above the temperatur range (750-950^oC) encount ed in a PFBC unit. Nevertheless, despite that formation of a highly porous material with a high specific surface area cannot take place under PFBC conditions, favorable desulfurization is known

to occur in PFBC units (Bulewicz et al., 1986; Hoy et al., 1982; Murthy et al., 1979). For dolomites, the situation is somewhat different since half-calcination (formation of a $MgO - CaCO_3$ product) is possible under 240 kPa of CO_2. Even in this case, however, if sorption of SO_2 occurred only in the pore space of the half-calcined solid, the utilization of the calcium content of dolomites should be much smaller than what is seen in practice under PFBC conditions.

The reaction of $CaCO_3$ with SO_2 may involve various reaction steps (Van Houte et al., 1981):

$$CaCO_3 + SO_2 \rightarrow CaSO_3 + CO_2 \quad (3.1)$$

$$CaSO_3 + \frac{1}{2}O_2 \rightarrow CaSO_4 \quad (3.2)$$

$$CaSO_3 + \frac{1}{2}SO_2 \rightarrow CaSO_4 + \frac{1}{2}S \quad (3.3)$$

$CaSO_3$ decomposes at temperatures higher than $650°C$, and therefore, under typical operating conditions in a PFBC unit, the overall reaction may be written as:

$$CaCO_3 + SO_2 + \frac{1}{2}O_2 \rightarrow CaSO_4 + CO_2 \quad (3.4)$$

For dolomites, one should also address the question of the reaction of MgO with SO_2.

Spatial variation of the partial pressure of CO_2 within the bed will obviously lead to calcination of $CaCO_3$ in the regions where CO_2 pressures lower than the equilibrium are prevailing. Calcination of $CaCO_3$ will yield a partially calcined product, the extent of calcination depending on the residence time of the solid in the low CO_2 concentration region. The CaO formed in the solid will then react with the SO_2 present in the bed in the same fashion as in the case of AFBC units:

$$CaCO_3 \rightarrow CaO + CO_2 \quad (3.5)$$

$$CaO + SO_2 + \frac{1}{2}O_2 \rightarrow CaSO_4 \quad (3.6)$$

When the partially calcined solid moves into regions rich in CO_2, where reaction (3.5) is favored to proceed from right to left, carbonation, i.e., recovery of $CaCO_3$, will take place, and reaction (3.4) will be competing with reaction (3.5) for CaO. Decomposition of

$CaCO_3$ may take place even if there is no variation of the CO_2 pressure in the reactor. Large variations in the temperature profile (100-140^oC) within the combustor unit have been reported by Smith et al. (1982). Therefore, if the solid particles move into regions where the temperature of the reactor is above the temperature at which $CaCO_3$ is stable at the average partial pressure of CO_2 in the reactor, decomposition of $CaCO_3$ may occur. However, only small amounts of CaO have been found in the reactor by Ljungstrom and Lindqvist (1982), suggesting that direct sulfation of limestones (equation (3.4)) is the main reaction occurring in the combustor. Similarly, PFBC data from Exxon (Hoke et al., 1977) with uncalcined Grove limestone showed that most of the unreacted Ca in the bed for CO_2 partial pressures above the equilibrium value existed in the form of $CaCO_3$.

Studies of SO_2 removal at high pressures have been carried out both with carbonates and precalcined solids. However, because of the aforementioned complexities, with the exception of the general conclusion that favorable desulfurization is possible under PFBC conditions, there is not much agreement in the literature on the effects of the various parameters on the process. Dennis and Hayhurst (1984, 1987) found that the reaction rate of precalcined limestones in a fluidized-bed reactor decreases with an increase in the operating pressure, both in the absence and presence of CO_2. On the basis of the experience gained from the study of the $CaO - SO_2$ reaction at atmospheric pressure, these results are reasonable since an increase in the pressure also leads to a smaller effective diffusion coefficient, but the change would be relatively small in view of the fact that diffusion takes place close to the knudsen diffusion regime. Also, the presence of CO_2 favors sintering of the porous solid, and if the carbonation reaction is favored, it may compete with reaction (3.4) for CaO. Working with a laboratory-size PFBC, Bulewicz et al. (1986) observed an increase in the sorption capacity of Ca-based sorbents (chalk, limestones and dolomites) with an increase in pressure up to 200 kPa, but further increase in pressure caused a reduction in the sorption capacity of all samples. Although there is no obvious explanation for the observed increase of the sulfation capacity of the sorbents for low pressures, the second observation of Bulewicz et al. can be explained from a thermodynamic standpoint. At an operating temperature of 835^oC, calcination of $CaCO_3$ takes place for pressures less than 200 kPa yielding a highly porous structure, while for pressures above 200 kPa, direct

sulfation of limestones would be the alternate route, where the absence of a developed porous matrix would result in lower sorption capacities. Such a behavior has also been observed by Jansson et al. (1982).

PFBC studies at Exxon (Hoke et al., 1977) showed better sulfur retention for precalcined limestones, but Stantan et al. (1982) observed no improvement in sorbent utilization by precalcination. Stantan et al. also reported that under weakly noncalcining conditions, a feed of uncalcined limestone gave better sulfur retention than that observed from thermogravimetric experiments. They postulated that no improvement was observed for precalcined solids because of the existence of a calcining zone near the base of the PFBC unit, which helps the uncalcined material achieve reactivity levels similar to those of the precalcined solid. Detailed tests done at the Illinois State Geological Survey (Chen, 1990) on several limestones and dolomites showed that some of the raw stones captured more SO_2 under noncalcining conditions than precalcined samples derived from these precursors. Moreover, an increase in pressure tended to increase sorbent utilization in the case of dolomites, but it had the opposite effect for solids with significant calcitic content.

It is possible to study the direct sulfation of calcium carbonate-containing sorbents under atmospheric pressure, provided that there is enough CO_2 in the reactor to prevent decomposition of the carbonate (simulated PFBC conditions). Tullin and Ljungstrom (1989), performed sulfation experiments in a thermogravimetric analyzer (TGA) under conditions inhibiting calcination of $CaCO_3$. They observed that the sulfation rate of uncalcined $CaCO_3$ was comparable with the sulfation rate of calcined material and concluded that desulfurization in PFBC units may proceed by direct sulfation of limestone. However, large amounts of sample and small particles (around 150 mg and 10-90 μm) were employed in the above study, and as a result, because of potentially strong interparticle diffusional limitations, extracting any quantitative information from the reported data is practically impossible. A similar procedure was employed by Snow et al. (1988) and Hajaligol et al. (1988), who also observed that the direct sulfation of $CaCO_3$ can reach, for some precursors, higher conversions than the sulfation of the calcines (CaO). They argued that the counter-diffusion of the CO_2 that is generated during the direct sulfation reaction (equation (3.4)) forms a porous product layer that offers less diffusion resistance than

the essentially nonporous layer formed during the $CaO - SO_2$ reaction. A shrinking core model was used by the above authors to analyze the experimental data, and the effective diffusivities they obtained were two to three orders of magnitude higher than the product layer diffusivity estimated from calcined limestone sulfation data.

A detailed experimental investigation of the direct sulfation of limestones with SO_2 is presented in this study. Reactivity evolution experiments were carried out in a thermogravimetric analysis system under simulated PFBC conditions, that is, in the presence of enough CO_2 to prevent decomposition of $CaCO_3$, as it was done in the studies of Snow et al. (1988) and Tullin and Ljungstrom (1989). The structure of precursor rocks and partially reacted samples was analyzed by gas sorption and mercury porosimetry. In order to examine the influence of the various experimental conditions and parameters on the overall rate of the limestone-SO_2 reaction, experiments were conducted using a broad range of particle size (53-350 μm), two temperatures (750 and 850^oC) and two SO_2 concentrations (1,500 and 6,000 mL/m^3). Three solids of high (> 95%) calcium carbonate content and different petrographic structure were employed in our experiments. The reaction of the calcined forms of these solids with SO_2 had been investigated in detail in a previous study (Zarkanitis and Sotirchos, 1989; Sotirchos and Zarkanitis, 1992), and as a result, a comparison of the rates of direct and indirect reaction of the same $CaCO_3$ solids with SO_2 is also presented in our study.

3.2. Materials and Procedures

Experiments were carried out using the following limestone specimens: a limestone of very high $CaCO_3$ content distributed by Greer Limestone Co. (Greer limestone), a calcitic marble (Tate White Aggregate) distributed by Georgia Marble Co. (Georgia marble), and a calcite(Iceland spar) distributed by Wards Inc. Chemical analysis of the solids showed that the calcium carbonate content was the highest in the Iceland spar (99.19 %), followed by those of the Greer limestone (97.89 %) and of the Georgia marble (95.19 %). Detailed chemical analyses of the three solids are given elsewhere (Krishnan, 1993). Mineralogical analysis of the stones revealed that the calcium carbonate was present in the form of calcite. Examination under a petrographic microscope showed that the Greer limestone

mainly consisted of calcitic, microgranular mud with inclusions of aggregates of small calcitic grains and that the Georgia marble consisted of coarse calcitic grains. The Iceland spar was found to be translucent and to consist of single crystals. More details on these materials are given by Zarkanitis (1991), who carried out a detailed investigation of the reaction of their calcined products with SO_2.

Direct sulfation experiments were carried out in a thermogravimetric analysis (TGA) system. A Cahn 2000 electrobalance capable of handling weights up to 2.5 g and sensing weight changes as small as 0.1 μg constitutes the main part of the TGA system. In order to avoid having significant interparticle diffusional limitations, a small amount of solid (3-10 mg) was used for reactivity experiments. The effects of particle size on conversion vs. time results were studied by carrying out experiments with particles in three size ranges (53-62, 88-105, and 297-350 μm) for each of the three solids. Two inlet concentrations of 1,500 and 6,000 mL/m^3 of SO_2 were employed to estimate the order of the reaction with respect to SO_2, which in past studies was assumed to be unity. The temperature effect was also studied by performing experiments at two different temperatures, 750 and 850^oC. The inlet gases were composed of a mixture of 70% CO_2 (99.99% purity), and 30% air (containing 0.5% SO_2 or 2% SO_2). The sample was heated to the desired reaction temperature of 750^oC or 850^oC in an environment of pure CO_2 to ensure that calcination would not take place. After temperature stabilization, the CO_2 stream was substituted with a mixture of 70% CO_2 and 30% N_2 to verify that calcination was inhibited under these conditions. The $CO_2 - N_2$ stream was then replaced by the reactive mixture, and the transient weight gain of the sample was recorded. A flow rate of 200 mL/min at standard conditions was employed in all experiments discussed in this study.

3.3. Reactivity Evolution Results

Figs. 3.1-3.3 present conversion vs. time data for the direct sulfation at 850^oC of 53-62, 88-105, and 297-350 μm particles of Greer limestone, Georgia marble, and Iceland spar, respectively, using 1,500 and 6,000 mL/m^3 SO_2 with 70% CO_2 (by volume) in air. Reactivity evolution results for the direct sulfation of the three solids (for the same particle sizes and SO_2 concentrations as in Figs. 3.1-3.3) at 750^oC are shown in Figs. 3.4-3.6. It is

obvious from the results of Figs. 3.1-3.6 that the particle size strongly influences the overall reactivity of limestone with SO_2, an indication that the reaction occurs under strong mass transportlimitations. The existence of heat transport limitations is not an issue under the reaction conditions used in our study. Because of the small concentrations of gaseous reactant, the amount of heat involved in the chemical reaction is too low to cause significant temperature gradients in the interior of the particles or in the surrounding gas phase.

The effect of particle size on the overall reaction rate of small Greer limestone particles appears to be considerably stronger, on a relative basis, than in all other cases. Increasing the particle size from 53-62 to 88-105 μm (that is, by a factor of 1.8) decreases the conversion level reached at large reaction times by more than 50%, while the corresponding decrease in the cases of Georgia marble and Iceland spar is less than 30%. This observation suggests that the overall mechanism of reaction of small Greer limestone particles may be qualitatively different from that of the other solids and of large particles of the same solid. For the 88-105 and 297-350 μm particles, the effects of particle size on the conversion evolution curves are in quantitative agreement, on a relative basis, for all three sorbents.

The reaction temperature has a strong influence on the overall rate of the $CaCO_3 - SO_2$ reaction, similar in extent to that of particle size. As a comparison of the results of Figs. 3.1-3.3 with the corresponding curves of Figs. 3.4-3.6 show, a 100^oC reduction in the reaction temperature causes a large drop in the sulfur uptake of the sorbents for a given reaction time. The sulfation temperature appears to influence both the kinetic and mass transport characteristics of the process. The initial slopes of the conversion evolution curves show that the overall reaction rate at the start of the process, where presumably there are no diffusional limitations, decreases significantly as the temperature goes from 850 to 750^oC, implying that a proportionate decrease is experienced by the intrinsic reaction rate. The variation of the slopes of the conversion vs. time curves with time indicates that the overall rates of reaction at the two temperatures are much different even at high conversion levels. Since the process is expected to be controlled at high conversion levels by diffusion through the product layer, one concludes that the mass transport resistance in the product layer must also be affected by temperature.

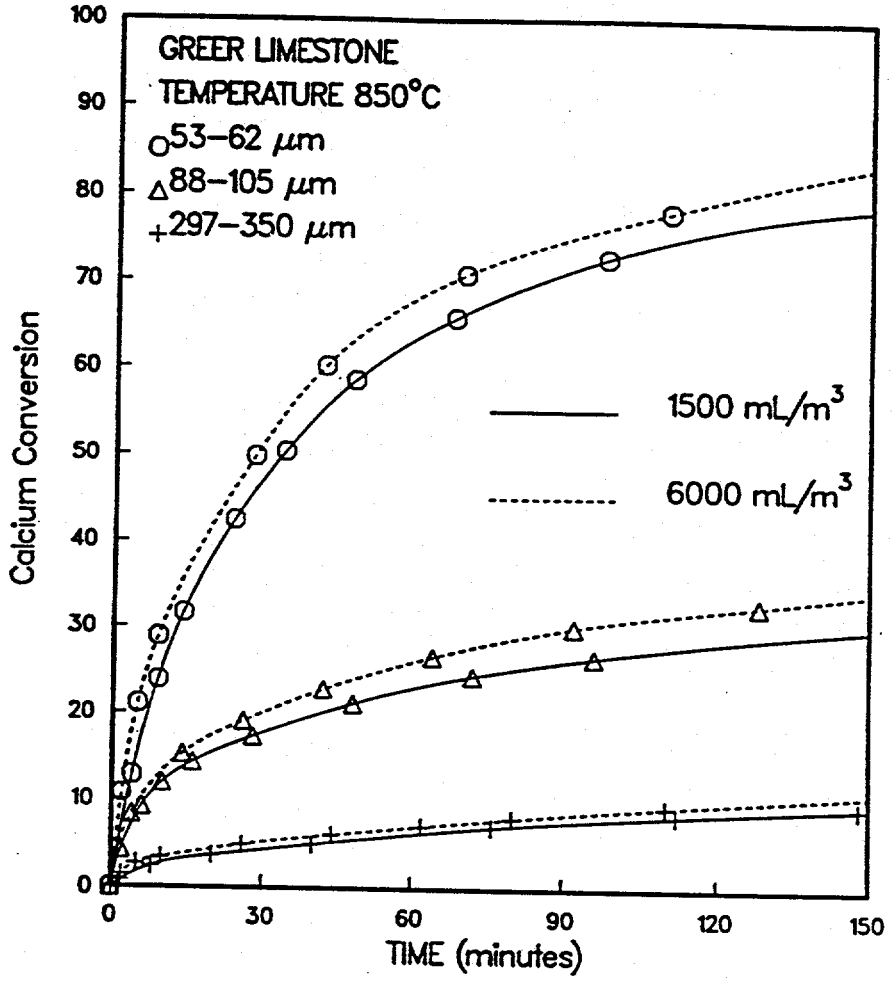

Figure 3.1: Conversion vs. time results during direct sulfation at $850°C$ of Greer limestone particles in an atmosphere of 30% air and 70% CO_2 (mole %).

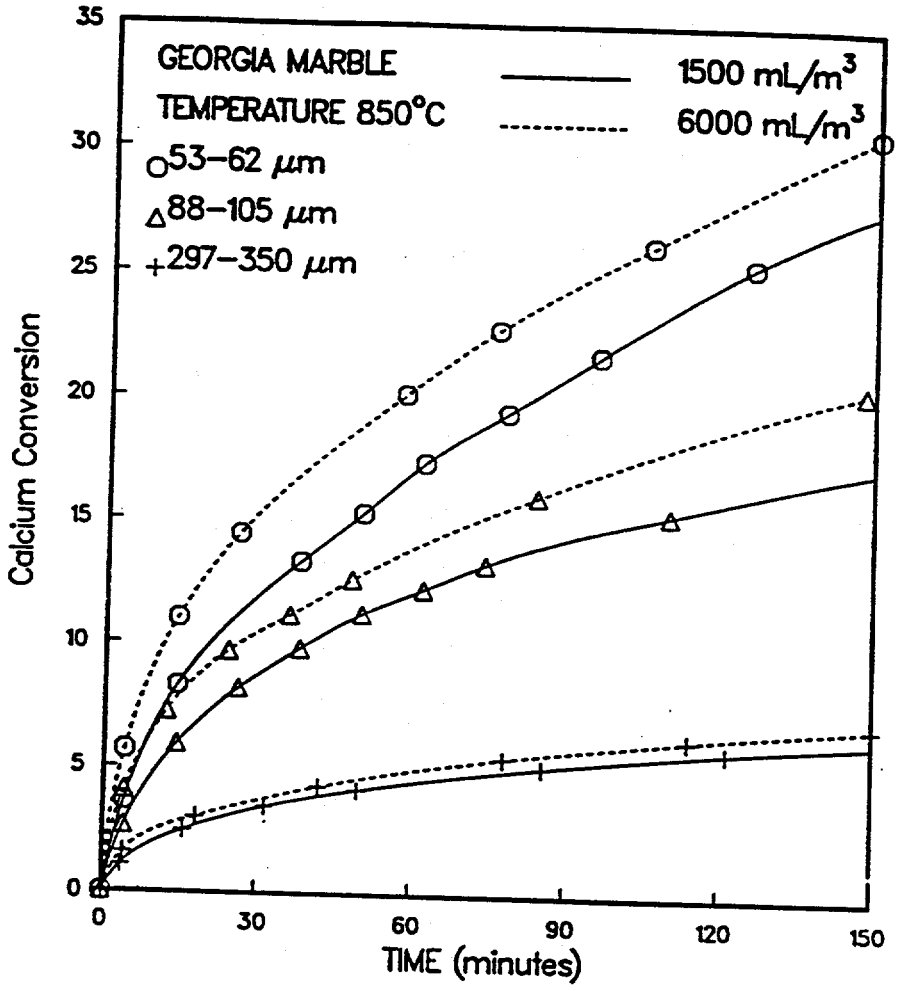

Figure 3.2: Conversion vs. time results during direct sulfation at $850°C$ of Georgia marble particles in an atmosphere of 30% air and 70% CO_2 (mole %).

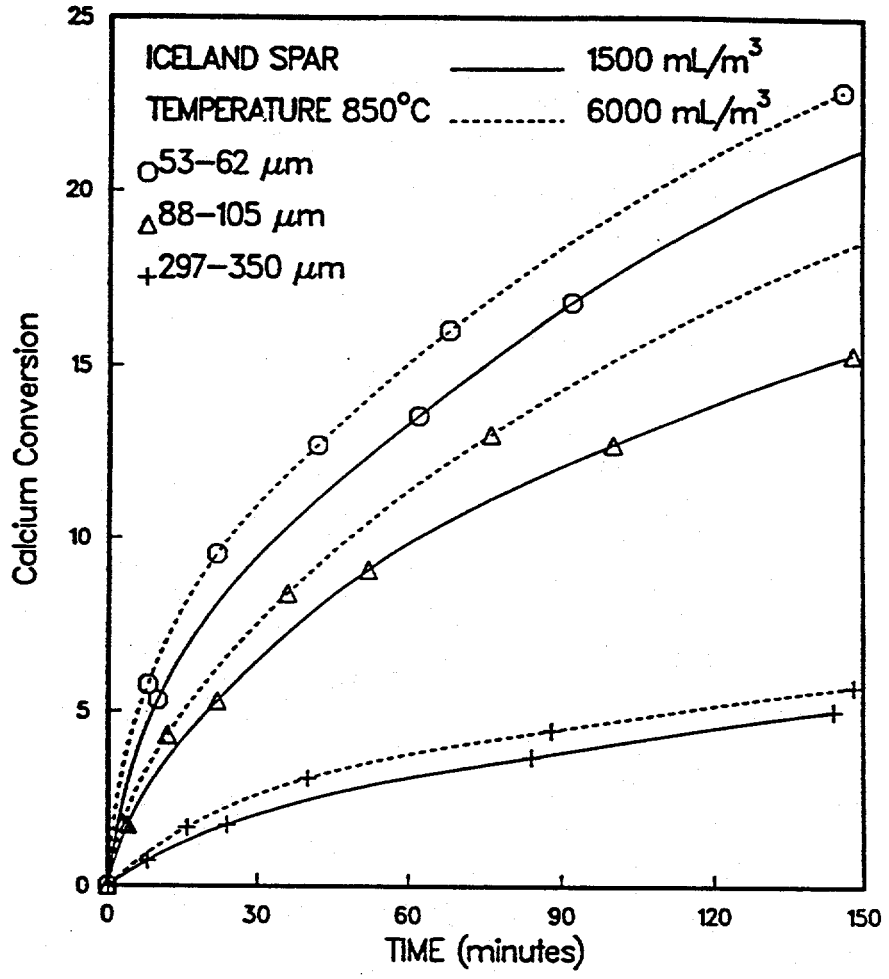

Figure 3.3: Conversion vs. time results during direct sulfation at $850°C$ of Iceland spar particles in an atmosphere of 30% air and 70% CO_2 (mole %).

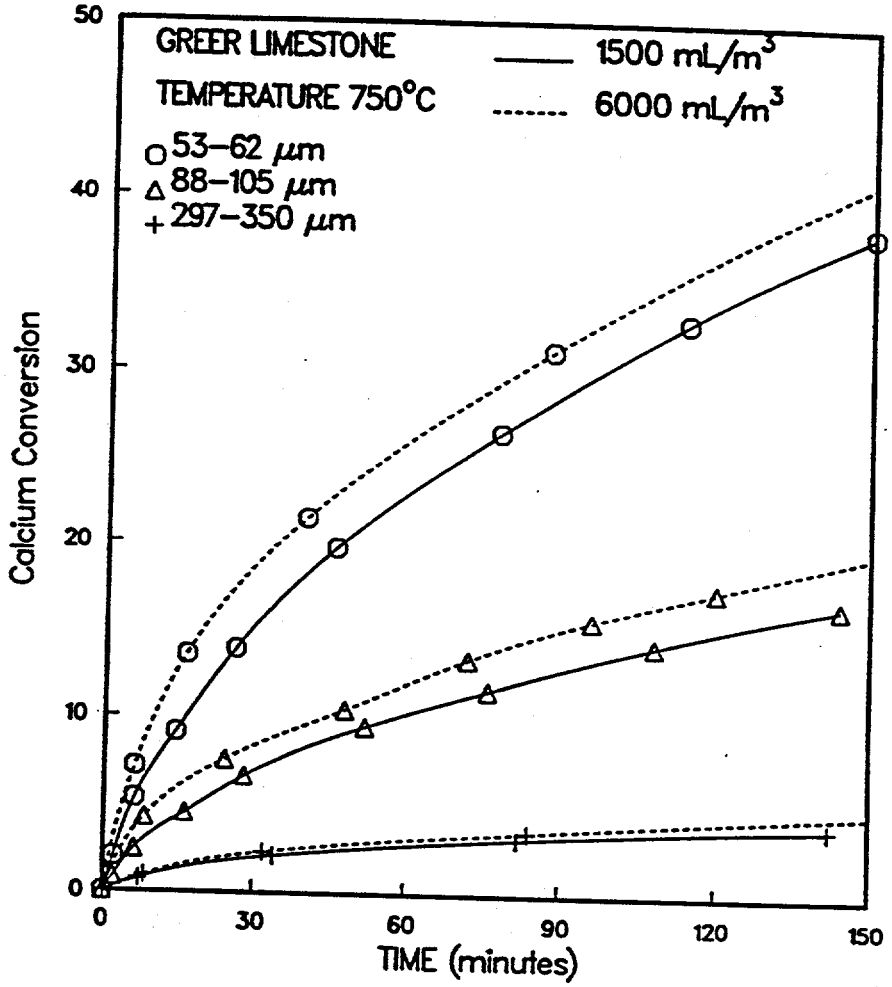

Figure 3.4: Conversion vs. time results during direct sulfation at 750°C of Greer limestone particles in an atmosphere of 30% air and 70% CO_2 (mole %).

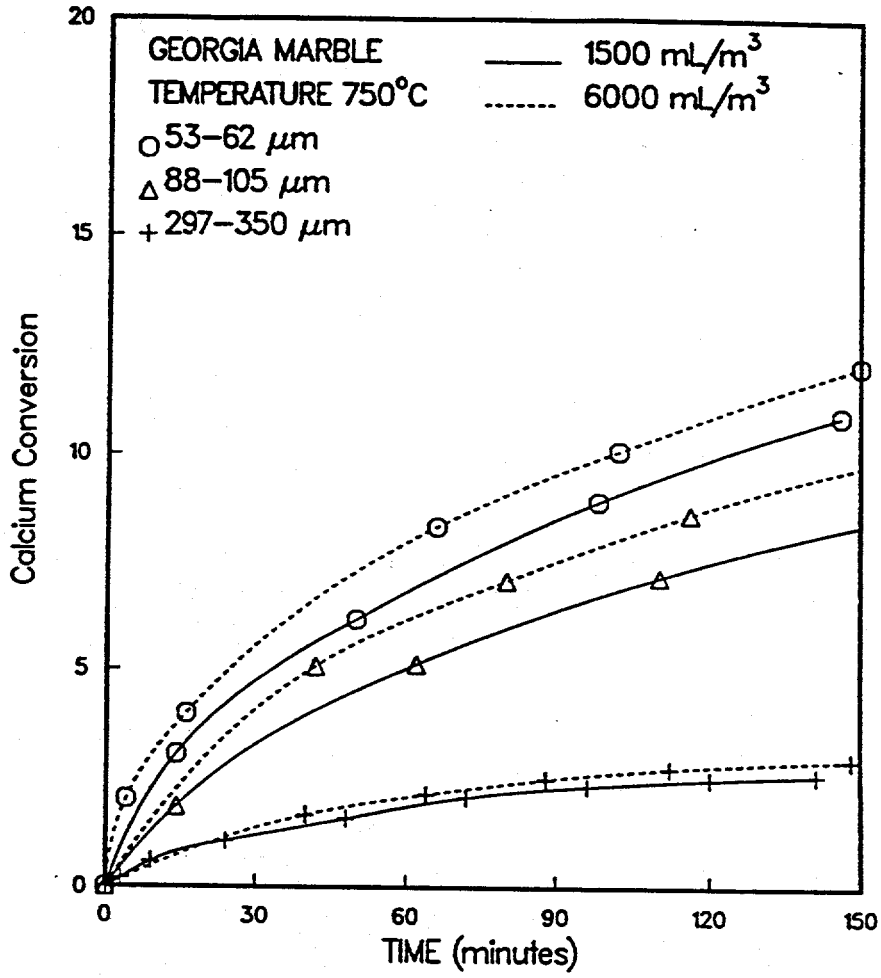

Figure 3.5.: Conversion vs. time results during direct sulfation at $750°C$ of Georgia marble particles in an atmosphere of 30% air and 70% CO_2 (mole %).

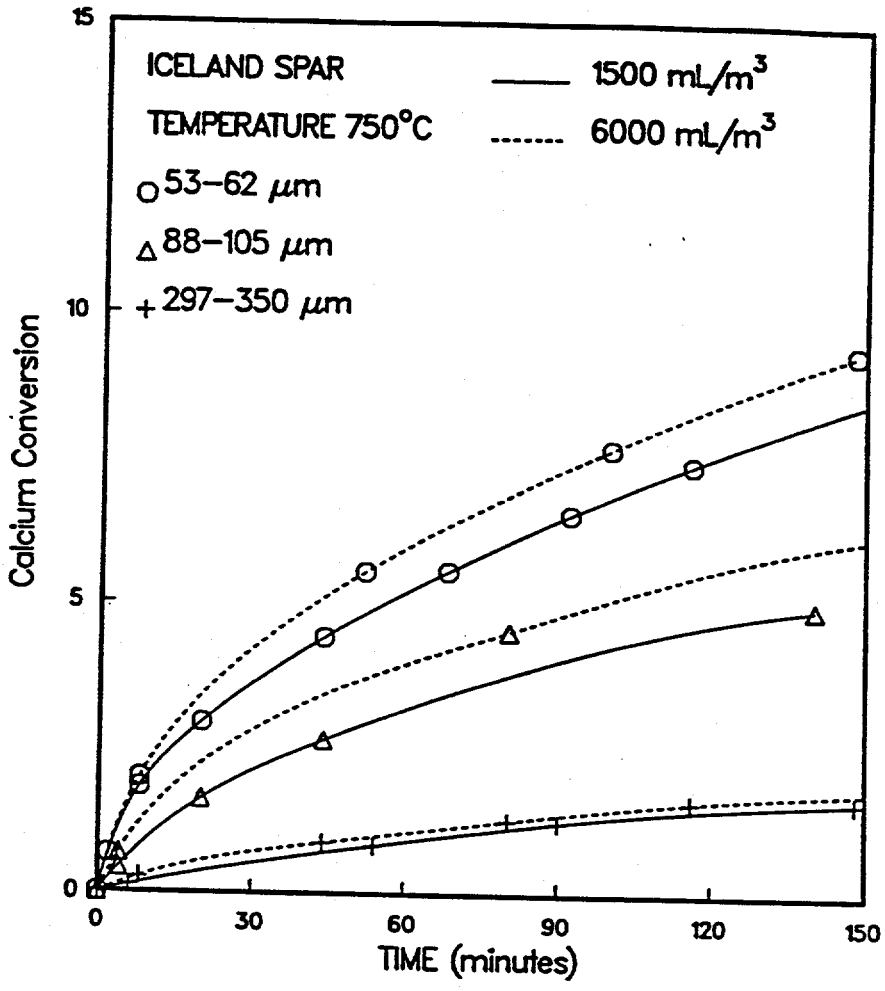

Figure 3.6: Conversion vs. time results during direct sulfation at $750°C$ of Iceland spar particles in an atmosphere of 30% air and 70% CO_2 (mole %).

Increasing the concentration of SO_2 leads to higher reaction rates and conversions, but the increase is for all combinations of limestone, particle size, and temperature much smaller than what should be expected for a four-fold increase in the concentration under conditions controlled by the intrinsic kinetics of the reaction for a first order (with respect to SO_2) reaction or by mass transport in the intraparticle space with the mass transport (diffusion) resistance being independent of the concentration. This result leads us to conclude that the order of reaction with respect to SO_2 is different from unity and that the diffusion coefficient in the product layer is a function of the SO_2 concentration.

Figs. 3.7 and 3.8 compare at 850 and 750°C, respectively, the conversion vs. time curves that we measured in this study for the direct reaction of 53-62 μm particles with 1500 mL/m^3 SO_2 with the corresponding curves that were obtained by Zarkanitis (1991) for the sulfation of the calcines of the three sorbents (same size particles). In the experiments of Zarkanitis (1991), the calcines were produced and sulfated at the same temperature. Sulfation was carried out using a mixture of 3000 mL/m^3 SO_2 and 12% (by volume) O_2 in N_2. Experiments for different SO_2 concentrations showed that the overall rate of reaction was of first order with respect to the concentration of SO_2 at all conversions. Thus, in order to make the results of Zarkanitis comparable with those obtained in our study for 1500 mL/m^3 of SO_2, the reaction time of his experiments was multiplied by 2.

It is seen in Figs. 3.7 and 3.8 that the overall reaction rate is much higher at low conversions for the sulfation of the calcines ($CaO - SO_2$ reaction) than for the sulfation of the precursors under conditions that prohibit decomposition to CaO ($CaCO_3 - SO_2$ reaction). However, the reaction rate of the calcines drops sharply after some conversion level (after about 10 min of exposure to the reactive environment), beyond which insignificant sorption of SO_2 takes place, whereas sulfation is seen to occur with significant rate for the uncalcined limestones throughout the 150 min window shown in Fig. 3.1. It is interesting to observe that in the case of the Greer limestone particles, the conversion of the uncalcined sorbent surpasses that of the calcine after about 30 min of reaction time.

The results of Figs. 3.7 and 3.8 cannot be used to determine the effect of temperature on the reaction of calcined limetones since the calcines of each figure were produced at different temperatures, and as a result, they have different pore structures. Zarkanitis and

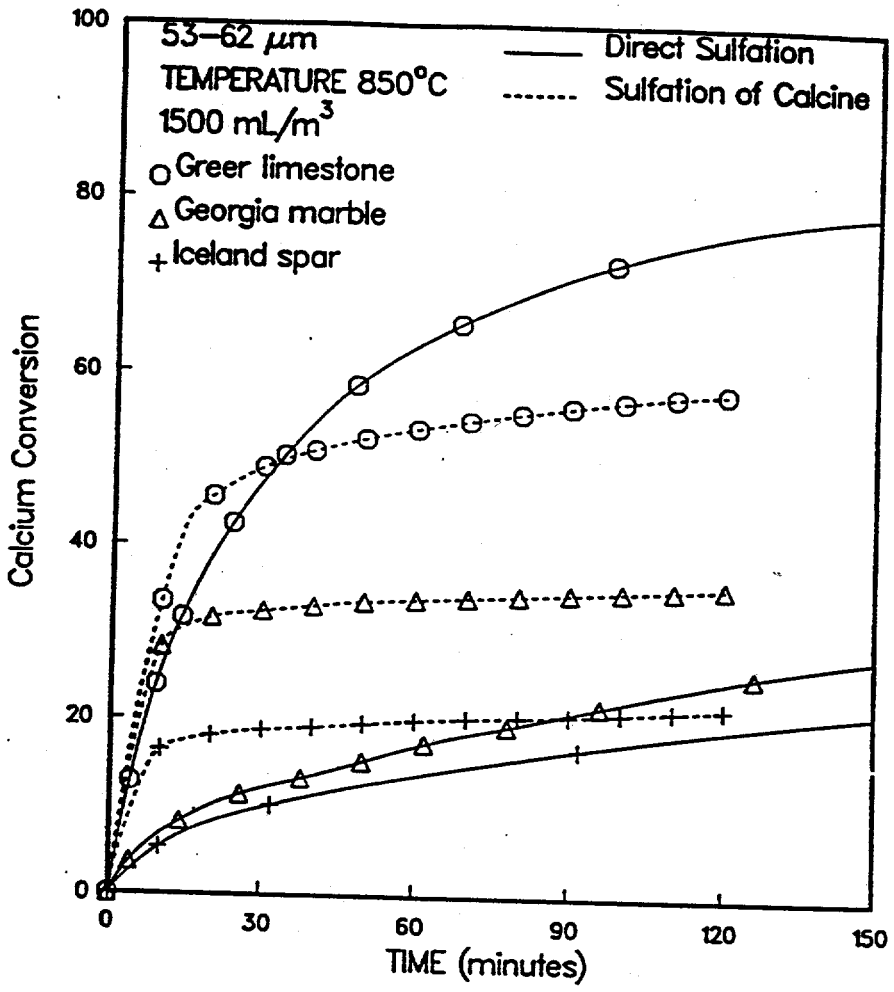

Figure 3.7: Comparison of the conversion evolution curves during direct sulfation of 53-62 μm particles at $850°C$ with those obtained during sulfation of same size particles of the calcined solids (Zarkanitis, 1991) at the same temperature. The calcines were prepared by calcination at $850°C$.

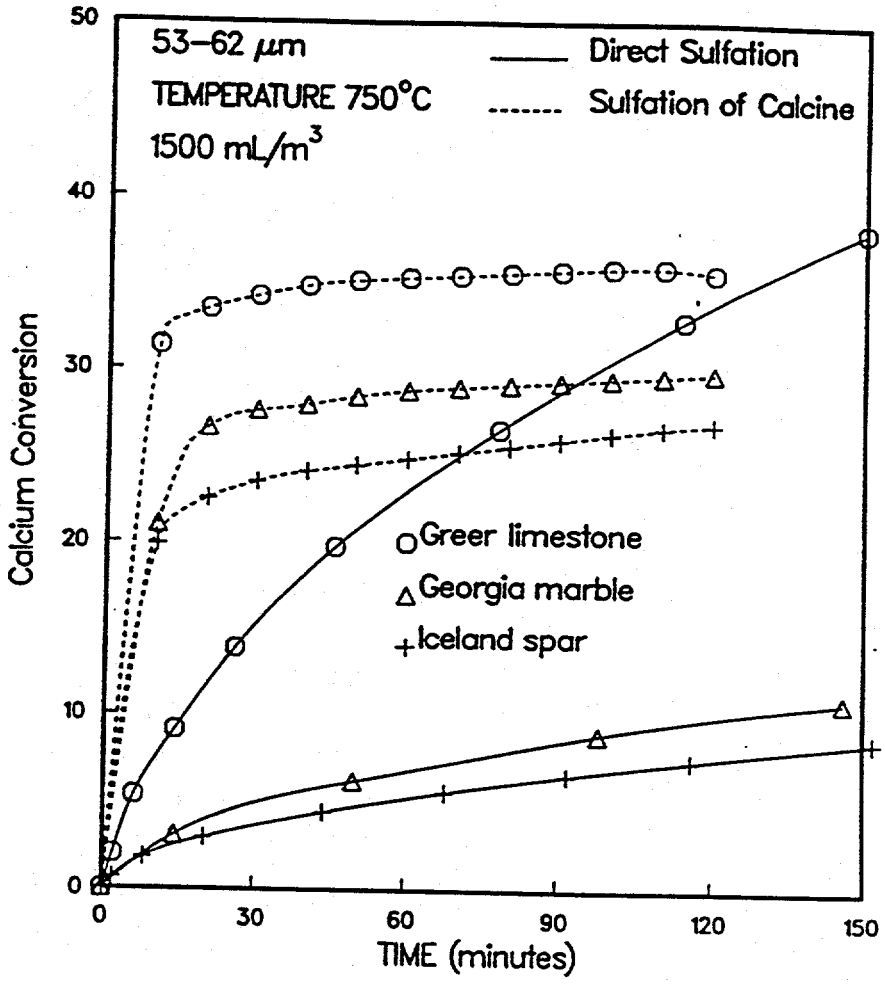

Figure 3.8: Comparison of the conversion evolution curves during direct sulfation of 53-62 μm particles at $750°C$ with those obtained during sulfation of same size particles of the calcined solids (Zarkanitis, 1991) at the same temperature. The calcines were prepared by calcination at $750°C$.

Sotirchos (1989) found that lowering of temperature does result in a decrease in the overall reaction rate for the sulfation of limestone calcines (Zarkanitis and Sotirchos, 1989), but of much smaller extent than for direct sulfation of limestones. The fact that temperature affects the two reactions differently lends further support to the conclusion that the overall mechanisms of the two processes are radically different.

Particle Size (μm)	Temp. (^oC)	GL (% Conv.) A B C	GM (% Conv.) A B C	IS (% Conv.) A B C
53-62	850	75 79 54	25 28 34	19 21 20
88-105	850	26 32 38	15 19 25	13 16 16
297-350	850	09 10 17	06 07 12	04 05 07
53-62	750	32 36 35	09 11 28	07 08 25
88-105	750	14 17 28	07 09 13	04 05 18
297-350	750	03 04 15	02 03 11	02 02 10

Table 3.1: Comparison of conversion levels obtained by direct sulfation or sulfation of calcined samples after 2 hours. GL=Greer Limestone, GM=Georgia Marble, and IS=Iceland Spar. A=Direct sulfation using 70% CO_2, 30% air(containing 0.5% SO_2), B=Direct sulfation using 70% CO_2, 30% air (containing 2%SO_2), and C=Sulfation of calcine using a mixture of 3000 ppm SO_2 and 12% O_2 (by volume) in N_2.

A quantity of much importance is the conversion level attained by the sorbent particles for reaction times comparable to the average residence time of the particles in a fluidized-bed combustor. Table 3.1 summarizes the comparison between conversion levels obtained through the two different routes of sulfation (direct and through calcination) after 2 hr of reaction time. The conversion level reached by the 53-62 μm particles of Greer limestone during direct sulfation at 850^oC for large exposure times (see Fig. 3.1 and Table 3.1) far exceeds the maximum allowable conversion for complete plugging of the pore space of its calcine with calcium sulfate (about 55%). For the other two sorbents, the conversions reached by the small (53-62 μm) particles during direct sulfation are comparable to those

attained by their uncalcined counterparts. However, because of the very strong effect of particle size on the rate of direct sulfation, which is much stronger than that on the calcined sorbent reaction, the conversion levels attained by larger particles are much lower for the direct sulfation reaction.

3.4. Pore Structure Results

Mercury penetration experiments using a Micromeritics 9220 II mercury porosimeter showed that the stones were nearly nonporous in their natural state as only minute quantities (typically, 0.01-0.02 mL/g) of mercury penetrated the void space of the samples. Mercury porosimetry was used by Hajaligol et al. (1988) to characterize the pore structure of the solids that were used in their studies. Since very small penetration volumes were observed in our experiments and mercury intrusion mainly occurred at high pressures, where sample and mercury compressibility introduce significant errors in the interpreted data for small intrusion volumes, it was decided to base the analysis of the pore structure of the samples of unreacted and partially reacted solids on gas sorption data instead. Gas sorption isotherms (N_2 at 77 K) were measured using a volumetric sorption instrument (Autosorb-1 by Quantachrome). The relatively large quantities of partially reacted samples needed for the porosimetry and sorption experiments were prepared in a fixed-bed reactor under differential operation at the same conditions used in the TGA experiments. The differential operation of the reactor was verified using a gas chromatograph (Varian 3300) equipped with a flame photometric detector to analyze the effluent stream.

Fig. 3.9 presents cumulative pore volume vs. pore radius results for the three limestones obtained through gas N_2 sorption at 77 K. The porosities for pores of radius smaller than 100 nm and the surface areas determined from BET analysis of the results of Fig. 3.9 are given in Table 3.2. Greer limestone is seen to have the highest natural porosity followed by Georgia marble and Iceland spar. The surface areas show the same trend as the porosities, with Greer limestone having about three times larger surface area than Georgia marble and four times than Iceland spar. Interestingly enough, the reaction rates and the sulfation efficiencies, both for direct and indirect (after calcination) sulfation (see Figs. 3.7 and 3.8), of the three solids increase in the same order as their porosities and

surface areas, while, on the contrary, their average grain size, as revealed by petrographic analysis, decreases. This observation indicates that the petrographic texture of a limestone plays an important role in determining its performance as a sorbent for SO_2 removal under both calcining and noncalcining conditions (AFBC and PFBC). In the case of sulfation of calcined stones, analysis of the reactivity evolution data using detailed models for transport, reaction, and structure change in porous solids (Sotirchos and Zarkanitis, 1992) suggested that the petrographic texture of the precursor affects the connectivity of the pores, which appears to increase with decreasing grain size. For the case in which direct sulfation takes place, the limestone characteristics influence the structure of the resulting product layer and, hence, the effective diffusion coefficient through it. Hajaligol et al. (1988) also attributed the differences among the various limestones they considered to the natural porosity of the samples.

Limestone	Particle size (μm)	Surface Area (m^2/g)	Porosity (pores of radius $<$ 100 nm)
Greer Limestone	53-62	0.91	0.015
Georgia Marble	53-62	0.31	0.007
Iceland Spar	53-62	0.23	0.004

Table 3.2: Surface Areas and Porosities of Georgia Marble, Greer Limestone, and Iceland Spar Precursors.

The analysis of the sorption isotherm of a Greer limestone sample exposed to the reactive mixture for 1 min only showed (Fig. 3.10) that its cumulative porosity was much smaller than that of the unreacted precursor. Since the direct sulfation of calcium carbonate involves formation of a bulkier solid product (calcium sulfate), it may be argued that the apparent porosity of the solid decreases immediately upon reaction because some of the pores of the precursor are plugged with solid product. However, gas sorption experiments on Greer limestone precursors that were heat-treated under N_2 revealed a similar decrease in cumulative porosity (Fig. 3.10). The pore size distribution of the heat-treated precursor

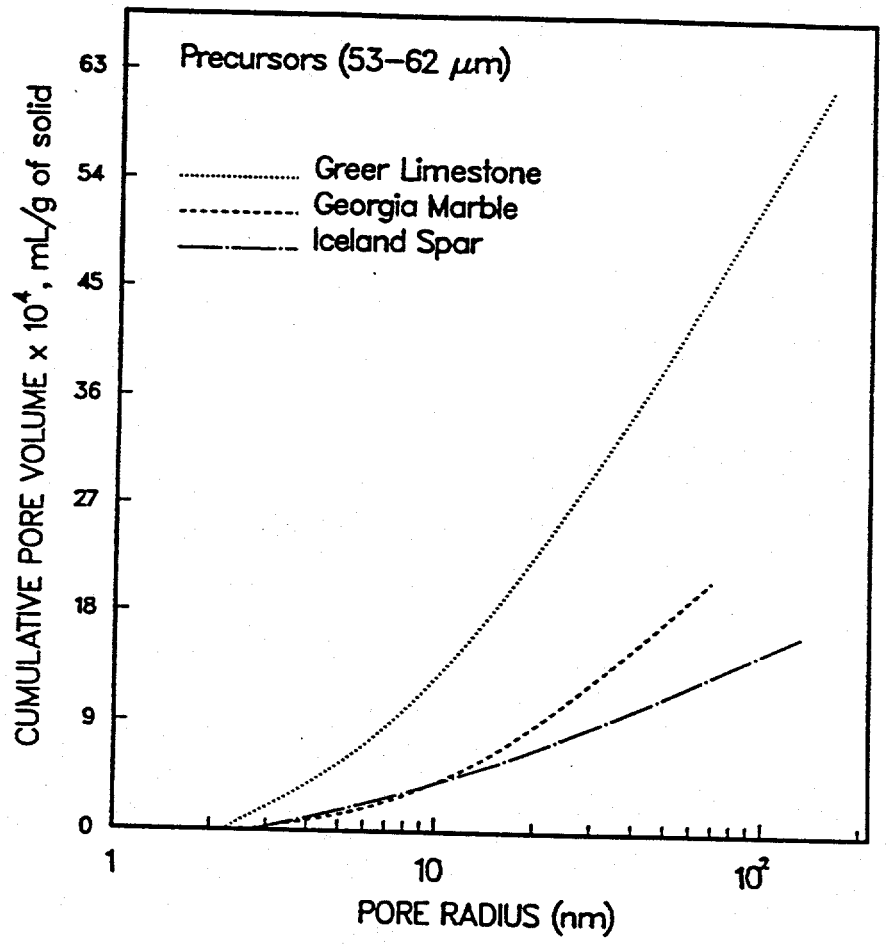

Figure 3.9: Cumulative pore volume vs. pore radius curves for the precursors obtained from N_2 sorption data.

was restored to its initial form after washing the sample in water and drying it in an oven at $150°C$. The last finding suggests that the main reason for the immediate decrease that the apparent cumulative porosity of Greer limestone undergoes during sulfation may be due to the exposure of the sample to high temperatures and not the formation of the solid product. Greer limestone contains 0.163% of P_2O_5 on a mass basis which has a melting point of 580-585$°C$ (Weast, 1987). During heat treatment at $850°C$, molten phosphorous pentaoxide may probably fill the interstitial space, blocking some of the pores and causing a reduction in apparent porosity. Washing with water dissolves the oxide and unplugs the pores, restoring the initial pore size distribution. A similar scenario was postulated by Huang and Daugherty (1988) in their attempt to explain the role of P_2O_5 in some of their results concerning the calcination of calcium carbonate solids. Heat treatment also affected the porosity of the Georgia marble sample, but it had practically no effect on Iceland spar. This behavior is in agreement with the postulated role of P_2O_5, since Georgia marble also contains P_2O_5, while Iceland spar contains very little.

Fig. 3.11 shows how the cumulative pore size distribution of Greer limestone changes with the conversion during sulfation at $850°C$ and 1500 mL/m^3 of SO_2 under noncalcining (70% CO_2) conditions. Partially reacted samples are seen to have smaller porosities than the original material at all conversions. The overall porosity tends to increase with increasing conversion, but the rate of increase appears to fall as the conversion increases. If it is assumed that the apparent pore size distribution of the unreacted material is the same as that of the heat treated sample of Fig. 3.10, the above result indicates that the average porosity of the reacted solid phase decreases with increasing conversion. The effect of conversion on the pore size distribution of the other two solids was qualitatively similar to that shown in Fig. 3.11 for Greer limestone. However, since the pore size distribution of these solids did not decrease as much at the outset of the process, the cumulative porosity varied less with the conversion. This behaviour may be seen in Fig. 3.12 which compares the original pore size distribution of Iceland spar with that of a 20% converted sample.

The $CaSO_4$ product of the 8% converted sample of Fig. 3.11 was removed by washing with water, and the remaining solid was dried in an oven at $150°C$. The weight of the washed solid was found to be in good agreement with that expected from the conversion

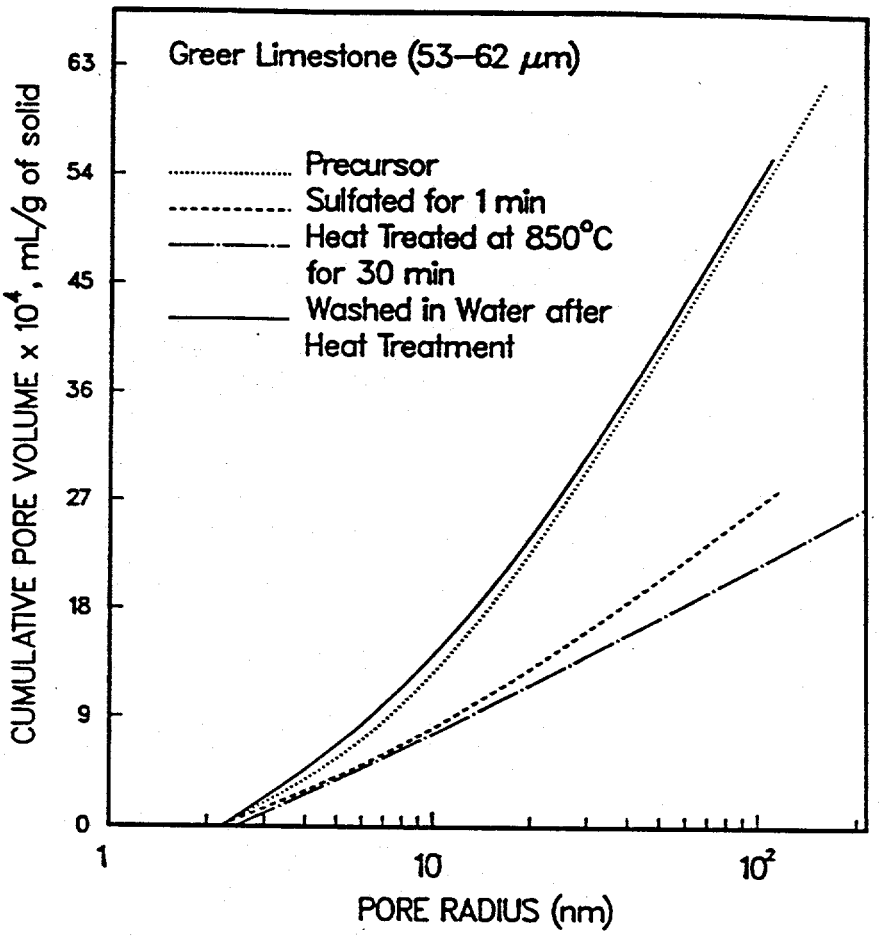

Figure 3.10: Effects of heat treatment and sulfation on the pore size distribution of Greer limestone. The sulfation was carried out in an atmosphere of 30% air (2% SO_2) and 70% CO_2 (mole %) at 850°C. The samples were heat treated in an atmosphere of 30% N_2 and 70% CO_2 (mole %).

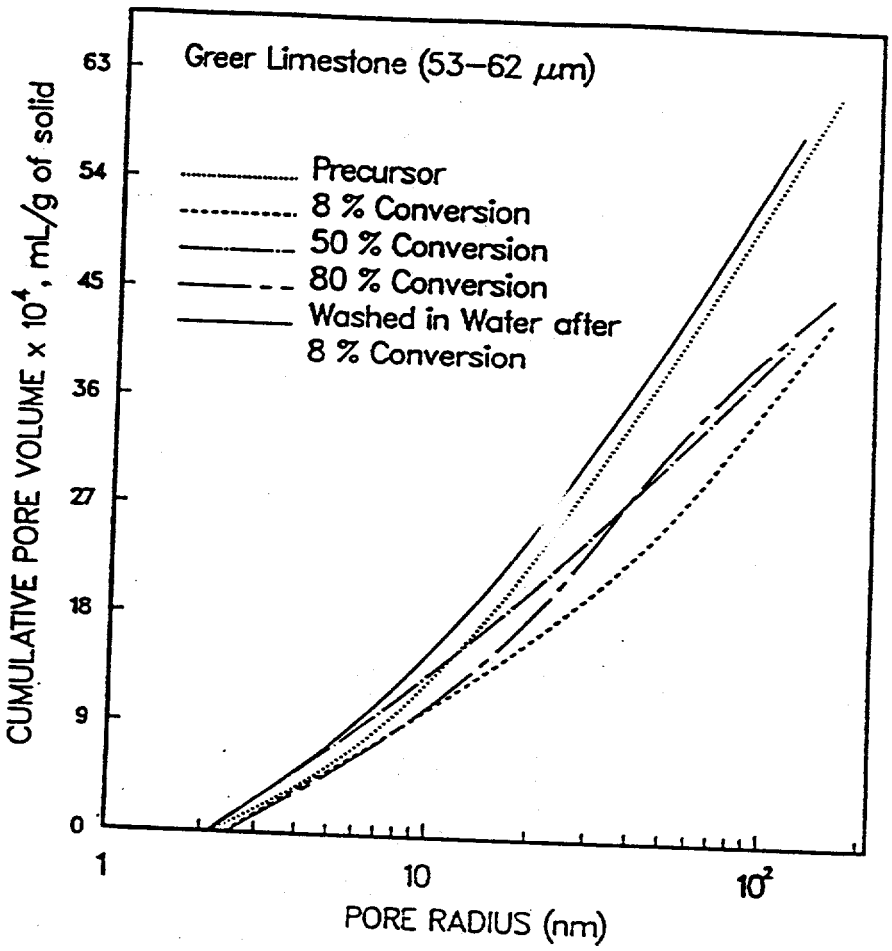

Figure 3.11: Effects of conversion on the pore size distribution of Greer limestone particles (53-62 μm). The sulfation was carried out in an atmosphere of 30% air (2% SO_2) and 70% CO_2 (mole %) at 850°C.

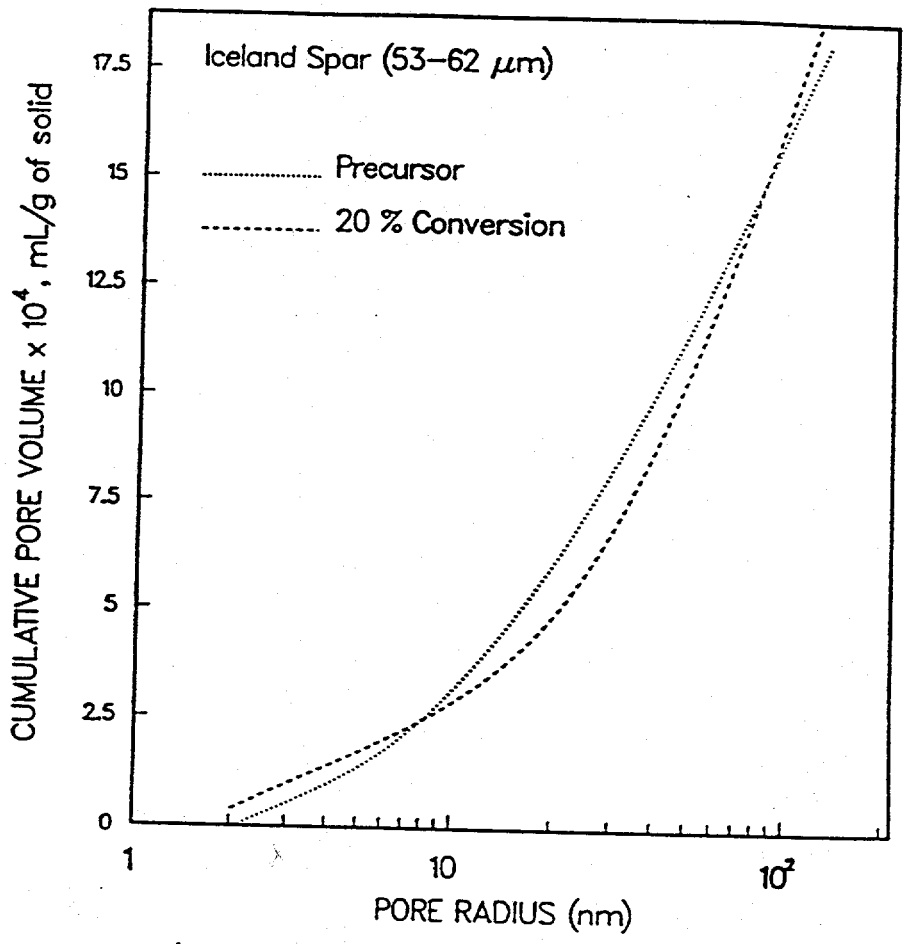

Figure 3.12: Effects of conversion on the pore size distribution of Iceland spar particles (53-62 μm). The sulfation was carried out in an atmosphere of 30% air (2% SO_2) and 70% CO_2 (mole %) at 850°C.

level, while gas sorption analysis (see Fig. 3.11) showed its pore size distribution to be almost the same as that of the original solid. This result offers a strong indication that the direct sulfation process proceeds in a shrinking-core fashion, in agreement with the scanning electron microsc ›y results of Hajaligol et al. (1988).

3.5. Discussion

Let the intrinsic reaction rate, expressed as mol/cm^2·s, be of the form $R_s = k_s c^n$, with c being the concentration of SO_2 at the reaction interface. The initial reaction rate data may be used to estimate the constant, k_s, and the order with respect to SO_2, n, of the intrinsic rate of the $CaCO_3 - SO_2$ reaction. Let a_0 be the initial particle size, c_s the concentration of SO_2 at the surface of the particle, and $\bar{R}_{obs}$ the observed overall reaction rate (mol/s). Because of the low porosity of the precursors, reaction at $t = 0$ will mainly take place on the external surface of the particle. Therefore, the initial rate observed experimenta'v, $\bar{R}_{obs}$, is directly proportional to the external surface area of the reacting particles anc ıence we can write:

$$\bar{R}_{obs} = 4\pi a_0^2 k_s c_s^n \tag{3.7}$$

The mass balance on SO_2 at the external surface of the particles requires that the following relationship be valid at all times:

$$\bar{R}_{obs} = 4\pi a^2 k_g (c_b - c_s) \tag{3.8}$$

with k_g being the mass transfer coefficient at the external surface of the particles, and c_b the concentration of SO_2 in the bulk. Equation (3.8) may be used to find the concentration of SO_2 at the surface of the particles at $t = 0$ needed for the estimation of k_s and n from equation (3.7). Use of standard cor ·lations for flow past freely suspended spheres (Bird et al., 1960) gives for all particle sizes used in our study a Sherwood number (Sh) of about 2 (based on diameter), that is, the value obtained for diffusion without flow around spherical particles. Since the particles are placed on the pan and are not uniformly exposed to the reactive mixture, this number should only be interpreted as an upper bound on the actual Sherwood number of the particles. However, when the mass transfer coefficient

for $Sh = 2$ is used in equation (3.8), it is found that even at the initial stages of the reaction – where the highest reaction rates are encountered – the concentration at the surface of the particles is practically identical to that in the bulk of the gas phase. At the conditions of our experiments, therefore, mass transfer from the bulk of the gas phase to the particles plays a minor role in the overall reaction process, and as a result, the exact value of Sherwood number – provided that is not much smaller than 2 – is immaterial for data analysis.

k_s and n can be obtained by linear regression on the logarithmic form of equation (3.7) with $c_s = c_b$. However, since for fixed particle size and reaction temperature, the initial rate of reaction is influenced only by the concentration of SO_2 (that is, by the order of reaction), a two-step procedure was employed to estimate n and k_s. It follows from equation (3.7) that for a given combination of particle size and temperature, the ratio of the initial reaction rates at the two concentrations used in our study must satisfy the equation:

$$\bar{R}_{obs}|_{1500\ mL/m^3} / \bar{R}_{obs}|_{6000\ mL/m^3} = (0.25)^n \tag{3.9}$$

The order of the reaction was estimated as the arithmetic mean of the six n values that are determined from equation (3.9) for each sorbent (three particle sizes and two temperatures). The n values that were estimated by this procedure for the three sorbents were very close to each other, and it was thus decided to use the same reaction order for all solids ($n = 0.4$), determined as the arithmetic mean of all n estimates. This value of n was then used to find k_s for each sorbent at each temperature as the arithmetic mean of the six values obtained from equation (3.7) (three particles and two concentrations).

The intrinsic reaction rate constants at the two temperatures of our experiments are given in Table 3.3. At least three independent measurements of the initial reaction rate for each combination of particle size, temperature, and concentration were employed to obtain each initial reaction rate value used to get the order of the reaction and the rate constants of Table 3.3. The rate constant decreases in the direction Greer limestone → Georgia marble → Iceland spar, that is, in the direction of decreasing overall reactivity, but the decrease is not enough to justify the observed overall reactivity differences. Hajaligol

et al. (1988) reported kinetic constants dependent on particle size, but such a trend was not evident in our results. The intrinsic reaction rate constant shows strong dependence on the temperature of the reaction, reflecting the strong influence of temperature on the conversion vs. time curves. Assuming Arrhenius-type dependence of the rate constants on temperature, the results of Table 3.3 yield 138.44 kJ/mol activation energy for Greer limestone, 109.73 kJ/mol for Georgia marble, and 113.57 kJ/mol for Iceland spar. In his study of sulfation of calcined samples of the same precursors, Zarkanitis (1991) determined activation energies of about 17.14 kJ/mol for all three solids. The higher values of activation energies of the direct sulfation reaction reflect the greater sensitivity of the kinetics of reaction (3.4) with respect to the reaction temperature than that observed for the reaction of CaO with SO_2 (reaction (3.6)).

Temp. (^oC)	Greer Limestone	Georgia Marble	Iceland Spar
750	9.06×10^{-6}	3.04×10^{-6}	2.28×10^{-6}
850	3.83×10^{-5}	9.53×10^{-6}	7.77×10^{-6}

Table 3.3: Reaction Rate Constant Values ($moles^{0.6}/cm^{0.8}\cdot s$) at 750 and 850$^oC$, n = 0.4.

Our pore structure characterization data (Fig. 3.11) suggested that the direct sulfation of limestones proceeds in a shrinking-core fashion. An attempt was thus made to analyze our conversion vs. time data using the shrinking-core model (Levenspiel, 1972; Szekely et al., 1976). However, the solid product formed during direct sulfation of limestones ($CaSO_4$) occupies more space than the solid it results from ($CaCO_3$). As a result, the particle size increases with increasing conversion, and it is necessary that this variation be accounted for in the shrinking- core model. Following the change of the particle size with the conversion requires knowledge of the volume of fully reacted solid per unit volume of unreacted solid, which in turn needs for its determination the porosities of the unreacted and fully reacted solids – and possibly their variation with the radial distance in the particle – and the volume of reacted dense solid phase per unit volume of unreacted dense solid phase (stoichiometric volume ratio, Z). Since the porosities of the three solids we used in

our study are very low in both unreacted and fully reacted form (see Figs. 3.9-3.12) and all solids have $CaCO_3$ as their main constituent, the volume of reacted solid per unit volume of unreacted solid in all cases can be approximated using the ratio of the molar volume of $CaSO_4$ to that of $CaCO_3$ (about 1.24).

With the intrinsic kinetics of the reaction and the mass transfer coefficient from the gas phase to the particles known, only the effective diffusion coefficient of SO_2 in the product layer is needed to apply the shrinking-core model to the experimental data. The predictions of the shrinking-core model are compared in Fig. 3.13 for three values of the effective diffusion coefficient of SO_2 in the reacted layer with the experimental data for 88-105 μm Greer limestone particles reacted at 850^oC. The results of Fig. 3.13 indicate that there is no effective diffusivity value that can bring the predictions of the shrinking-core model into agreement with the experimental data. The overall reaction rate decreases much faster with the extent of the reaction than what the shrinking-core model predicts. If the effective diffusive coefficient is chosen so that the experimental conversion matches the theoretical one at some reaction time, the model would give lower conversions below that time and overpredict the conversion past it. Results similar to those shown in Fig. 3.13 were obtained by applying the shrinking-core model to other precursors, particle sizes, and reaction temperatures.

The behavior seen in Fig. 3.13 suggests that the average resistance for mass transport in the product shell increases with the progress of the reaction. Therefore, the diffusion coefficient in the product shell must be varied with the progress of the reaction (that is, be decreased) in order to be able to reproduce the results using the shrinking-core model. The formation of a solid product that occupies more space that the solid reactant it replaces is most probably the main reason for the occurrence of this situation. Nascent solid product formed at the reaction interface at conversions different from zero has to push against a progressively thicker product layer to accommodate itself within the product shell. This in turn causes the density of the product layer to increase away from the external surface of the particles and the effective diffusion coefficient to decrease. This explanation is in qualitative agreement with the pore structure data, which, as we pointed out when we discussed the results of Fig. 3.11, suggest that the average porosity of the reacted solid

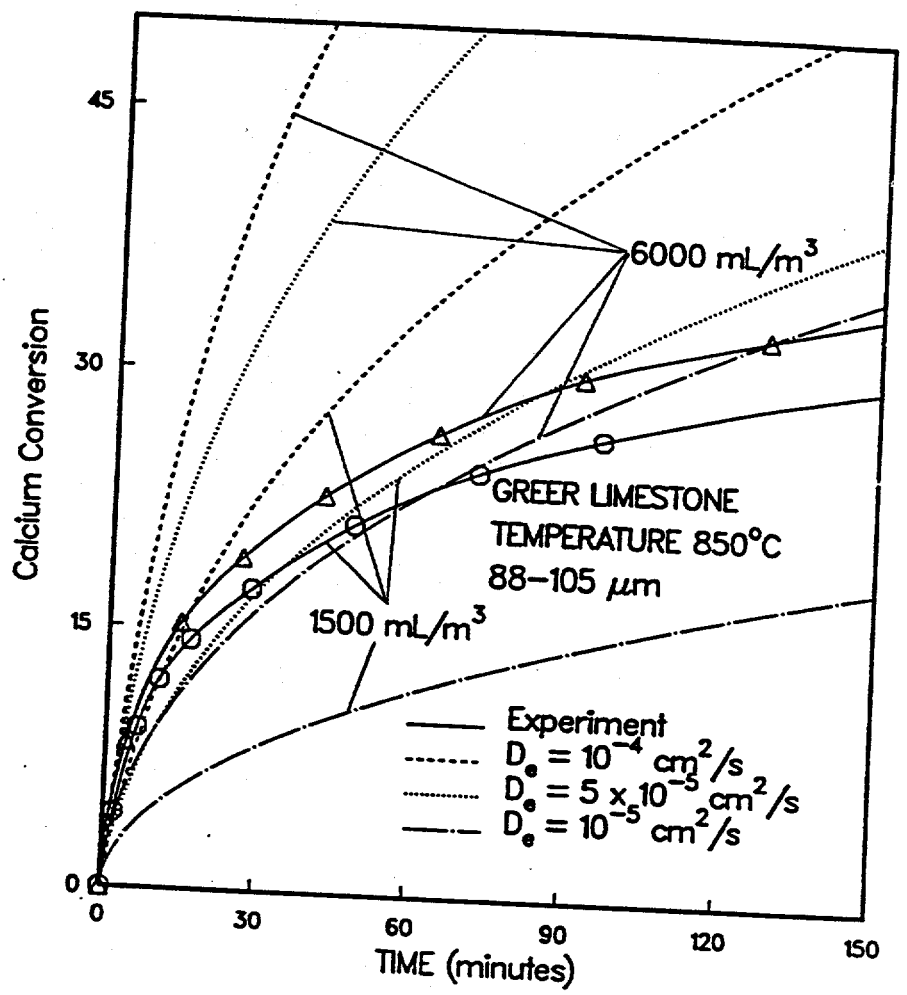

Figure 3.13: Comparison of the experimental data for 88-105 μm Greer limestone particles at 850^oC with the predictions of a shrinking core model for various effective diffusivities.

phase decreases with increasing conversion. It also agrees with the observed increase of the overall reactivity of the solids in the direction of increasing precursor porosity, in view of the fact that the average product layer porosity varies among the three precursors in the same way as their initial porosity (see Figs 3.11 and 3.12).

Hajaligol et al. (1988) reached a similar conclusion when they attempted to analyze their direct sulfation data using the shrinking-core model. They treated the average diffusion coefficient in the product layer as function of time (or, equivalently, of conversion) and determined its value at selected conversion levels by fitting the shrinking-core model predictions to the experimental data. The results they obtained showed some scattering but suggested the existence of a correlation between average effective diffusivity in the product layer and conversion. The experimental data that we obtained here are analyzed using a variable diffusivity shrinking-core model in another study (Krishnan and Sotirchos, 1993). Since the effective diffusivity is treated as a function of distance from the external surface of the particles, its functional form is determined through a parameter estimation procedure under the constraint that the diffusivity expression be the same for all particles of the same solid at the same reaction conditions.

3.6. Conclusions

The reaction between $CaCO_3$ and SO_2, which is of immense importance in a PFBC unit, was studied in depth in this work. Three types of limestones, each consisting of more than 95% $CaCO_3$ on a mass basis, were directly sulfated for this purpose. The sulfation of these stones were carried out in a TGA system in an atmosphere of 70% CO_2 to prevent the decomposition of $CaCO_3$ at the reaction temperatures of 750 and 850^oC. A broad range of particle size (53-350 μm) and two concentrations of SO_2 (1500 and 6000 mL/m^3) were employed in this investigation.

The particle size was found to have a strong influence on the conversion-time profile for all limestones under all reaction conditions indicating that the reaction was controlled by mass transport in the intraparticle space. Small Greer limestone particles tended to show a stronger influence of particle size on the conversion profile, but the larger size ranges were in agreement, quantitatively on a relative basis, with the profiles seen for the other

stones. Temperature was also found to strongly influence the conversion-time profiles for all stones, and the strong dependence of the conversion trajectory on the reaction temperature was noticeable throughout the duration of the experiment. This indicated that temperature had a strong impact on both the kinetics (the controlling factor during the initial stages of the reaction) and mass transport (the controlling factor during the later stages). The concentration of SO_2 had rather small effects on the conversion-time profile. The lack of aproportionate change in the reaction rate with the concentration of SO_2 in the bulk at either the earlier or the later stages of the reaction led us to conclude that the order with respect to SO_2 was different from unity and that the mass transport coefficient was a function of reactant concentration.

The conversion-time profiles for the $CaCO_3 - SO_2$ reaction that we obtained in this study were found to be markedly different from those for the $CaO - SO_2$ reaction obtained with the same limestones in an earlier investigation (Sotirchos and Zarkanitis, 1992). The $CaO - SO_2$ reaction proceeded much faster initially on account of a developed porous structure, but leveled off beyond certain exposure time or, equivalently, conversion, because of pore closure. On the contrary, the $CaCO_3 - SO_2$ reaction proceeded at a relatively lower rate during the initial stages of the process, but even after prolonged exposure times reacted at a significant rate. This rather striking difference between the two reactions has been attributed to a lower mass transport resistance offered by the product shell of the $CaCO_3 - SO_2$ reaction compared to that of the $CaO - SO_2$ reaction. A strong correlation between desulfurization capacity and initial porosity of the solids was observed, in agreement with a similar observation made by Hajaligol et al. (1988). Interestingly, the limestones showed the same order of performance as in the $CaO - SO_2$ reaction. The fact that the reactivity increased with decreasing grain size in the solid led us to conclude that the petrographic texture of limestones plays an important role in determining their capacity for SO_2 removal.

The structure of unreacted and partially reacted solids was analyzed using N_2 sorption and the results were used to study the changing morphology of the product layer. The measurements showed that both the fresh and partially reacted solids possessed very little porosity, and that the average porosity of the fully reacted part of the solid decreased with

increasing conversion or equivalently product layer thickness. Therefore, based on the ratio of molar volume of the solid product to that of the solid reactant, the change of $CaCO_3$ (the main reactant) to $CaSO_4$ (the main product) caused approximately a 25% change in volume. Furthermore, the pore structure results of unreacted solid and a solid washed with water after sulfation indicated that the direct sulfation of limestones proceeded in a shrinking-core fashion.

The initial reaction rates were used to determine the intrinsic reaction rate constant and the order of the reaction with respect to SO_2. The order of the reaction was found to be similar for the three different stones and an average value of 0.4 was estimated. The intrinsic reaction rate constant was found to decrease among the three solids in the same order as the overall reactivity but not enough to justify the drop in overall reactivity. The kinetic data were used in a shrinking-core model with constant effective diffusivity in the product shell, but this simple model failed to bring any agreement between theory and experiment. It was observed that an increasing mass transport resistance through the product layer was needed to yield agreement between model predictions and experimental results. Therefore, a variable diffusivity shrinking- core model must be employed to describe the direct sulfation of limestones. The increase in the average resistance for mass transport in the product layer with increasing conversion is most probably caused by the formation of denser product layer away from the external surface of the particles.

3.7. Notation

a	outer radius of the particle, cm
a_0	initial radius of the particle, cm
c_b	concentration of SO_2 in the bulk, mol/mL
c_s	concentration of SO_2 at the surface of the particle, mol/mL
D_m	molecular diffusivity of SO_2-gas mixture, cm^2/s
D_e	effective diffusivity of SO_2 in the product layer, cm^2/s
k_g	external mass transfer coefficient, cm/s
k_s	intrinsic reaction rate constant, $mol^{0.6}/cm^{0.8} \cdot s$
n	order of reaction with respect to SO_2

$\bar{R}_{obs}$ observed overall reaction rate, mol/s

R_s intrinsic reaction rate, $mol/cm^2 \cdot s$

Sh Sherwood number, $2k_g a/D_m$

t real time, s

Z volume of dense reacted solid phase per unit volume of dense unreacted solid phase

3.8. Literature References

Bird, R.B.; Stewart, W.E., Lightfoot E.N., *Transport Phenomena*, John Wiley & Sons, New York (1960).

Borgwardt, R.H.; Harvey, R.D.,"Properties of Carbonate Rocks Related to SO_2 Reactivity," Environ. Sci. Technol., **6**, 350-360 (1972).

Bulewicz, E. M.; Kandefer S.; Jurys C.,"Desulphurization during the Fluidized Combustion of Coal using Calcium-based Sorbents at Pressures up to 600 kPa," J. Inst. Energy, **59** 188-195 (1986).

Chen, W.T., Private Communication, Illinois State Geological Survey (1990).

Dennis, J.S.; Hayhurst, A.N.,"The Effect of Pressure on the Kinetics and Extent of Sulphation of Calcareous Materials," Inst. Chem. Eng. Symp. Ser., **87**, 61-68 (1984).

Dennis, J.S.; Hayhurst, A.N., "The Effect of CO_2 on the Kinetics and Extent of Calcination of Limestone and Dolomite Particles in Fluidised Beds," Chem. Eng. Sci., **42**, 2361-2372 (1987).

Fox, E.C.; Krishnan, R.P.; Daw C.S.; Jones, J.E., Jr., " A Review of Fluidized-bed Combustion Technology in the United States," Energy, **11**, 1183-1200 (1986).

Gullett, B.K.; Bruce, K.R., "Pore Distribution Changes of Calcium-based Sorbents Reacting with Sulfur Dioxide," AIChE J., **33**, 1719-1786 (1987).

Hajaligol, M.R.; Longwell, J.P.; Sarofim, A.F., "Analysis and Modeling of the Direct Sulfation of $CaCO_3$," Ind. Eng. Chem. Res., **27**, 2203-2210 (1988).

Hartman, M.; Coughlin, R.W., "Reaction of Sulfur Dioxide with Limestone and the Influence of Pore Structure," Ind. Eng. Chem. Process Dec. Dev., **13**, 248-253 (1974).

Hartman, M.; Coughlin, R.W., "Reaction of Sulfur Dioxide with Limestone and the Grain Model," AIChE J., **22**, 490-498 (1976).

Hoke, R.C.; Bertrand, R.R.; Nutkis, M.S.; Kinzler, I .D.; Ruth, L.A., "Studies of the Pressurized Fluidized-bed Coal Combustion Process," Technical Report EPA-600/7-77-107, (September 1977).

Hoy, H.R.; Roberts, A.C.; Phillips, R.N.; Carpenter, L.K., "Performance of a Small Combustor at Pressures up to 20 Bar," Proc. Int. Conf. Fluid. Bed Combust., **7**, 473-481 (1982).

Huang, J-M; Daugherty, K.E., "Inhibition of the Calcination of Calcium Carbonate," Thermochim. Acta, **130**, 173-176 (1988).

Jansson, S.A.; O'Connell, L.P.; Stantan, J.E., "Effect of Carbon Dioxide Pressure on Desulfurization in Coal Fired PFBC Systems," Proc. Int. Conf. Fluid. Bed Combust., **7**, 1095-1100 (1982).

Krishnan, S.V., "Mass Transport of Gases in Porous Media of Evolving Morphology. Application to Desulfurization of Flue and Coal Gases. Ph.D. Thesis, University of Rochester (1993).

Krishnan, S.V.; Sotirchos, S.V., "A Variable Diffusivity Shrinking-Core Model and its Application to the Direct Sulfation of Limestones," Can. J. Chem. Eng., **71**, 734-745 (1993).

Levenspiel, O., *Chemical Reaction Engineering*, John Wiley & Sons, New York (1972).

Ljungstrom, E., Lindqvist, O., "Measurements of In-bed Gas and Solid Compositions in a Combustor Operating at Pressures up to 20 Bar," Proc. Int. Conf. Fluid. Bed Combust., **7**, 465-472 (1982).

METC, "Pressurized Fluidized-Bed Combustion. Technology Status Report," DOE/METC-86/0235, Morgantown, West Virginia (1984).

Murthy, K.S.; Howes, J.E.; Nack, H.; Hoke, R.C., "Emissions from Pressurized Fluized-bed Combustion Processes," Environ. Sci. Technol., **13**, 197-204 (1979).

Newton, G.H.; Chen, S.L.; Kramlich, J.H., "Role of Porosity Loss in Limiting SO_2 Capture by Ca-based Sorbents," AIChE J., **35**, 988-994 (1989).

Simons, G.A.; Garman, A.R., "Small Pore Closure and the Deactivation of the Limestone Sulfation Reaction," AIChE J., **32**, 1491-1499 (1986).

Smith, D.; Anderson, J.S.; Atkin, J.A.R.; Bekofske, K.L.; Brown, R.A.; Cavanna, J.; Christianson, S.; Failing, K-H; Friedman, M.A.; Glenn, J.C.; Hebden, D.J.; Mainhardt, P.J.; Schuetz, M.; Wheeldon, J.M.; Carls, E.L., "IEA Grimethorpe 2m × 2m Pressurised Fluidised Bed Combustion Project - Experimental Performance Results and Future Plans," Proc. Int. Conf. Fluid. Bed Combust., **7**, 439-452 (1982).

Snow, M.J.H., Longwell, J.P.; Sarofim, A.F., "Direct Sulfation of Calcium Carbonate," Ind. Eng. Chem. Res., **27**, 268-273 (1988).

Sotirchos, S.V.; Zarkanitis, S., "Inaccessible Pore Volume Formation during Limestone Sulfation," to appear in AIChE J., **38**, 1536-1550 (1992).

Stantan, J.E., Barker, S.N.; Wardell, R.V.; Ulerich, N.H.; Keairns, D.L., "Calcination of Limestones in Pressurised Fluidised-bed Combustors," Proc. Int. Conf. Fluid. Bed Combust., **7**, 1064-1075 (1982).

Szekely, J.; Evans, J.E.; Sohn, H.Y., *Gas-Solid Reactions*, Academic Press, London (1976).

Tullin, C.; Ljungstrom, E., "Reaction between Calcium Carbonate and Sulfur Dioxide," Energy & Fuels, **3**, 284-287 (1989).

Ulerich, N.H; O'Neill, E.P.; Keairns, D.L., "The Influence of Limestone Calcination on the Utilization of the Sulfur-Sorbent in Atmospheric Pressure Fluid-Bed Combustors," EPRI FP-426, Final Report, Westinghouse Electric Corp., Pittsburgh, Pennsylvania (1977).

Van Houte, G.; Rodrique, L.; Genet, M.; Delmon, B., "Kinetics of the Reaction of Calcium Sulfite and Calcium Carbonate with Sulfur Dioxide and Oxygen in the Presence of Calcium Chloride," Environ. Sci. Technol., **15**, 327-332 (1981).

Weast, R.C., Ed., *CRC Handbook of Chemistry and Physics*, 68th ed., Chem. Rub. Publ. Co., Boca Raton, Florida (1987).

Wen, C.Y.; Ishida, M., "Reaction Rate of Sulfur Dioxide with Particles Containing Calcium Oxide," Environ. Sci. Technol., **7**, 703-708 (1973).

Yu, H.C., "Theoretical and Experimental Studies on Gas-Solid Reactions with Solid Product," Ph.D Thesis, University of Rochester (1987).

Zarkanitis, S., "Pore Structure and Reactivity Evolution during Limestone Sulfation," Ph.D. Thesis, University of Rochester (1991).

Zarkanitis, S.; Sotirchos, S.V., "Pore Structure and Particle Size Effects on Limestone Capacity for SO_2 Removal," AIChE J., **35**, 821-830 (1989).

4. A VARIABLE DIFFUSIVITY SHRINKING-CORE MODEL AND ITS APPLICATION TO THE DIRECT SULFATION OF LIMESTONES

4.1. Introduction

In an earlier investigation (Krishnan and Sotirchos, 1993), we carried out an extensive study of the direct reaction of high purity limestones with SO_2 under various reaction conditions in a thermogravimetric analyzer (TGA). Reactivity experiments were performed at atmospheric pressure in the presence of CO_2 in order to inhibit the decomposition of $CaCO_3$ and, thereby, simulate conditions met in pressurized fluidized-bed combustion (PFBC) units. Various interesting results concerning the influence of particle size, temperature, and concentration were obtained in that study. Analysis of the initial reactivity data yielded a value of 0.4 for the order of the reaction with respect to SO_2 and enabled us to obtain values for the intrinsic rate constant of the $CaCO_3 - SO_2$ reaction for two temperatures and three limestone precursors.

One of the most interesting observations from our earlier study was that the rate of the direct sulfation of limestones (limestone-SO_2 reaction) could be larger at high conversion levels than that of the sulfation of the corresponding calcines ($CaO - SO_2$ reaction), in qualitative agreement with similar observations made by Snow et al. (1988) and Tullin and Ljungstrom (1988). Since at high conversion levels, the reaction rate is primarily controlled in both cases by diffusion of SO_2 through the product layer (mainly $CaSO_4$), a major conclusion arrived at on the basis of the above finding was that the product layer exhibits lower diffusional resistance in the case of direct sulfation.

In order to gain better insight into the overall mechanism of the direct sulfation of limestones, mercury penetration porosimetry and gas sorption were used to characterize the pore structure of precursors and partially reacted samples. Because of very small mercury penetration volumes and, consequently, large relative errors in the interpretation of mercury penetration data, only the gas sorption data (N_2 at 77 K) were used to extract quantitative information on the pore structure of the solids (for pores smaller than about 200 nm in diameter). Our measurements showed that both the fresh (unreacted) and partially reacted solids possessed very small porosity (smaller than 1.5%) and that the

average porosity of the fully reacted part of the solid decreased with increasing conversion or, equivalently, product layer thickness. Moreover, characterization of the pore structure of samples in which the reacted solid had been removed by washing in water suggested that the reaction proceeded in a shrinking-core fashion. Qualitatively similar conclusions were reached by Hajaligol et al. (1988) from mercury porosimetry and scanning electron microscopy measurements on partially reacted solids.

An attempt was made to reproduce the experimentally observed behavior using a shrinking-core model with constant diffusivity in the product layer, but it failed. Specifically, a comparison of model predictions and experimental data showed that the overall reaction rate in the experimental data fell more rapidly with the reaction time (or, equivalently, the conversion of the solid), especially during the initial stages of the reaction, than what the shrinking-core model predicted, indicating that the average resistance for mass transport in the product shell increased with the progress of the reaction. This result and the results from our pore structure characterization experiments led us to conclude that because of the formation of a solid product ($CaSO_4$) that occupies more space than the solid reactant ($CaCO_3$) – about 25% more – and the presence of the product shell around the unreacted core, progressively denser layers of solid product are formed during reaction away from the external surface of the particles. Therefore, an effective diffusion coefficient that decreases with the distance from the external surface of the particles should be used in the shrinking-core to reproduce the behavior seen in the experimental data. A similar conclusion led Hajaligol et al. (1988) to use a conversion dependent diffusivity in the shrinking-core model in order to reproduce their experimental data. Good agreement between model predictions and experimental data was observed by these investigators. However, aside from assuming uniform effective diffusivity in the product layer, their assumption that the variation of the effective diffusivity with conversion was independent of the particle size is difficult to justify on physical grounds inasmuch as the same conversion level corresponds to significantly different product layer thicknesses for different size particles.

A variable diffusivity shrinking-core model is developed and used in this study to analyze the experimental data obtained by Krishnan and Sotirchos (1993) for the reaction

of SO_2 with limestones under simulated PFBC conditions. The effective diffusivity in the product layer is assumed to vary with the distance from the external surface of the particles, and a parameter estimation procedure is developed to handle the ill-posed numerical problem that arises when one tries to extract the effective diffusivity as a distributed parameter from the experimental data.

4.2. Model Equations and Parametric Sensitivity

The physical picture that needs to be mathematically modeled for the direct sulfation of limestones involves a shrinking core of unreacted material surrounded by an expanding shell of reacted solid. At the interface, gas A and solid S react to produce solid P according to the reaction

$$A + S + ... \rightleftharpoons P + ... \tag{4.1}$$

where ... stands for other gaseous species that may participate in the reaction but do not have to be considered to describe the process. In the case of limestone sulfation, the overall chemical reaction has the form

$$CaCO_3 + SO_2 + 1/2O_2 \rightleftharpoons CaSO_4 + CO_2 \tag{4.2}$$

Several sources of the literature (e.g., Szekely et al. (1976) and Levenspiel (1972)) describe models involving the above general features, and thus, we will provide details only for the most important aspects of the model that is developed here.

Assuming isothermal conditions and pseudosteady-state for the concentration profile of the gaseous reactant (SO_2 in the case of limestone sulfation), a mass balance on the gaseous reactant yields

$$(1/r^s)\frac{\partial}{\partial r}(r^s D_e(r)\frac{\partial c}{\partial r}) = 0 \tag{4.3}$$

s is the particle shape factor (0: slab; 1: cylinder; 2: sphere), c is the concentration of the reactive species in the product layer, and $D_e(t,r)$ is the effective diffusivity in the product layer varying in time, t, and locally along the radial direction, r. At the external surface of the particles, we have the boundary condition

$$D_e(r,t)(\partial c/\partial r)|_{r=a} = k_g(c_b - c_s) \tag{4.4}$$

k_g is the external mass transfer coefficient, c_b the bulk concentration of SO_2, c_s the concentration of SO_2 at the external surface of the particle, and a the size of the particle. In our previous study, it was found that even for the highest reaction rates measured in our experiments, c_s was practically equal to c_b even when the Sherwood number (Sh) was given values much lower than 2, the value corresponding to spherical particles exposed to a stagnant environment. Therefore, for all practical purposes Eq. (4.4) can be replaced by

$$c|_{r=a} \equiv c_s = c_b \tag{4.5}$$

At the reaction front ($r = a_c$), a mass balance on the gas gives

$$D_e(r,t)(\partial c/\partial r)|_{r=a_c} = R_s(c_c) \tag{4.6}$$

whereas a mass balance on the solid leads to

$$da_c/dt = -v_s R_s(c_c) \tag{4.7}$$

v_s is the volume of unreacted core per mole of solid reactant, c_c is the concentration at the reaction front, and $R_s(c)$ is the reaction rate per unit surface area, which is assumed to be related to the concentration at the reaction front by the equation

$$R_s(c) = k_s c^n \tag{4.8}$$

k_s is the intrinsic reaction rate constant, and n the order of the reaction with respect to reactant A (SO_2). Before reaction starts (i.e., at time zero), we obviously have

$$a = a_c = a_0 \tag{4.9}$$

with a_0 being the initial size of the particle.

The conversion of the solid is related to the core size by the obvious equation

$$X = 1 - (a_c/a_0)^{s+1} \tag{4.10}$$

An equation relating a, a_c, and a_0 is obtained from an overall balance on the solid reactant. Let ϵ_0 be the porosity of the unreacted solid and $\epsilon(r,t)$ the porosity of the product shell at position r and time t. Then we have

$$Z({a_0}^{s+1} - {a_c}^{s+1}) = (1/1-\epsilon_0)\int_{a_c}^{a}(1-\epsilon(r,t))dr^{s+1} \tag{4.11}$$

Z is the stoichiometric volume ratio of the solid product-solid reactant system, that is, the volume of reacted solid phase per unit volume of unreacted solid phase. If the unreacted solid phase consists of solid reactant only, then Z is equal to the ratio of the molar volume of solid product to the molar volume of solid reactant. This value can also be used for solids that contain very small amounts of inert solids, like the three limestones used to obtain the results reported in our previous study. For the direct sulfation of $CaCO_3$, Z is equal to 1.24 (based on densities for $CaSO_4$ and $CaCO_3$ given in Perry et al. (1984)). For very small values of ϵ_0 and $\epsilon(r,t)$ – as it was found to be the case for the limestones used in our direct sulfation experiments – Eq. (4.11) can be simplified to

$$a^{s+1} = Z{a_0}^{s+1} + (1-Z){a_c}^{s+1} \tag{4.12}$$

Integration of Eq. (4.3), using Eqs. (4.5) and (4.6) as boundary conditions, yields

$$\int_{a_c}^{a} (1/D_e(r,t)r^s)dr = (c_b - c_c)/{a_c}^s R_s(c_c) \tag{4.13}$$

With the kinetics of the reaction (i.e., the form of $R_s(c)$) and $D_e(r,t)$ known, Eqs. (4.7), (4.10), (4.12) (or (4.11) given ϵ_0 and $\epsilon(r,t)$), and Eq. (4.13) canbe solved numerically to determine the evolution of the conversion with time. In the application of the mathematical model to the direct sulfation of limestones, it will be assumed that D_e is determined only by the distance from the external surface of the particles, x, i.e.,

$$D_e(r,t) = D_e(a(t)-r) \equiv D_e(x);\ x = a - r \tag{4.14a,b}$$

Some results regarding the dependence of the model predictions on the model parameters are shown in Fig. 4.1 for $D_e(x) = \alpha\exp(-\beta x)$. The results shown in the figure are for sulfation of 53-62 μm limestone particles of spherical shape ($s = 2$) at 850^oC with 1500 mL/m^3SO_2. The reaction rate was assumed to be given by Eq. (4.8), and the various combinations of n and k_s were chosen so that the initial reaction rate (${k_s}{c_b}^n$) was the same for all cases and similar in value to the rate measured by Krishnan and Sotirchos (1993) for Iceland spar at 850^oC and 1500 mL/m^3SO_2. Therefore, differences among the various curves of Fig. 4.1 are solely due to the existence of diffusional limitations in the product shell.

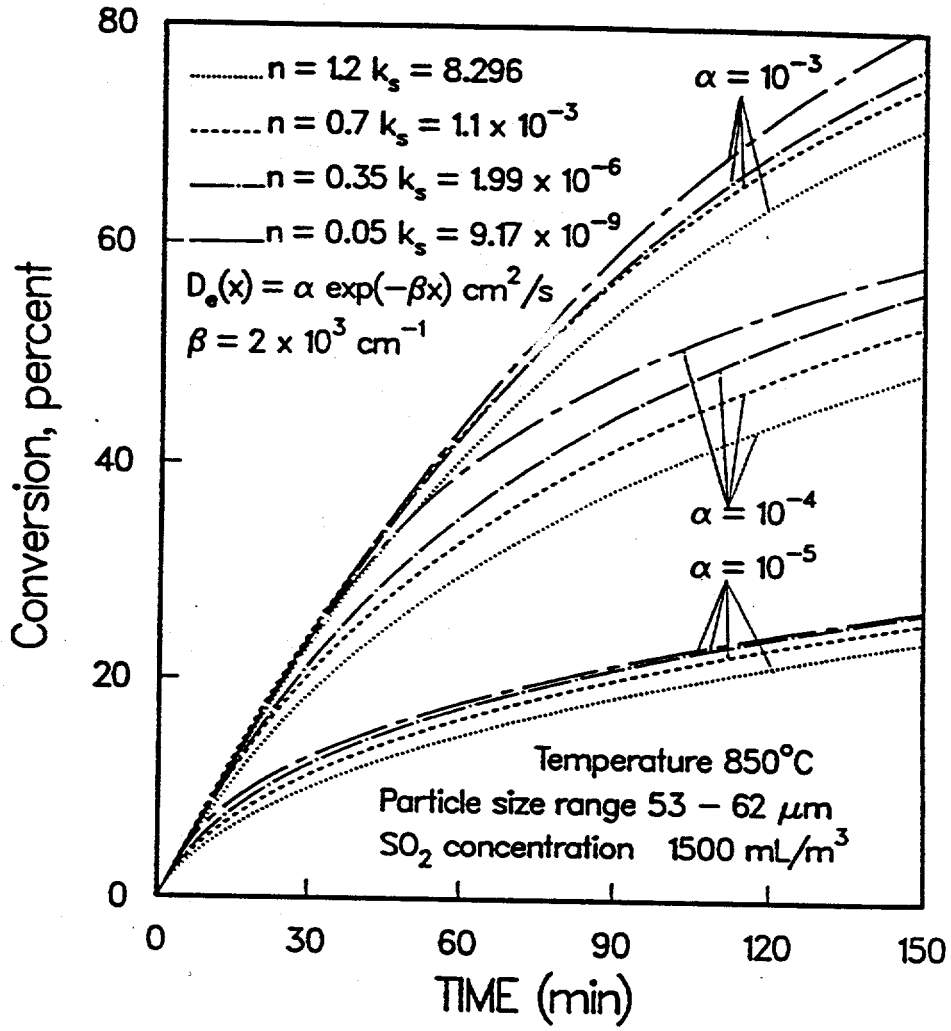

Figure 4.1: Conversion-time trajectories predicted by the variable diffusivity shrinking-core model for several forms of effective diffusivity varying exponentially along the product layer for identical kinetics. Results shown are for sulfation of spherical ($s = 2$) particles (53-62 μm) at 850°C and 1500 mL/m^3 of SO_2. The units of k_s are $mol^{0.6}/cm^{0.8} \cdot s$.

As expected, lowering the value of α (i.e., the effective diffusivity at the external surface of the particles) causes a proportionate change to the value of effective diffusivity at all depths and slows the overall reaction. For higher vales of α (in other words, lower diffusional resistance), the kinetics of the reaction controls the process until the shell thickness becomes large enough to effect significant diffusional limitations. Thus, notice that there is confluence of all curves (for different combinations of n and k_s) for $\alpha = 10^{-3} cm^2/s$ up to nearly 20% conversion, whereas the four curves diverge from each other much earlier for $\alpha = 10^{-5} cm^2/s$.

Parameter β dictates how the effective diffusivity falls with distance in the product shell, and therefore, how the average resistance for diffusion in the product layer increases with the product layer thickness. A value of $\beta = 0$ was employed in our previous study, but, as we have already mentioned, it failed bring any agreement between theory and experiment. Nonzero values of β cause the overall rate of reaction to decrease faster with time, and our computations revealed that this effect can be intensified by increasing β. Therefore, the variable diffusivity shrinking-core is capable of describing, at least qualitatively, the behavior seen in our experimental data.

It can be shown using the model equations that for a diffusion coefficient varying according to Eq. (4.14), the variation of the product layer with time for slab geometry particles (s=0) is independent of the particle size. This is also approximately valid for other geometries (spherical or cylindrical particles) for relatively small product layer thickness, that is, before the curvature of the particles (see Eqs. (4.11), (4.12), and (4.13)) starts to influence significantly the predictions of the mathematical model. Product layer thickness, d, vs. time curves can be constructed from experimentally measured conversion vs. time profiles by using Eqs. (4.10) and (4.12) to compute a and a_c (and hence $d = a - a_c$) at each conversion level. This procedure was applied to our experimental data, and Fig. 4.2 presents the variation of the product layer thickness with time for three sizes of Iceland spar particles reacted at $850°C$ under 1500 mL/m^3 of SO_2. In order to get the results of Fig. 4.2, the particles were assumed to be of spherical geometry, in which case $d = a_0[(Z + (1 - Z)(1 - X))^{1/3} - (1 - X)^{1/3}]$. This geometry was also employed for all other results we will present in this study.

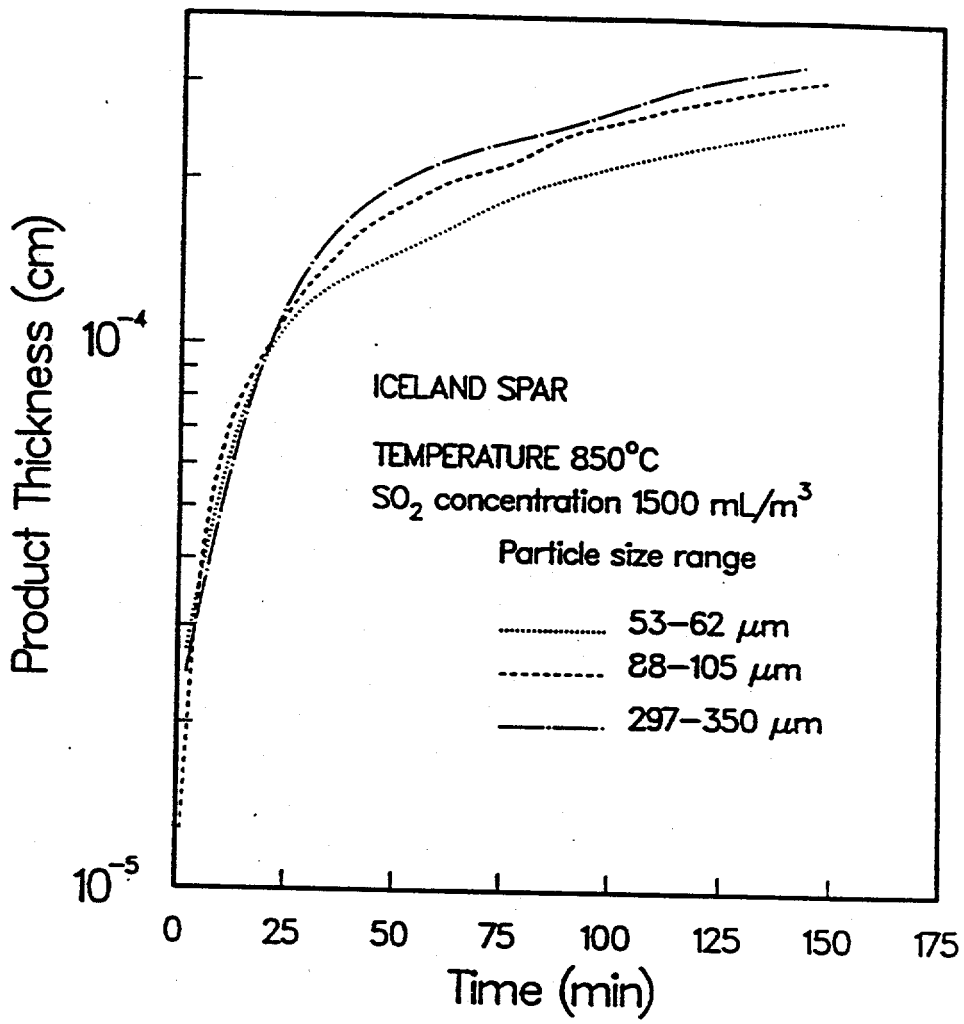

Figure 4.2: Development of product layer thickness for Iceland spar sulfated directly at $850°C$ and 1500 mL/m^3 of SO_2 in an atmosphere of 70% $CO_2(mol\%)$.

The results of Fig. 4.2 show that the product layer has the same thickness at a given time for all particle sizes during the initial stages of the reaction, thus supporting our assumption that the variation of the diffusivity is given by Eq. (4.14). Significant differences among the three d vs. t curves appear only as the product layer thickness increases, and curvature starts to influence significantly the behavior of small particles. Qualitatively similar results to those shown in Fig. 4.2 were obtained from the experimental data for all other cases involving Iceland spar and Georgia marble particles. The product layer also developed at the same rate during the initial stages of the reaction of the 88-105 and 297-350 μm particle size ranges of Greer limestone samples, but 53-62 μm particles of this solid tended to react much faster. This behavior can be seen in Fig. 4.3 which presents product layer thickness vs. time curves for Greer limestone particles reacted at $850°C$ under 1500 mL/m^3 of SO_2. Lack of confluence between the smallest particle size range and the other two size ranges was seen at all reaction conditions for the Greer limestone sample. A similar behavior was observed in sulfation data of calcined samples of the same solid (Sotirchos and Zarkanitis, 1992).

All these results indicate that the small Greer limestone particles react differently from all other samples used in our experiments. The origins of this difference in behavior most probably lie in the different petrographic texture of the three solids. As it was pointed out in previous studies (Zarkanitis and Sotirchos, 1992; Krishnan and Sotirchos, 1993), petrographic characterization revealed that whereas Georgia marble and Iceland spar exist in the form of coarse, mm-size calcitic grains and large single crystals, respectively, the structure of Greer limestone is spanned by small calcitic grains, a few μm in size. For the particle sizes used in our experiments, therefore, each Georgia marble or Iceland spar particle is essentially part of a single grain, while each Greer limestone particle is an aggregate of small grains. Since the small Greer limestone particles are only a few grains thick, the mechanical stresses that are developed in their interior by the formation of a bulkier solid product could cause movement of the individual grains relative to each other and particle expansion. This in turn would reduce the average resistance for diffusion in the intraparticle space and lead to larger conversions than those expected from the behavior of larger particles.

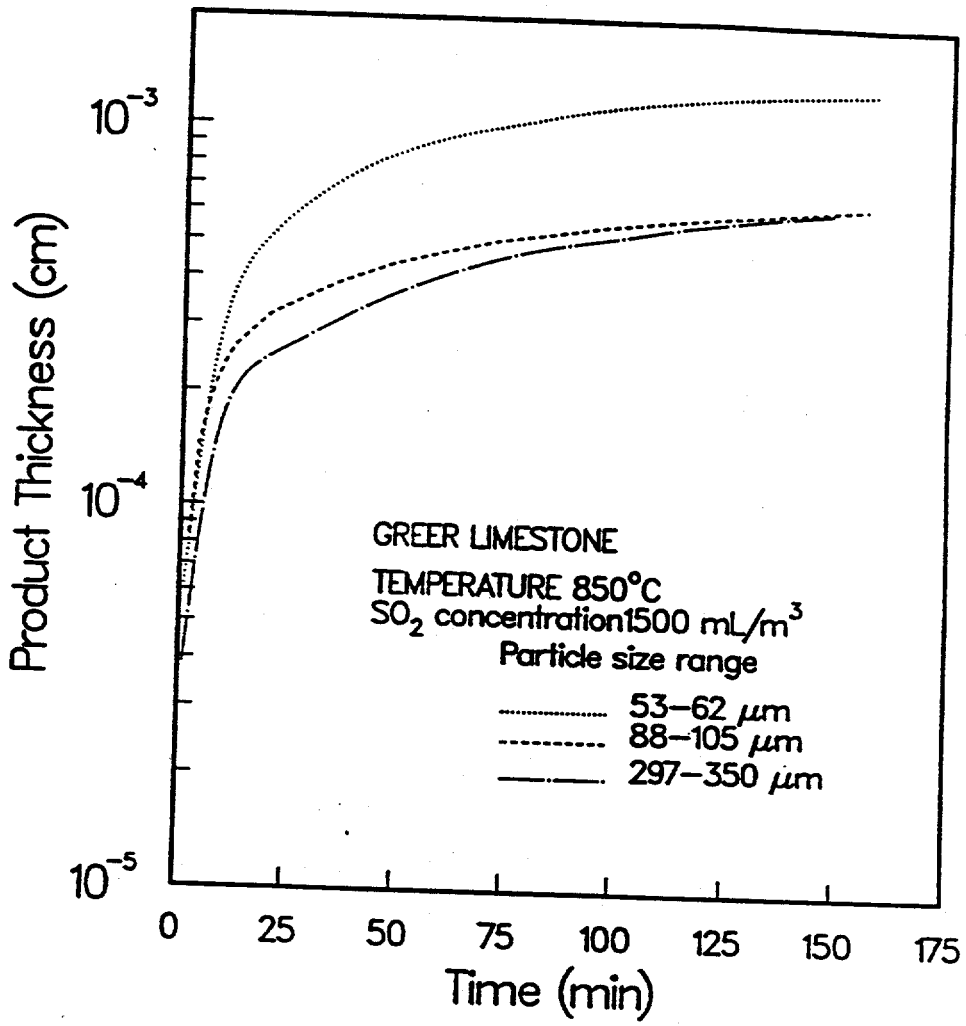

Figure 4.3: Development of product layer thickness for Greer limestone sulfated directly at 850°C and 1500 mL/m^3 of SO_2 in an atmosphere of 70% $CO_2(mol\%)$.

It follows from Eq. (4.7) that a similar growth rate for the product layer implies similar reactant concentrations at the reaction front. Fig. 4.4 gives reactant concentration at the interface (c_c) vs. time curves obtained from the experimental conversion vs. time data for Greer limestone particles reacted at $750°C$ and 6000 $mL/m^3 SO_2$. The conversion values were converted to concentration by using Eq. (4.10) to compute a_c, differentiating the $a_c(t)$ function to get (da_c/dt), and solving Eq. (4.7) to find c_c. IMSL routines CSAKM and CSDER, based on a method by Akima (1970), were used to compute the derivative from the values of a_c at the sampling time instants. The k_s and n values for each solid were those obtained from the initial reaction rate data in our previous study and are listed in Table 4.1. In agreement with the results of Fig. 4.3, it is seen that the concentration of SO_2 at the reaction front has similar values for the two larger sizes. However, the concentration for the 53-62 μm particles is much higher than that of the other two size ranges, implying the existence of a much smaller resistance for diffusion in the product layer of the small particles. The different behavior of the small Greer limestone particles will be discussed in more detail during the analysis of our experimental data using the variable diffusivity shrinking-core model.

Rate Constant $(mol^{0.6}/cm^{0.8} \cdot s)$			
Temp. $(°C)$	GL	GM	IS
750	9.06×10^{-6}	3.04×10^{-6}	2.28×10^{-6}
850	3.83×10^{-5}	9.53×10^{-6}	7.77×10^{-6}

Table 4.1: Reaction Kinetics at 750 and 850°C, n = 0.4. GL=Greer limestone, GM=Georgia Marble, and IS=Iceland Spar.

4.3. Parameter Estimation Procedure

The order of the reaction with respect to SO_2, n, and the intrinsic reaction rates, k_s, have been estimated by Krishnan and Sotirchos (1993), and the procedure used for their estimation is described in detail there. The stoichiometric volume ratio, Z, can be estimated from the composition of the precursor, but for high purity stones – as it is the case here – it can be approximated by the ratio of the molar volumes of $CaSO_4$ to $CaCO_3$

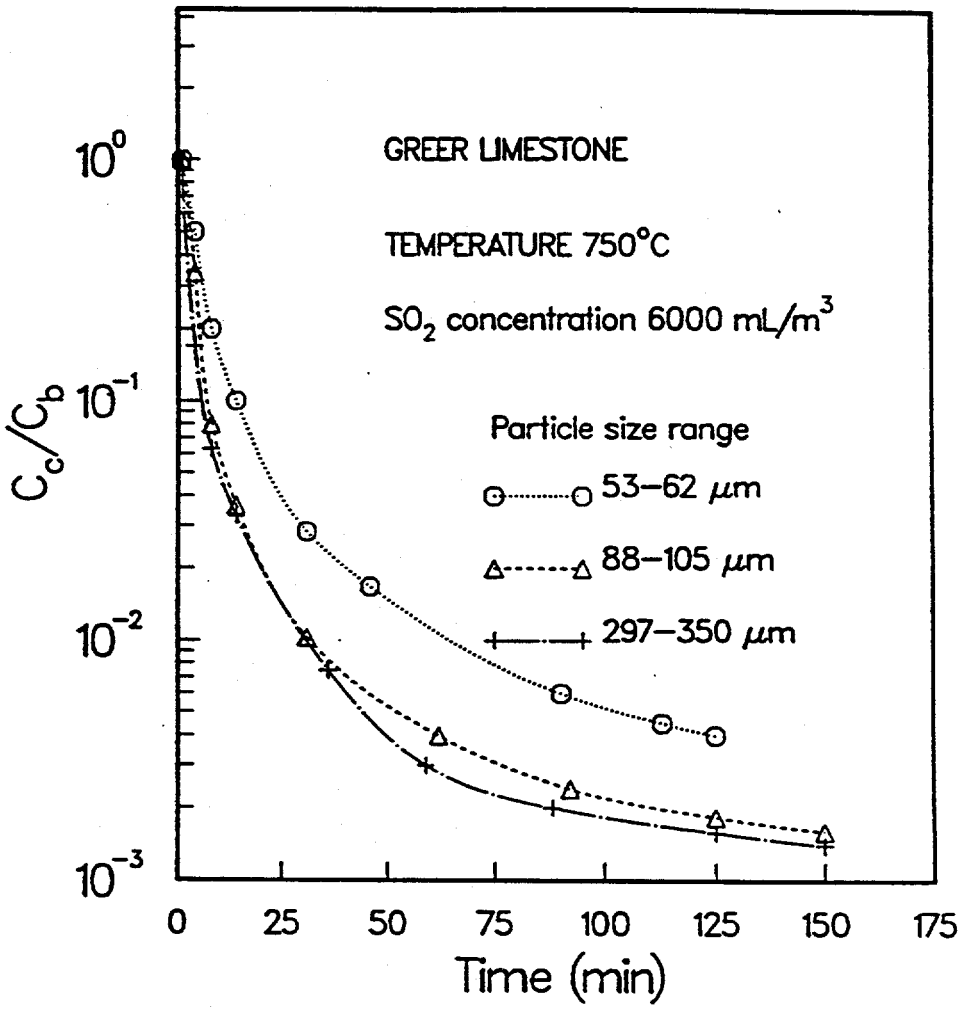

Figure 4.4: Concentration of SO_2 at the reaction interface for Greer limestone sulfated directly at $750°C$ and 6000 mL/m^3 of SO_2 in an atmosphere of 70% $CO_2(mol\%)$.

(=1.24). The porosities of the unreacted and reacted solid are very low, and as a result, we can use Eq. (4.12) instead of Eq. (4.11) to relate a, a_0, and a_c. Therefore, the sole parameter that needs to be determined is the effective diffusivity through the product shell.

Using the procedure that we used to obtain the results shown in Figs. 4.2-4.4, all the experimental conversion vs. time data obtained from our thermogravimetric analysis experiments can be converted to equivalent d vs. time, c_c vs. time, and a_c vs. time curves. Once the experimental data are available in these forms, Eq. (4.13) can be used to determine the effective diffusivity as a function of x. Using Eq. (4.8) and (4.14) and changing the integration variable from r to x, Eq. (4.13) is written

$$\int_0^d [1/(D_e(x)(a-x)^s)]dx = (c_b - c_c)/{a_c}^s k_s {c_c}^n \tag{4.15}$$

Eq. (15) can be written in the general form of Fredholm integral equations of the first kind as

$$\int_{p_1}^{p_2} F_1(t,x)F_2(x)dx = g(t) \tag{4.16}$$

by defining, $F_1(t,x) = 1/(a-x)^2$, $F_2(x) = 1/D_e(x)$, and $g(t) = (c_b - c_c)/{a_c}^2 k_s {c_c}^n$. $g(t)$ and $F_1(t,x)$ are known from the experimental data, and the objective is to find $F_2(x)$.

$F_2(x)$ can be expressed as a linear expansion of a set of known functions,

$$F_2(x) = \sum_{i=1}^{N} A_i \phi_i(x) \tag{4.17}$$

Eq. (4.17) is introduced in Eq. (4.16) to give

$$\sum_{i=1}^{N} A_i \int_{p_1}^{p_2} F_1(t,x)\phi_i(x)dx = g(t) \tag{4.18}$$

Application of Eq. (4.18) to M data points ($M > N$), using some quadrature formula to compute the integral appearing in it, yields an overdetermined set of linear equations

$$\mathbf{BA} = \mathbf{g} \tag{4.19}$$

which may be solved by using the least-squares method for A_i and, therefore, the form of $D_e(x)$. $\mathbf{B}$ is an $M \times N$ matrix, $\mathbf{A}$ is the N-dimensional vector of coefficients in the

expansion of $F_2(g)$, and $\mathbf{g}$ is an M-dimensional vector consisting of the right-hand side of Eq. (4.13) at the data points.

Unfortunately, the inversion of Eq. (4.16) is a well known ill-posed problem, and as a result, the above described procedure yields oscillatory solutions (Allison, 1979). This difficulty may be avoided by using a regularization method (Tikhonov and Arsenin, 1977). Such a method has been used, among others, by Brown and Travis (1983) to extract pore size distributions of porous media from effective diffusivity measurements. However, the application of the regularization method requires the values of $F_2(x)$ at the limits of integration (p_i), whereas such information is not available for the problem at hand. For this reason, we will use a method based on the concept of singular value decomposition of matrices (Golub and Van Loan, 1983), which can yield smooth solutions from the overdetermined set of equations (Eq. (4.19)) that result from discretization of Eq. (4.16) at the data points, but it does not require knowledge of $F_2(x)$ at p_i for its application.

Singular value decomposition decomposes an $M \times N$ matrix $\mathbf{B}$ into a product of three matrices, an $M \times N$ column-orthogonal matrix $\mathbf{U}$, an $N \times N$ diagonal matrix with positive or zero elements $\mathbf{W}$, and the transpose of an $N \times N$ orthogonal matrix $\mathbf{V}$:

$$\mathbf{B} = \mathbf{U}\mathbf{W}\mathbf{V}^{\mathbf{T}}; \mathbf{W} = \mathbf{diag}(w_1, w_2, ...w_m) \tag{4.20}$$

In terms of the elements of these three matrices, the least squares solution of Eq. (4.19) is given by

$$\mathbf{A} = \sum_{i=1}^{N} (\mathbf{u_i} \cdot \mathbf{g}/w_i)\mathbf{v}_i \tag{4.21}$$

where $\mathbf{u_i}$ and $\mathbf{v_i}$ are the ith columns of matrices $\mathbf{U}$ and $\mathbf{V}$, respectively. When $\mathbf{A}$ is computed from Eq. (4.21), oscillating solutions arise because some of the singular values of the matrix $\mathbf{B}$ are very small, tending to amplify the experimental errors present in the data used to form $\mathbf{B}$ and $\mathbf{g}$. Therefore getting smooth solutions from Eq. (4.21) amounts to filtering out the small singular values, that is, omitting from the summation the terms that correspond to small singular values. An algorithm described by Press et al. (1986) was employed to compute the singular value decomposition of matrix $\mathbf{B}$ and $\mathbf{A}$ from Eq. (4.21).